

Some Notes on Neurovascular Coupling Models

Tim David

September 14, 2016

0.1 NVU Version control details

Version 1.0: Farr & David (2011).

Version 1.1: Dormanns et al (2014), expanded on Farr & David model, added Ostby astrocyte model, removed Ca^{2+} in the astrocyte and EET pathway.

Version 1.2: Version 1.1 + nitric oxide pathway by Dormanns et al (2016), astrocytic Ca^{2+} from Farr & David (2011), and TRPV4 channel by de Ruijter. Currently on **master** branch in OO-NVU.

Version 2.0 Version 1.2 + Elshin/Chang neuron and ECS model. Currently on NVU2.0 branch in OO-NVU. Not yet complete.

Version 2.1: Version 2.0 + Ca^{2+} in the neuron (TvG). Not yet implemented.

0.2 Parbrain Version Control

Version 1.1: NVU Version 1.1 without diffusion. Currently on **master** branch.

Version 1.1.1: NVU Version 1.1 with extracellular K^+ diffusion. Currently on NVU11-ECSdiffusion branch in parbrain repo.

Version 1.2: NVU Version 1.2 with extracellular K^+ diffusion. Currently on NVU12-ECSdiffusion branch in parbrain repo.

Version 2.0: NVU Version 2.0 with extracellular ion diffusion. Not yet implemented - to be done when NVU Version 2.0 complete.

Version 2.1: NVU Version 2.1 with extracellular ion diffusion. Not yet implemented - to be done when NVU Version 2.1 complete.

Todo list

need to check if the VOCCs are modelled in the astrocyte. If not then we need to do it	12
equations required here	13
look at paper by Andrews et al [3] and [2] for experimental evidence on endothelial NO production.	20
up to this point NVS versions exist beyond we will need to put code through NVS	24
has the above been implemented in the nitric oxide model ?	25
check Elshin's model coupled with correct version 1.1	25
need to explain the difference between extracellular space and synaptic cleft	25
check dilation dynamics of ver 2.0 are the same compared to ver 1.2 . . .	26
what is the nernst potential at this stage for potassium?	31
redo buffering in ECS	32
proper oxygen model that fits with Cloutier is crucial see section 2.2.1 and section 1.4	34
black-box Beard and link to Cloutier or black-box Cloutier and link to Beard	35
email sasha.bulik@charite.de for the code	35
look at integrating mitochondrial models into a single model linked with NVU	35
need to find this reference	38
can we use this, by implementing a spatially averaged value of concentra- tions in the NVU model?	41
look at GABA interneurons and the glutamatergic pyramidal neurons forming a COX-1 type pathway via AA and EETs. In contrast to the K+ pathway that we currently support.	50
Rejuvinate the BACE1/hypoxic hypothesis for another HRC grant appli- cation	52
investigate energy model of mitochondrial oxygen consumption of [7] per- haps we should compare with the model of [21]	52

Chapter 1

NVU

1.1 Background

Latest version Functional hyperemia is an important metabolic autoregulation mechanism by which increased neuronal activity is matched by a rapid and regional increase in blood supply. This mechanism is facilitated by a process known as ‘neurovascular coupling’, the orchestrated communication system involving neurons, astrocytes and arterioles. Over the past five years the Canterbury group has developed an increasingly complex model of neurovascular coupling. This started with the work of Hannah Farr [38] and it has been updated with the work of Dormanns et al [29]. These notes are intended to document historical and future development.

1.1.1 some general references

The following are some papers that those of us have either forgotten how things work or we are new to the area **should read !** [46], [40], [42], [41], [104], [60, 61], [116] and of course [52]. A review article looking at the blood brain barrier dysfunction as a cause of Alzheimer’s is well worth reading [36].

1.2 Model version 0

This model was based on the work of Farr and David [38] who investigated the experiments and hypothesis of Filosa and other workers [41]. The model is a compartmental one where neuron, astrocyte and coupled smooth muscle and endothelial cell make up the full model. Here the basic premise was that neuronal activity mediated glutamate release into the synaptic cleft. The mGluR receptors release via the membrane bound G-protein phospholypase C and subsequently IP₃. The IP₃ receptors on the sarcoplasmic reticulum in the astrocyte release cytosolic Ca²⁺. Increased concentration of cytosolic Ca²⁺ mediates the EET pathway. In addition the Na/K ATPase pump allows synaptic cleft K⁺ to

be pumped into the astrocyte. Both K^+ and EET mediate the opening of the BK ion channel situated on the end feet of the astrocyte which is adjacent to the perivascular space. This space divides the end feet from the SMC. K^+ in the PVS allows the opening of the inwardly rectified K^+ ion channel situated on the SMC (in contrast to the model of Koenigsberger et al [68] which did not include a K_{IR} channel). The pathways are shown schematically in Figure 1.1. The dilation/contraction of the arteriole is determined by using the model of Hai and Murphy [52] and second order o.d.e modelling the mass acceleration of a unit mass of vessel tissue. The acceleration term is small and neglected (this means that one boundary condition is not able to be specified). The force produced by the phosphorylated myosin and activated phosphorylated myosin provides data for the Young's modulus of the tissue. The model successfully accounts for several observations seen in experiment. The model is capable of simulating the approximate 15% arteriolar dilation caused by a 60-s neuronal activation (modelled as a release of potassium and glutamate into the synaptic cleft). This model also successfully emulates the paradoxical experimental finding that vasoconstriction follows vasodilation when the astrocytic calcium concentration (or perivascular potassium concentration) is increased further. It is suggested that the interaction of the changing smooth muscle cell membrane potential and the changing potassium-dependent resting potential of the K_{IR} channel are responsible for this effect. Finally, the model demonstrates that a well controlled mechanism of potassium buffering is potentially important for successful neurovascular coupling.

1.2.1 Notes

This model was successful but fairly simple. Indeed the neuron model was non-existent and only relied on synaptic K^+ release and the action of mGluR to provide Ca^{2+} and EET concentrations in the astrocyte. K^+ concentration was not considered in the astrocyte as it was deemed that influx at the "head" was balanced by efflux at the "feet" with the BK channel. VOCCs are not modelled for the astrocyte [17]

There is a pump in the astrocyte and Ca^{2+} in the ER was obtained by allowing the rate of change of cytosolic Ca^{2+} to be equal and opposite to the store Ca^{2+} (with a volume change variable to maintain proper concentration). EET was assumed to "shift" the equilibrium state of the open probability for the BK channel. A simple shift to the membrane potential component of the equilibrium was used. This is based on experiments from Lu et al [82] where a variation in EET derived DHET provided a proportional variation in the half-maximal probability. It is noted that the DHET concentration was very small (of the order of 5 nM).

The K_{IR} channel's Nernst potential is a function of extracellular potassium (in this case the concentration in the PVS), Farr and David modelled it using the data from Quayle et al [97] as a log/linear relationship. The maximum conductance of the channel was a simple square root function of extracellular K^+ . This would be changed in version 1.0 (see section 1.3).

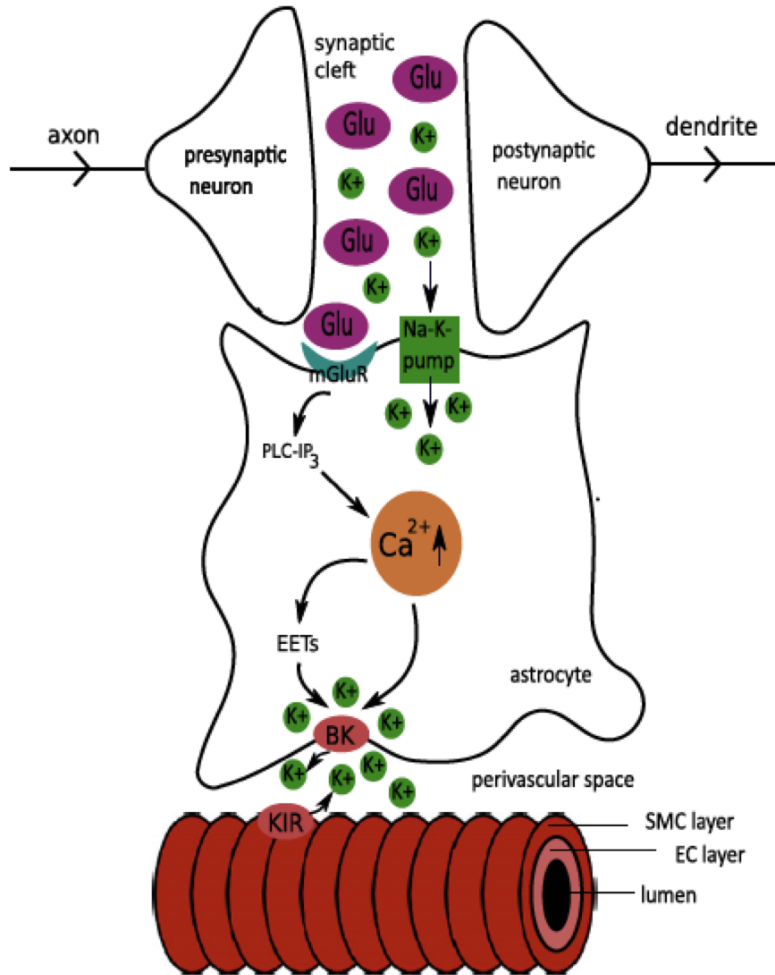


Figure 1.1: Overview of the complete NVC Model due to Farr and David [38].

The dilation took some time to reach peak value of radius change. This was thought to be due to the reaction constants for the Hai and Murphy model.

Although the results were encouraging in comparison with the experimental data of Edwards [35] they were qualitative at best. Increasing perivascular potassium did reverse the dilation but the figures in the paper seemed contradictory. For example Figure 2 shows a change in perivascular potassium from 4.2 to 5.2 mM and the corresponding radius changes from 16 to approximately 20 μm . Yet Figure 4 shows that changes in radius only occur for potassium concentrations of 8 mM and above.

1.3 Versions 1.*

1.3.1 version 1.0:

Farr and David [38]

After much discussion it was decided to completely rebuild NVU with new neuron and astrocyte models based on the work of Ostby et al [93]. A schematic of the pathways is given in Figure 1.2. As in version 0 the model did not include any detail in the internal concentrations of ions etc in the neuron but simply a release of K^+ and Na^+ into the synaptic cleft and its re-distribution back to the neuron via the NaKATPase pump. The time-dependent input for the neuronal activity is treated as a pulse like release of K^+ into the synaptic cleft and a simultaneous equal influx of Na^+ from the neuron following activity using an input signal, $f(t)$. In contrast to Farr and David conservation equations are developed in the astrocyte and the SMC and ECs for K^+ , Na^+ , Cl^- and HCO_3^- . All Nernst potentials for the K^+ , Na^+ , Cl^- and HCO_3^- channels are log functions of the ratio of external to internal concentrations where the external concentration is defined as the concentration in the synaptic cleft. This is important as the concentrations in the cleft vary over time and especially when the neuron is active.

One of the main questions that this model version answered was whether Ca^{2+} was a necessary and sufficient component for neurovascular coupling as proposed by [41, 40]. The model utilises only the K^+ pathway, excluding both Ca^{2+} and the subsequent AA/EET/20-HETE components in the astrocyte. The second question related to the possible action of ATP as an agonist in flowing blood on the endothelium and smooth muscle cells. Experiments indicated that the P2Y receptor on the luminal side of the endothelium would, if activated by ATP, mediate the production of IP_3 in the endothelial cell. IP_3 flowing through the myo-endothelial gap junction into the SMC will allow cytosolic Ca^{2+} to be released from the SR. Due to the calcium dependent receptors on the SR the cytosolic Ca^{2+} will mediate further release of Ca^{2+} into the cytosol, a process known as calcium induced calcium release (CICR) [48]. Results showed that this effect was dramatic and the paper by Dormanns et al. [30] indicated that increased reaction of ATP on the endothelial surface reduced the dilation of the perfusing arteriole due to the SMC oscillating and providing an increased average value of Ca^{2+} .

It should be noted that work by Simard et al. [104] showed that the purinergic G protein-coupled receptor P2Y was **not** expressed in cerebral endothelial cells but were expressed at the "glio-vascular interface" (not really sure what the authors meant by this or how the glio-vascular interface was defined). In addition from immunolabelling experiments by the same group showed that the connexin Cx43 was strongly expressed at the end feet of astrocytes.

1.3.2 Notes

Again as in version 0 the model is based on a compartment system with seven compartments as shown in 1.2. A BK channel was added to the Ostby model of the astrocyte providing a flux of K^+ into the perivascular space. This channel is formulated on the basis of the work by [49] with the Nernst potential of the channel a function of the ratio of internal to external K^+ along with the equilibrium of the open probability and characteristic time constant functions of the membrane potential v_k , which in contrast to [38] is independent of Ca^{2+} . It is assumed that the external $[K^+]_e$ is a constant. Importantly because the model does not include Ca^{2+} there is no sarcoplasmic reticulum. This will be included in version 1.1 (see section 1.3.3).

Luminal agonists acting on P2Y receptors on the endothelial cell surface provide a flux of IP_3 into the endothelial cytosol. This concentration of IP_3 is transported via gap junctions between endothelial and smooth muscle cells providing a source of sarcoplasmic derived Ca^{2+} in the smooth muscle cell. The model is able to relate a neuronal input signal to the corresponding vessel reaction. Results indicate that blood flow mediated IP_3 production via the agonist ATP has a substantial effect on the contraction/dilation dynamics of the SMC. The resulting variation in cytosolic Ca^{2+} can enhance and inhibit the flow of blood to the cortical tissue. IP_3 coupling between endothelial and smooth muscle cells seems to be important in the dynamics of the smooth muscle cell. The VOCC channels are, due to the hyperpolarisation from K^+ SMC efflux, almost entirely closed and do not seem to play a significant role during neuronal activity. The current model shows that astrocytic Ca^{2+} is not necessary for neurovascular coupling to occur in contrast to a number of experiments outlining the importance of astrocytic Ca^{2+} in NVC, however this Ca^{2+} pathway is not the only one mediating NVC. Importantly agonists in flowing blood have a significant influence on the endothelial and smooth muscle cell dynamics.

1.3.3 version 1.1:

Dormanns et al [29],[30] this is the **STABLE VERSION**

1.3.4 version 1.11:

version 1.1 + astrocytic Ca^{2+} + EET (mediation of BK channel) pathway

NOT YET IMPLEMENTED but is a topic branch

For this version the model contains the Ca^{2+} pathway originally developed by [38] in addition to the K^+ in the astrocyte. The astrocyte (AC) model contains different types of active and passive ion channels. These ion channels and pumps are captured in a set of differential equations to describe the conservation of mass for the corresponding species concentrations in the SC, the AC and the PVS. The ion channels for potassium (J_{KCC1} , J_{NKCC1} , J_K , J_{NaK} and J_{BK}), sodium (J_{NBC} , J_{NKCC1} , J_{NaK} and J_Na), chloride (J_{KCC1} , J_{NKCC1} and J_{Cl})

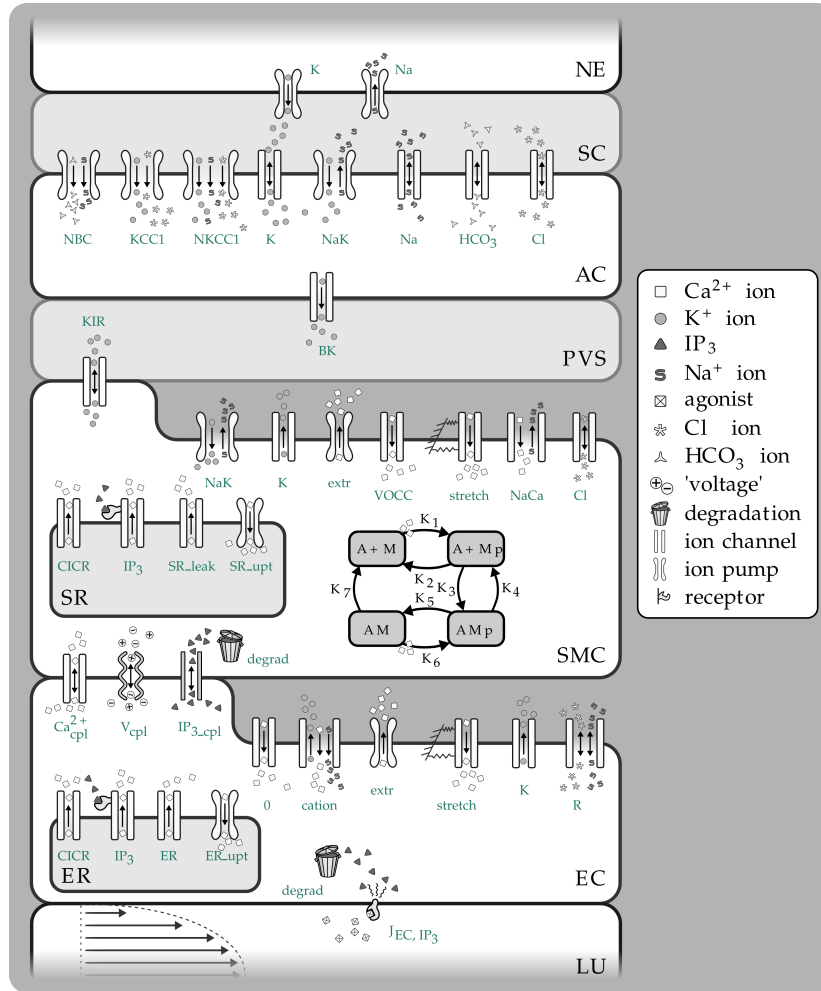


Figure 1.2: Overview of the complete NVC Model of version 1.0 including all subsystems. Abbreviations: NE - Neuron, SC - Synaptic cleft, AC - Astrocyte, PVS - Perivascular space, SMC - Smooth muscle cell, SR - Sarcoplasmatic reticulum, EC - Endothelial cell, ER - Endoplasmatic reticulum, LU - Lumen. NBC - Sodium bicarbonate pump, KCC1 - Potassium chloride cotransporter pump, NKCC1 - Sodium potassium chloride cotransporter pump, BK - Large conductance potassium channel, VOCC - Voltage-operated calcium channel, CICR - Calcium induced calcium release channel, R - Residual current regrouping channel, K₁ - K₇ - reaction rate constants, M - free nonphosphorylated cross bridges, Mp - free phosphorylated cross bridges, AMP - attached phosphorylated cross bridges, AM - attached dephosphorylated latch bridges.

and bicarbonate (J_{HCO_3}) are included. Note that the bicarbonate and chlorine fluxes are coupled with the Na⁺ and K⁺ fluxes to obtain a neutral in- or efflux

membrane voltage-wise.

The release of glutamate from the neuron in the synaptic cleft is simulated by creating a smooth pulse function ρ that describes the ratio of bound to total glutamate receptors on the synapse end of the astrocyte. This induces an IP_3 release into the cell, causing the release of Ca^{2+} from the ER into the cytosol, which then leads to the production of EET. The K^+ release into the PVS is controlled by the BK-channels. The opening of the BK-channels is regulated by the membrane voltage, as well as the EET and Ca^{2+} concentration. Figure 1.3 shows the whilst Figure 1.4 shows the full model.

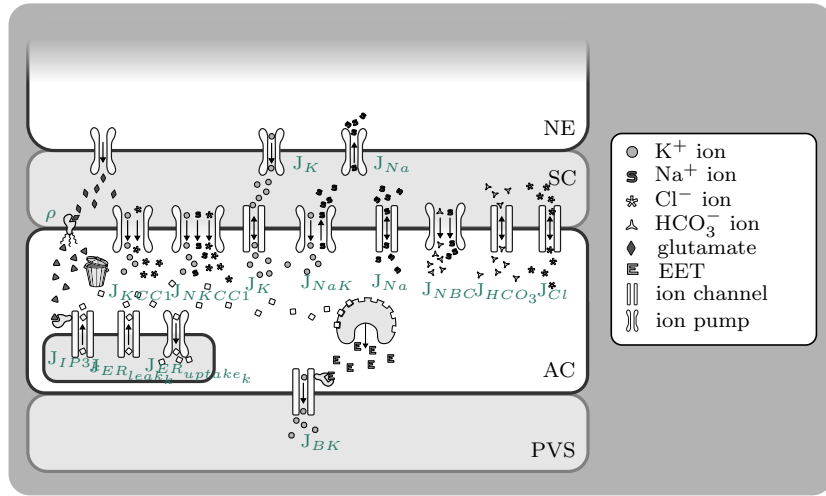


Figure 1.3: Overview of the Astrocyte ion channels showing additional Ca^{2+} and EET pathways which mediate the BK K^+ channel.

Results from this model indicate a similar profile to that found in version 1.0 however, when the neuronal pulse stops the flux through the BK potassium channel on the astrocyte is reduced compared to version 1.0 . The flux in the K_{IR} channel on the SMC is larger due to the increased K^+ in the PVS. This leads to a variation in the radius profile. Figure 1.5 shows the BK potassium channel flux, Figure 1.6 the flux in the K_{IR} and Figure 1.7 the radius profile. All Figures compare version 1.0 and 1.1 . In the original Farr and David model [38] the BK channel equation for the equilibrium open probability was given as

$$n_\infty = \frac{1}{2} [1 + \tanh(\frac{v + eet_{shift}[EET] - v_3}{v_4})] \quad (1.3.1)$$

$$v_3 = -\frac{v_5}{2} \tanh(\frac{[Ca] - Ca_3}{Ca_4}) + v_6 \quad (1.3.2)$$

Hence the BK channel is mediated by both EET and Ca^{2+} . In version 1.0 no Ca^{2+} was present hence the equilibrium value needed to be altered and this is

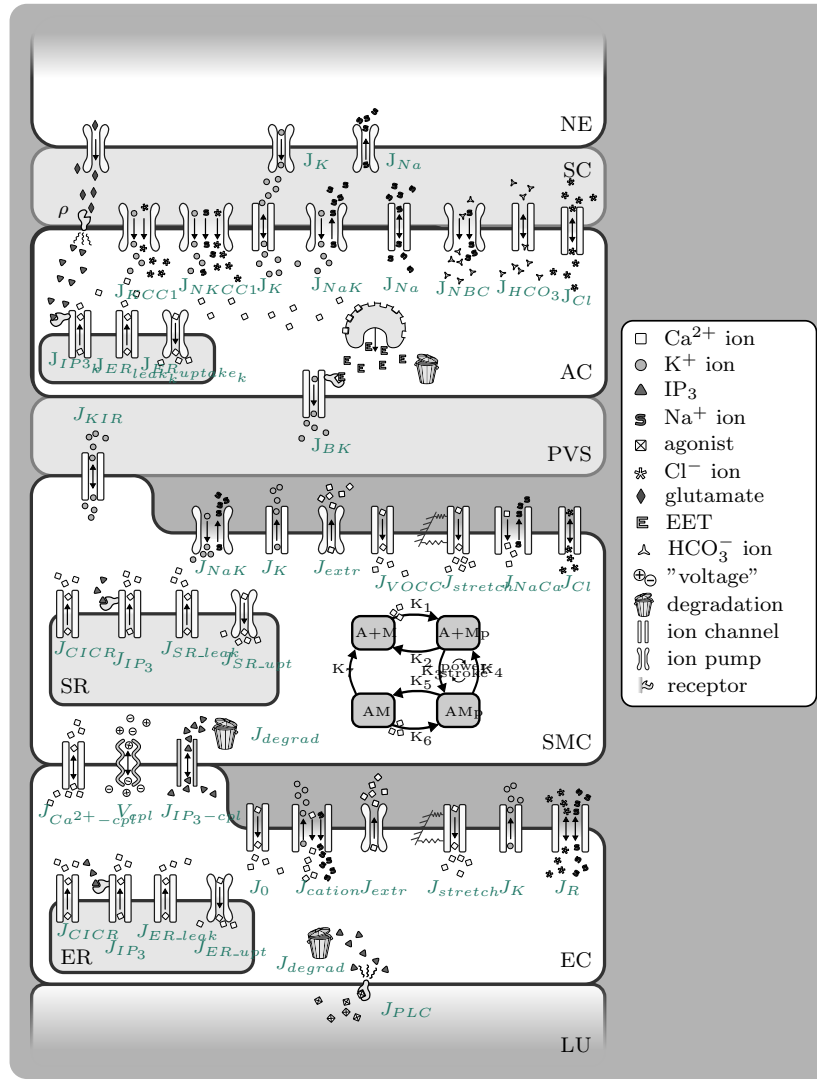


Figure 1.4: Overview of the version 1.1 model showing the glutamate influx into the SC.

given below.

$$n_\infty = \frac{1}{2} [1 + \tanh(\frac{v + v_6}{v_4})] \quad (1.3.3)$$

$$v_6 = 22mV \quad (1.3.4)$$

Results comparing the version 1.0 with version 1.1 shows that $v_3 \ll v_6$. The lower value therefore induces the BK channel to close earlier and leave an increased amount of potassium in the PVS. It should also be noted that the time

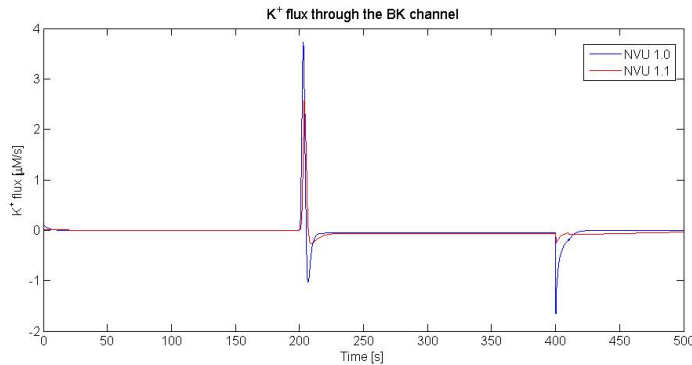


Figure 1.5: Comparison of versions 1.0 and 1.1 for the astrocyte BK channel

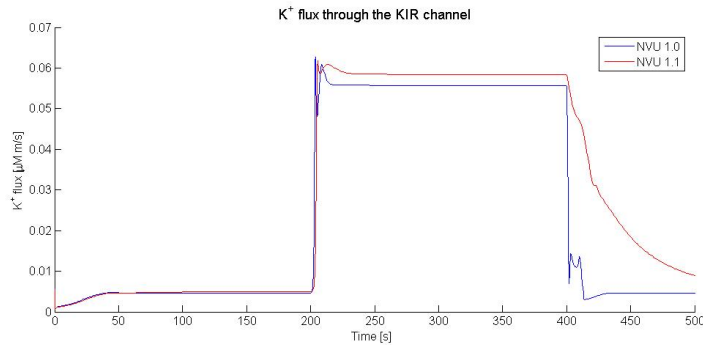


Figure 1.6: Comparison of versions 1.0 and 1.1 for the astrocyte K_{IR} channel

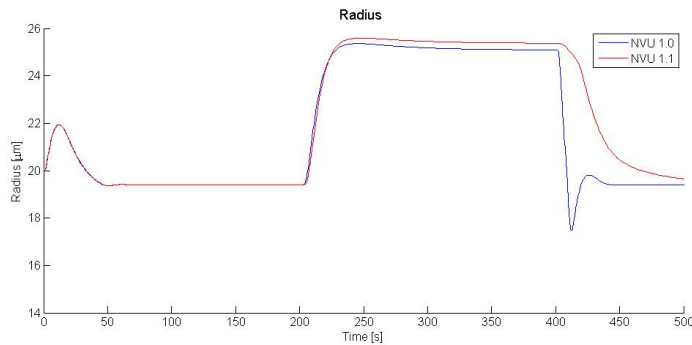


Figure 1.7: Comparison of versions 1.0 and 1.1 for the radius change during neuronal activation

constants for the channel opening/closing are different for the different models

since for version 1.0 (i.e.no astrocytic Ca^{2+}) we have

$$\phi_w = \cosh\left(\frac{v + v_6}{2v_4}\right) \quad (1.3.5)$$

with $v_6 = \text{constant}$, whereas for version 1.1 we have that

$$\phi_w = \cosh\left(\frac{v + v_3}{2v_4}\right) \quad (1.3.6)$$

with v_3 a function of Ca^{2+} . It is interesting to note that Ca^{2+} is not a necessary condition for neurovascular coupling as stated by Filosa [41] (see the work of Nizar et al. [92]), however their group did then indicate the importance of K^+ [42].

Lastly in this section work by Hadfield et al. [50] utilised the paper of Rzegalinski et al. [99] to model the role of arachidonic acid in the pathway towards the production of EET and 20-HETE from Ca^{2+} . Harder et al. [55] looked at (a review of) the role of cytochrome P450 enzymes as part of the pathway to EET and 20-HETE.

1.3.5 version 1.2:

version 1.11 + TRPV4 channel **IMPLEMENTED** and currently on master branch in **OO-NVU**

Experiments by Dunn et al. [34] seemed to show that TRPV4 ion channels produced enhanced Ca^{2+} concentrations in the endfeet of astrocytes and in contrast to Tran et al. [108] amplifies the neurovascular coupling response. Furthermore, previous work by Girouard et al. [47] indicated that the K^+ ion BK channel was mediated by astrocytic "endfoot" Ca^{2+} and that increasing Ca^{2+} caused a reversal of dilation to constriction. **it is unknown at present whether NVU version 1.1 can show this.** Work by intern Joerik de Ruijter (during first half of 2015) has produced a model which models the constriction/dilation experimental results of [34].

need to check if the VOCCs are modelled in the astrocyte. If not then we need to do it

Interestingly increasing PVS K^+ as we know induced both dilation and constriction however the evidence from [47] indicated that when the K_{IR} channel was blocked by Ba^{2+} it removed the dilation but not the constriction. **what was causing the constriction?**. It is suggested that the "switch" is based on both "endfoot" Ca^{2+} and PVS K^+ . Suppose a K^+ such that in normal circumstances it induces a dilation then blocking that particular BK channel changes a dilation to a constriction via the astrocytic "endfoot" Ca^{2+} . There is some experimental data in [47] with which we can compare our own dilation/constriction (as a function of ECS K^+) see Figure 7 in [29]. It seems from the work of [47] that ECS K^+ concentration plays an important part in the dilation/constriction phenomenon. Girouard et al's experiments show that "astrocytes regulate arteriolar tone through modulation of smooth-muscle

membrane potential with Kir-mediated hyperpolarization inducing vasodilation by closing VOCCs and K⁺ -mediated depolarization activating smooth-muscle VOCC to induce vasoconstriction”.

equations required here

Myoendothelial feedback

Tran et al. [108] hypothesised the existence of feedback between the SMC contraction and the EC. The proposed feedback pathway on the activation of the SMC contraction is such that the depolarisation of the SMC induces IP₃ which crosses the myoendothelial gap junction and triggers Ca²⁺ release from IP₃Rs. The resulting Ca²⁺ activate Ca²⁺-mediated IK K⁺ channels resulting in hyperpolarisation and a reduction in the contraction.

This process seems to have a number of problems. Firstly it assumes that the SMC contraction is done without any EC influence, i.e. that the contraction is triggered by agonists in the ECS. How this comes about is unclear. Secondly the hyperpolarisation of the SMC is done via some form of voltage gap junction. Yet membrane voltage variations in space can only occur if there is ion movement from one cell to another. How or what ions move is unclear.

1.3.6 version 1.2:

version 1.12 plus nitric oxide model NOW IMPLEMENTED as version 1.2 in NVU

A model of NO production from both neuron and endothelial cell is now available. Experimental work by Andrews et al [3] shows the importance of stress induced NO production and its dependence on ATP autocrine signalling and CCE. This work can provide some validation data. Figure 11 in the paper also provides a possible pathway that our model has yet to look at (although we may have already done this !). In addition the same group [2] has provided experimental data that our model needs to utilise. **this work was submitted to the Journal of Theoretical Biology and successfully published in [31]** basic method is set out below

1.3.7 Model Development

The potential of NO as an important vasodilating messenger molecule is assessed using a holistic mathematical model that includes the dynamics of NO in the NVU. With the help of this model the most crucial signalling pathways are analysed and the influence of NO in NVC investigated, including the localisation of the main contributing source.

Therefore, our previous foundation NVU model [38, 29] is extended by mathematical equations that represent production, diffusion and consumption of NO in different cell types, as well as the interaction of NO with other biochemical species and ion channel open probabilities.

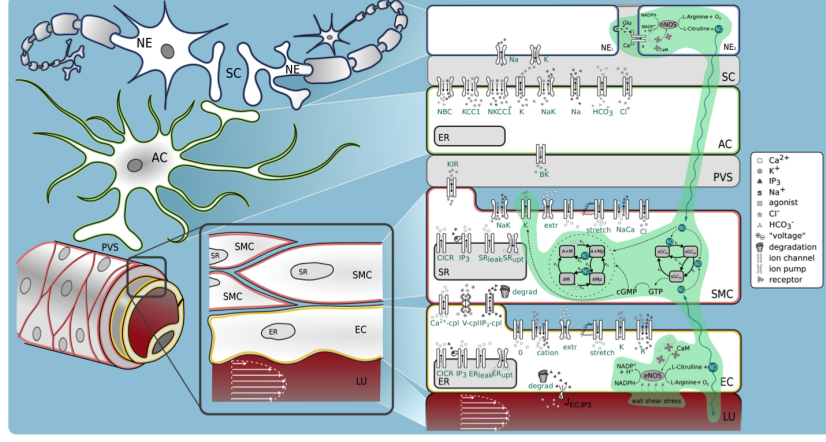


Figure 1.8: Overview of the complete NVC Model of version 1.0 with NO pathway.

As in the previous models of an NVU [38, 29] we divide the full model into seven compartments: the neuron (NE), the synaptic cleft (SC), the astrocyte (AC), the perivascular space (PVS), the smooth muscle (SMC) and endothelial (EC) compartments and the arteriolar lumen (LU). Connectivity is provided by inputs and outputs in form of values or time-dependent functions for ion fluxes, membrane potential and ion channel open probability of each of the compartments which act as a coupling between them.

Our NO model focusses on the NO production by the two constitutive isoforms of nitric oxide synthase, nNOS and eNOS [28]. Both enzymes' activation is mediated by intracellular Ca^{2+} in the NE and EC, respectively. In addition, eNOS gets activated by blood flow induced wall shear stress in the cerebral arterioles [?]. Due to its high diffusion coefficient NO diffuses rapidly into other compartments, shown in experiments [64] and in kinetic simulations [74]. When NO reaches the SMC it interacts with intracellular enzyme activation and regulates SMC relaxation[113].

A schematic representation of the compartments and the NO signalling pathway in the NVU is given in Figure 1.9, reaching from its synthesis in the NE and the EC to the relaxation of the SMC.

The dynamics of NO in the involved compartments are mathematically described using mass balance formulations. Like this, the concentration of NO in each domain is determined by the production $P_{NO,m}$, subtracted with the consumption $C_{NO,m}$ within the cell, i.e. the reaction with oxygen or other molecules, and the diffusion $D_{NO,m}$ from and into other compartments.

The NO concentration $[NO]_m$ is given by the solution of the following generic first-order non-linear differential equation:

$$\frac{d[NO]_m}{dt} = P_{NO,m} - C_{NO,m} + D_{NO,m}, \quad (1.3.7)$$

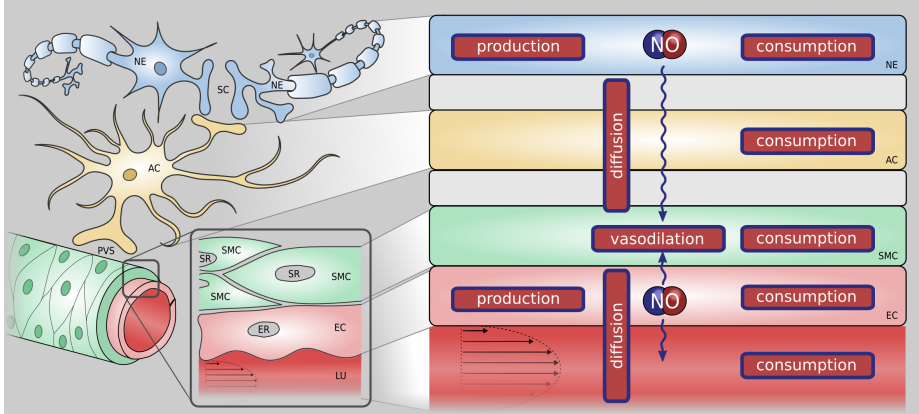


Figure 1.9: NO signalling pathway in NVC. NO is produced in the neuron (NE) and the endothelial cell (EC) and diffuses into other compartments, where it gets consumed by chemical reactions. In the smooth muscle cell (SMC) it leads to relaxation and therefore vasodilation. SC - Synaptic cleft, AC - Astrocyte, ER - Endoplasmic reticulum, PVS - Perivascular space, SR - Sarcoplasmic reticulum, LU - Lumen.

where $m \in \{n, k, i, j\}$ notates the cell indices for NE, AC, SMC and EC, respectively.

1.3.8 NO Production

The production rate of NO is dependent on the concentration of activated nitric oxide synthase. L-Arginine (L-Arg), oxygen (O_2) and nicotinamide adenine dinucleotide phosphate (NADPH) are the biochemical substrates needed for the NO production [19], where L-Arg is the requisite and sole nitrogen donor [45]. L-Arg is oxidized to L-Citrulline and the biochemical reaction leads to the production of $NADP^+$, water and NO. This five-electron oxidation reaction takes place in two steps, the overall stoichiometric chemical formula reads as follows:



For the reaction several biomolecule cofactors such as flavin mononucleotide (FMN), flavin adenine dinucleotide (FAD) and tetrahydrobiopterin (H_4B) are needed.

Constitutive NOS isoforms, nNOS and eNOS, are thought to be the most influential NO producers and are critical for maintenance of homeostasis [44, 45]. On the basis of this we consider NEs and ECs as most influential producers of NO and assume no production in other cell types, therefore $P_{NO,k}$, $P_{NO,i} = 0$.

Neuronal NO Production

NO synthesis in the NE is catalysed by nNOS in response to glutamate-induced calcium influx into the post-synaptic neuron. An overview of the model detail is given in Figure 1.10.

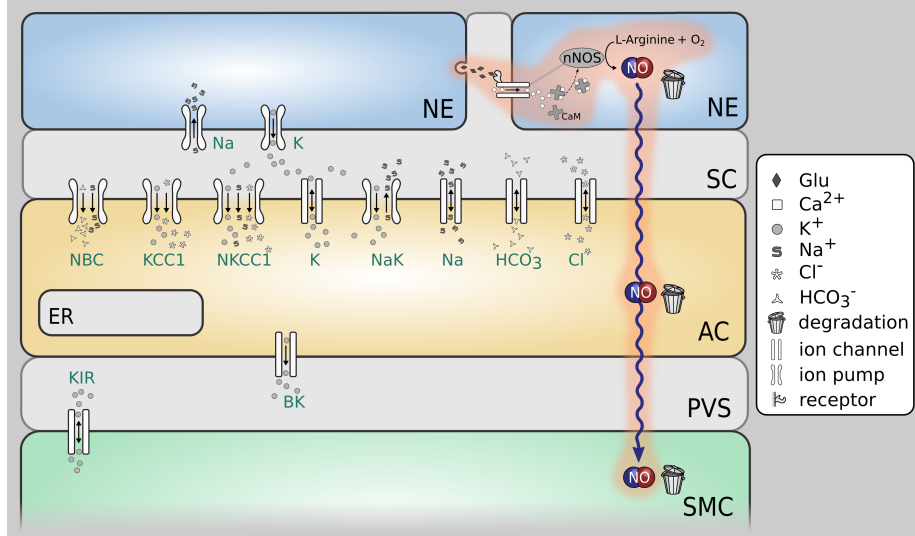


Figure 1.10: Graphical representation of the mathematical model, detail. The biochemical reaction that produces NO in the NE is catalysed by the enzyme nNOS and depends on the available concentration of L-Arg and O_2 . The model addition to our previous foundation model [29] is highlighted in orange. NE - Neuron, SC - Synaptic cleft, AC - Astrocyte, PVS.

The NO production in the NE depends on the amount of activated nNOS $[nNOS_{act}]$ [?], whose catalytic activity is sensitive to the availability of the substances O_2 and L-Arg [19]. We express it mathematically as

$$P_{NO,n} = P_{max} \frac{[O_2]_n}{K_{m,n}^{O_2} + [O_2]_n} \frac{[L\text{-Arg}]_n}{K_{m,n}^{L\text{-Arg}} + [L\text{-Arg}]_n}, \quad (1.3.8)$$

where P_{max} is the maximum neuronal production rate and given by

$$P_{max} = V_{NO,n_{max}} [nNOS_{act}], \quad (1.3.9)$$

with the maximum nNOS catalytic rate $V_{NO,n_{max}}$ and the neuronal O_2 and L-Arg concentrations, $[O_2]_n$ and $[L\text{-Arg}]_n$, respectively. $K_{m,n}^{O_2}$ and $K_{m,n}^{L\text{-Arg}}$ are the associated Michaelis constants [19, 20].

The nNOS activation in the NE is triggered by the chemical neurotransmitter glutamate (Glu) in response to neuronal activation. In a chemical synapse, when an action potential reaches the axon terminal of the presynaptic NE, it allows the release of Glu from vesicles into the synaptic cleft (SC) which then binds to

Glu-sensitive receptors of the postsynaptic NE's dendrite and is subsequently removed from the synaptic cleft by diffusion and hydrolysis [?].

As a stimulation input to the model we give a Glu concentration of $[2] \times 10^{-6}$ mol/m³ in the SC during neuronal activation. Before and after stimulation we assume a zero value of $[\text{Glu}]_{sc}$. Neuronal NOS is often colocalised with ionotropic N-methyl-D-aspartate receptors (NMDA-Rs) [85? , 15], which are receptor complexes including transmembrane ion channels in the NE that are opened or closed in response to the binding of Glu [?]. These channels provide Ca²⁺ influx into the cytosol. The two subtypes of NMDA-Rs, NR2A and NR2B, show different opening probability kinetics and expressed values. We model the open probabilities w of NMDA-Rs with different subunits with dependency of neuronal Glu concentration using a Michaelis-Menten kinetics formulation to fit the experimental data from [102] (see Figure ??):

$$w_{NR2,i} = \frac{[\text{Glu}]_{sc}}{K_m^i + [\text{Glu}]_{sc}}, i \in \{A, B\}, \quad (1.3.10)$$

where K_m^A and K_m^B are fitted Michaelis constants.

At an open state NMSDA-Rs are highly permeable to calcium ions [62]. The equation for the neuronal inward calcium current I_{Ca} in femtoamps (fA) per open NMDA-R is given by [102]:

$$I_{Ca} = \frac{4v_n G_M (P_{Ca}/P_M)([\text{Ca}^{2+}]_{ex}/[M^+])}{1 + e^{(\alpha_v(v_n + \beta_v))}} \cdot \frac{e^{(2v_n F/(RT))}}{1 - e^{(2v_n F/(RT))}} \quad (1.3.11)$$

with the Faraday's constant F , the neuronal membrane potential v_n (assumed to be constant during activation, an average value of the neuronal spiking activity of multiple action potentials. This is a simplified mathematical description, but suitable for our purpose as the model is focusing on Glu-effected Ca²⁺ changes in the NE), the conductance G_M , the ratio of the NMDA-R permeabilities to Ca²⁺ and to monovalent ions, respectively, P_{Ca}/P_M , the external Ca²⁺ concentration $[\text{Ca}^{2+}]_{ex}$, the concentration of monovalent ions (intra- and extracellular $[M^+]$, translation factors α_v and β_v , the temperature T and the universal gas constant R .

Santucci and Raghavachari arrive at estimates of 0.63 NR2A- and 11 NR2B-NMSDA-Rs, on average, per synapse [102]. Therefore, the total calcium current $I_{Ca,tot}$ reads as follows:

$$I_{Ca,tot} = I_{Ca}(0.63w_{NR2,A} + 11w_{NR2,B}). \quad (1.3.12)$$

The rate of change in neuronal cytosolic Ca²⁺ concentration in $\mu\text{M s}^{-1}$ is given by [102]:

$$\frac{d[\text{Ca}^{2+}]_n}{dt} = \frac{(I_{Ca,tot}/(2FV_{spine})) - \kappa_{ex}([\text{Ca}^{2+}]_n - [\text{Ca}^{2+}_{rest}]_n)}{1 + \Lambda}. \quad (1.3.13)$$

here V_{spine} is the volume of the neuronal dendritic spine (used together with F to convert the electrical flux $I_{Ca,tot}$ (in fA) into a molar flux (in $\mu\text{M s}^{-1}$)),

the decay rate constant of internal Ca^{2+} concentration κ_{ex} , the resting Ca^{2+} concentration $[\text{Ca}^{2+}_{rest}]_n$ and the buffer capacity Λ [102].

We formulate the concentration of activated neuronal NO synthase $[nNOS_{act}]_n$ in $\mu\text{M s}^{-1}$ as the solution of the following rate equation [57]:

$$\frac{d[nNOS_{act}]_n}{dt} = V_{max_{NOS}} \frac{[CaM]_n}{K_{act_{NOS}} + [CaM]_n} - \mu_2 [nNOS_{act}]_n , \quad (1.3.14)$$

where $V_{max_{NOS}}$ is the maximal rate of nNOS activity, μ_2 is the deactivation rate [22], and $K_{act_{NOS}}$ is the corresponding Michaelis constant [57].

The concentration of calmodulin / calcium complexes is given by [24]:

$$[CaM] = \frac{[\text{Ca}^{2+}]_n}{m_c} \quad (1.3.15)$$

with m_c , the number of Ca^{2+} bound per calmodulin:

$$m_c = \frac{[\text{Ca}^{2+}]_n}{\phi_n} \frac{d\phi_n}{d[\text{Ca}^{2+}]_n} , \quad (1.3.16)$$

where ϕ_n , the sum of all states of bound Ca^{2+} with respect to free $[\text{Ca}^{2+}]_n$, is

$$\phi_n = 1 + Q_1 [\text{Ca}^{2+}]_n + Q_1 Q_2 [\text{Ca}^{2+}]_n^2 + Q_1 Q_2 Q_3 [\text{Ca}^{2+}]_n^3 + Q_1 Q_2 Q_3 Q_4 [\text{Ca}^{2+}]_n^4 \quad (1.3.17)$$

with the binding constants Q_1 to Q_4 [24].

Endothelial NO Production

NO production in the EC is catalysed by the constitutive enzyme isoform eNOS, whose catalytic activity is sensitive to the availability of the substances O_2 and L-Arg [19]. An overview of the model detail is given in Figure 1.11.

The endothelial NO production can be mathematically expressed by

$$P_{NO,j} = V_{NO,j_{max}} [\text{eNOS}_{act}] \frac{[\text{O}_2]_j}{K_{m,j}^{O_2} + [\text{O}_2]_j} \frac{[\text{L-Arg}]_j}{K_{m,j}^{L-Arg} + [\text{L-Arg}]_j} . \quad (1.3.18)$$

The maximal activity of eNOS $V_{NO,j_{max}}$ is controlled by the intracellular calcium concentration $[\text{Ca}^{2+}]_j$ [19] and additionally it depends on the wall shear stress (wss) which occurs due to the blood flow through the perfusing arteriole [22].

Fluid shear stress activates a pathway involving phosphatidylinositol 3-kinase (PI3K) and the serine/threonine-specific protein kinase enzyme, which phosphorylates eNOS [43].

[96] and [22] describe the elastic strain energy stored within the vessel membrane by adapting mathematical models of [110] and [83], who focus on quantifying exogenous Ca^{2+} -entry via shear stress-gated ion channels.

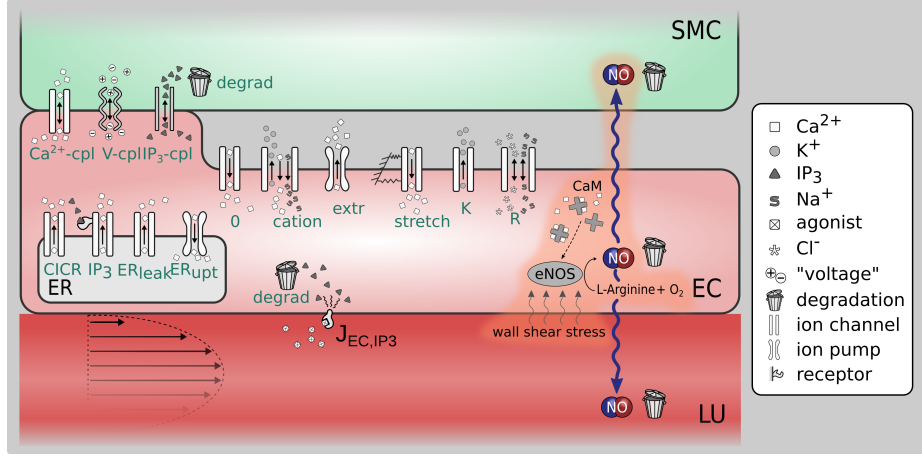


Figure 1.11: Graphical representation of the mathematical model, detail. The biochemical synthesis of NO in the EC is catalysed by the enzyme eNOS. It depends on the available concentration of the substances L-Arg and O₂ and is mediated by wall shear stress. The model addition to our previous foundation model [29] is highlighted in orange. SMC - Smooth muscle cell, EC - endothelial cell, LU - lumen.

The concentration of activated eNOS is given by the solution of the following differential equation [22]:

$$\frac{d[eNOS_{act}]}{dt} = \lambda \frac{K_{dis}[Ca^{2+}]_j}{K_{eNOS} + [Ca^{2+}]_j} + (1-\lambda)g_{max}F(\tau_\omega) - \mu_2[eNOS_{act}] . \quad (1.3.19)$$

The activation of eNOS by the cytosolic free calcium concentration in EC, $[Ca^{2+}]_j$, is given by the first term of the equation, where K_{dis} describes the eNOS-caveolin disassociation rate and K_{eNOS} is the Michaelis-Menten constant. g_{max} the maximal wss-induced eNOS activation rate, μ_2 denotes the deactivation rate [22].

The function $F(\tau_\omega)$ describing the elastic strain energy stored within the membrane is given by [110]:

$$F(\tau_\omega) = \frac{1}{1 + \alpha_j e^{-W(\tau_\omega)}} - \frac{1}{1 + \alpha_j} . \quad (1.3.20)$$

Here α_j is a zero shear open channel constant [22]. Note that we have added the term $\frac{1}{1 + \alpha_j}$ in order to deactivate the endothelial synthase of NO in the presence of no wss.

The strain energy density function $W(\tau_\omega)$ is taken from [110]:

$$W(\tau_\omega) = W_0 \frac{\left(\tau_\omega + \sqrt{16\delta_{WSS}^2 + \tau_\omega^2} - 4\delta_{WSS} \right)^2}{\tau_\omega + \sqrt{16\delta_{WSS}^2 + \tau_\omega^2}} \quad (1.3.21)$$

with W_0 , a shear gating constant and δ_{WSS} , the membrane shear modulus [22].

The wall shear stress τ_ω in the arteriolar wall depends on the regional cerebral blood flow (rCBF) Q . We assume Hagen-Poiseuille flow for cerebral arterioles:

$$Q = \frac{\Delta P \pi r^4}{8\eta L}, \quad (1.3.22)$$

where $\Delta P/L$ is the pressure drop over a given length of pipe (arteriole) and η is the dynamic viscosity of the fluid (blood). Both are assumed to be constant. The radius r of the arteriole is determined by the dynamics of the actin-myosin phosphorylation model by Hai and Murphy [51] used in our NVU model [29].

The wall shear stress, i.e. the frictional force per unit area, reads as follows:

$$\tau_\omega = \frac{4\mu Q}{\pi r^3}. \quad (1.3.23)$$

This creates a positive feedback mechanism, since increased wall shear stress will result in higher NO production from the EC, leading to vasodilation and further variation in wall shear stress.

look at paper by Andrews et al [3] and [2] for experimental evidence on endothelial NO production. These papers give some indication of the importance of ATP and capacitive calcium entry CCE mediated production of NO.

look at paper by Andrews et al [3] and [2] for experimental evidence on endothelial NO production.

1.3.9 Nitric Oxide Diffusion

The mathematical description of the NO diffusion is approached in many references [112? , 75]. It can be derived from Fick's second law describing a general diffusion of a substance over time in space. Steady-state conditions can be assumed, because diffusivity of NO is very high (diffusion coefficient $D_{c,NO} = 3300 \text{ } \mu\text{m}^2 \text{ s}^{-1}$) whereas the consumption of NO, represented by R_{NO} , is shown to be rather slow [?]. Instead of using complex partial differential equations, we simplify the diffusion formulation, using the Einstein-Smoluchowski equation to describe the characteristic time $\tau_{\Delta x}$ that is needed for NO to diffuse over a certain distance, Δx , from the centre of one cell to another, which reads as [75]:

$$\tau_{\Delta x} = \frac{\langle \Delta x \rangle^2}{2D_{c,NO}}. \quad (1.3.24)$$

The distance between the centre of the EC layer and the centre of the SMC layer, x_{ji} , is 3.75 μm [66] and the distance between the centre of the NE layer and the one of the SMC layer is estimated to be 50 μm with the astrocyte in the middle between them.

For the diffusion of NO from one compartment into another, we can write

$$D_{NO,m} = \frac{[NO]_{out} - [NO]_{in}}{\tau_{\Delta x}}; m \in \{n, k, i, j\}. \quad (1.3.25)$$

NO diffusivity is assumed to be constant even though Vaughn *et al.* propose that the value of $D_{c,NO}$ varies for different regions [?]. Furthermore, we do not consider concentration gradients within the cytosol (lumped parameter approach).

The compartment model above describes the diffusion between the different domains, but does not consider the amount of NO that is released in the lumen and is scavenged by reactions with haemoglobin. Butler *et al.* and Kavdia and Popel, who base their results on numerical simulations, find that the NO concentration in the lumen is zero after a distance of approximately half of the radius [? 65]. Therefore, the diffusion flux J , i.e. the amount of ions leaving the EC per unit area and time, described by Fick's first law can be approximated as:

$$J = -D_{c,NO} \frac{\partial [NO]_j}{\partial x} \approx -D_{c,NO} \frac{\Delta [NO]_j}{\Delta x} \approx -D_{c,NO} \frac{[NO]_j}{r/2} \quad (1.3.26)$$

J is converted into a concentration leaving the region per unit time by multiplying with the arteriolar surface area and dividing by the volume. The arteriole is treated as a hollow cylinder with radius r and a given length δz :

$$D_{NO,j} = \frac{2\pi r \delta z}{\pi r^2 \delta z} \left(-D_{c,NO} \frac{[NO]_j}{r/2} \right) \approx \frac{-4D_{c,NO}[NO]_j}{r^2} \quad (1.3.27)$$

1.3.10 NO Consumption

As a free radical, NO reacts readily with biochemical species containing unpaired electrons, such as molecular oxygen, superoxide anions and metals [85]. NO gets scavenged in the cytosol of all cell types through which it diffuses. Mathematically, the scavenging term for all model compartments is given as (following [66]):

$$R_{NO} = k_m [NO]_m C_m; m \in \{n, k, i, j\}, \quad (1.3.28)$$

where C_m is the concentration of reactive species in the cell type and k_m represents the reaction rate constant.

1.3.11 NO in the SMC

NO diffuses through all cell types and clearly reaches the SMC, which forms the contractile core of the NVU model [29]. NO, via its second messenger cyclic guanosine monophosphate (cGMP), influences the SMC contraction mechanism and the open probability of the big potassium channel (BK), see Figure 1.12.

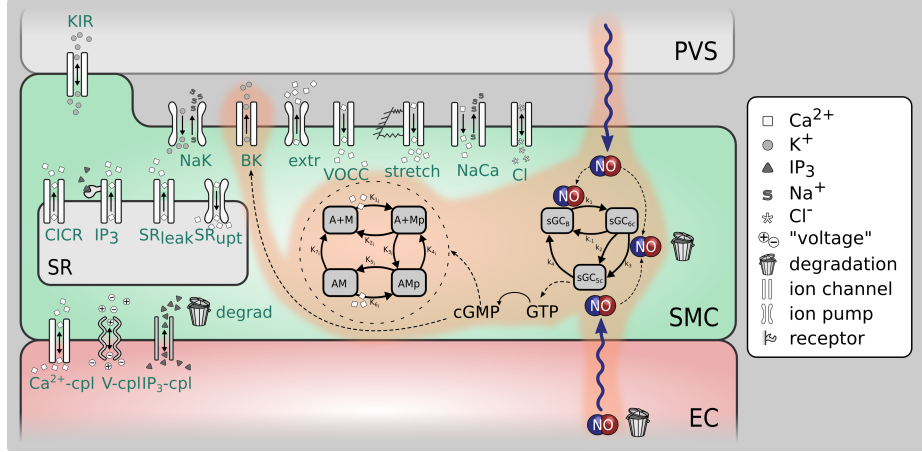


Figure 1.12: Graphical representation of the mathematical model, detail. NO in the smooth muscle cell (SMC) influences the contraction mechanism and the open probability of the big potassium channel (BK). The model addition to our previous foundation model [29] is highlighted in orange. PVS - Perivascular space, EC - endothelial cell.

The time rate of change of NO concentration in the SMC $[NO]_i$ is the sum of the diffused concentrations from the NE and the EC subtracted by the amount of NO that is scavenged by reactions with oxygen. This is written as:

$$\frac{d[NO]_i}{dt} = \frac{[NO]_n - [NO]_i}{\tau_{ni}} + \frac{[NO]_j - [NO]_i}{\tau_{ij}} - k_i[NO]_i , \quad (1.3.29)$$

where the NO consumption rate constant k_i reflects the activity of various NO scavengers [113].

In the SMC NO activates soluble guanylyl cyclase (sGC), an enzyme catalysing the formation of the second messenger cGMP. The kinetics of sGC and its complexes are described by Yang *et al.* with reaction rate constants from Condorelli and George [113, 23]. The sGC system with E_b , the fraction of sGC in the basal state, E_{6c} , the fraction of sGC in the intermediate form and E_{5c} , the fraction of sGC in the fully activated form, is described by the following set of equations [113]:

$$\begin{aligned} \frac{dE_b}{dt} &= (-k_1[NO]_i - k_{-1})E_b + (k_4 - k_{-1})E_{5c} + k_{-1} \\ \frac{dE_{5c}}{dt} &= (-k_3[NO]_i - k_2)E_b + (-k_3[NO]_i - k_2 - k_4)E_{5c} + k_3[NO]_i + k_2 \\ E_{6c} &= 1 - E_b - E_{5c} , \end{aligned} \quad (1.3.30)$$

where k_{-1} to k_4 are rate constants, of which k_4 depends on the cGMP concen-

tration:

$$k_4 = C_4[cGMP]^m . \quad (1.3.31)$$

Here m reflects the strength of the cGMP feedback and C_4 is a rate constant [113]. The cGMP concentration is determined by

$$\frac{d[cGMP]}{dt} = V_{max,sGC}E_{5c} - \frac{k_{pde}[cGMP]^2}{K_{m,pde} + [cGMP]} , \quad (1.3.32)$$

where $V_{max,sGC}$ is the maximum cGMP production rate, $K_{m,pde}$ the Michaelis-Menten constant and k_{pde} the phosphodiesterase rate constant [113].

1.3.12 NO-mediated dilation

Yang *et al.* suggested two pathways as to how NO can lead to local vasodilation of arterioles in the brain [113]. Firstly, by indirectly influencing the SMC contractile system that is determined by the formation of cross bridges between the actin and myosin filaments and that was first described by Hai and Murphy [51]. There are four possible states for the formation of myosin: free nonphosphorylated cross bridges (M), free phosphorylated cross bridges (Mp), attached phosphorylated cross bridges (AMp) and attached dephosphorylated latch bridges (AM). The second messenger of NO, cGMP changes the rate constants K_2 and K_5 for the dephosphorylation of Mp to M and AMp to AM by myosin light-chain phosphatase (MLCP) [113]. In our previous fundamental NVU model [29] we used the rate constants based on the model of [68] where $K_2, K_5 = [0.5]/s$. [113] used the following reduced two-state model to describe the phosphorylation kinetics:



where

$$k_{mlcp} = k_{mlcp}^b + k_{mlcp}^c \frac{[cGMP]^{n_{H,mlcp}}}{[cGMP]^{n_{H,mlcp}}} \quad (1.3.34)$$

with an estimated Hill coefficient $n_{H,mlcp}$ of 2.

To adjust the reduced model to the [51] model used by [68], we scale the two factors k_{mlcp}^b and k_{mlcp}^c in order to achieve $K_2, K_5 = [0.5]/s$ for no NO production.

The second pathway concerns the open probability, w_i , of the BK channel in the SMC, which is a function of the membrane potential, v_i and is shifted to the left (in the membrane potential space) by cGMP, as shown in Figure 1.13 [?].

In the NVU model [29] the open probability of the BK channel in the SMC is described by the equation of [68]:

$$\frac{dw_i}{dt} = \lambda_i (K_{act_i} - w_i) , \quad (1.3.35)$$

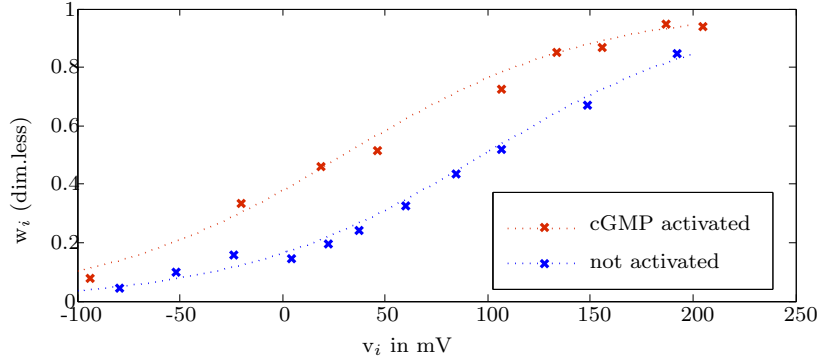


Figure 1.13: cGMP activation of the open probability of the BK channel in the SMC [?].

with the equilibrium state K_{act_i} given by

$$K_{act_i} = \frac{([Ca^{2+}]_i + c_{wi})^2}{([Ca^{2+}]_i + c_{wi})^2 + \beta_i \exp(-([v_i - v_{Ca3i}] / R_{Ki}))}. \quad (1.3.36)$$

Here the constants β , v_{Ca3i} and R_{Ki} describe the channel activation. We assume that in the v_i range of interest there is an approximately constant shift of w_i when activated by cGMP that can be modelled by making c_{wi} a function of cGMP, so that :

$$c_{wi} = \frac{1}{1 + \alpha_i \exp(\gamma_i [cGMP])} \quad (1.3.37)$$

with α_i and γ_i as translation factors that are chosen to give the desired shift of w_i upon cGMP stimulation as observed in experiments [?].

up to this point NVS versions exist beyond we will need to put code through NVS

Influence of the Blood fluid flow on Nitric Oxide production

Our current model does not provide a viable influence of the blood flow in the arterioles. We have shown through simple models that the flux of IP₃ has a substantial influence yet fluid shear stress and the transport mechanisms through the endothelial cell (essentially the blood brain barrier) are not modelled in a sufficient manner. Fadel et al. [37] produces a computational model of NO production and transport in a parallel plate flow chamber. The work looks at (using an FE model to solve the resulting pdes) NO concentration in both the fluid (simple Poiseuille flow) and the "tissue". In the case of integrating with NVU our main concern is the rate at which NO is produced in the EC. The production rate can come about through a shear mediated ion channel and the activation of the P2Y receptor by ATP. The spatial concentration of ATP in the

fluid boundary layer is a function of the wall shear stress. An analytical solution has been done by [27] which could help in determining the ATP concentration and hence NO in the EC. A review paper by Ngai and Yao [90] provides a substantial amount of data and Figure (1) indicates helpful possible pathways.

has the above been implemented in the nitric oxide model ?

We need to be mindful of the relationship between cGMP baseline and the SMC BK open probability . The reason for this is that if we change the radius of the perfusing arteriole then the shear stress changes and there is a consequential change in the baseline of cGMP due to variations in the activation of eNOS. We can therefore get a non-physiological negative concentration of cGMP for the resting baseline ! At present this issue is dealt with by never allowing the cGMP concentration to go below zero.

1.4 version 2.0:

Elshin/Chang model of neuron and extracellular space **NOT YET IMPLEMENTED**

check Elshin's model coupled with correct version 1.1

This model includes the work of Chang et al. [18] which was originally developed to investigate the propagation of large potassium waves in the cortex as a model for cortical spreading depression. The major difference between version 1.1 and 1.2 is that the neuron model of Østby et al. [93] has now been replaced by a neuron consisting of a soma (includes axon) and dendrite along with an extracellular space.

need to explain the difference between extracellular space and synaptic cleft

1.4.1 Model Development from work of Chang et al

An eight-compartment continuum mathematical model comprised of a soma, dendrite, extracellular space compartment, astrocyte, perivascular space, smooth muscle cell, endothelial cell, and lumen compartment will be compiled from different existing models. For simplicity reasons, the neurovascular unit is divided into two components namely a neuron component and a vascular component. The neuron component is comprised of the somatic, dendritic and extracellular space compartment. The vascular component is comprised of the astrocyte, perivascular space, smooth muscle cell, endothelial cell, and lumen compartment. Importantly the new model now includes the effects of oxygen on the metabolism.

1.4.2 Neuron Components, based on the model by Chang et al [18]

There are many different types of neurons, with differences in size, shape and physiological properties. In this project we have considered a generic neuron model with its basic features. The neuron component is a three compartment model consisting of a soma compartment, dendrite compartment and extracellular space compartment. The three major ions sodium, potassium, and chlorine and their associated channels are considered. Inter compartmental communications is enabled in the three compartments using a lumped parameter approach. Figure 1.14 shows the complete model.

we need to check that the dynamics of the astrocyte and the consequential dynamics of the SMC/EC and dilation/contraction model are the same for this model as they are for version 1.2

check dilation dynamics of ver 2.0 are the same compared to ver 1.2

Membrane potential and Cross-membrane currents

The total cross membrane currents is the sum of the voltage dependent sodium and potassium currents, sodium, potassium and chlorine leak currents, and the sodium-potassium exchange current. The membrane potentials of the neuronal components, $E_{m,*}$ (* is either s for somatic or d for dendritic), are governed by the coupled partial equations

$$C_m \frac{\partial E_{m,s}}{\partial t} = -I_{s,tot} + \frac{1}{2R_a\delta_d^2}(E_{m,d} - E_{m,s}) \quad (1.4.1)$$

$$C_m \frac{\partial E_{m,d}}{\partial t} = -I_{d,tot} + \frac{1}{2R_a\delta_d^2}(E_{m,s} - E_{m,d}) \quad (1.4.2)$$

where C_m is the membrane capacitance per unit surface area (μ farad/cm 2), R_a is the input resistance of the effective dendritic tree(ohms), δ_d is the half length of the effective dendritic tree(cm). $I_{s,tot}$ and $I_{d,tot}$ are the total cross-membrane ionic currents per unit surface area(mA/cm^2) for soma and dendrite and are given by

$$I_{s,tot} = I_{s,Na,tot} + I_{s,K,tot} + I_{s,Cl,tot} \quad (1.4.3)$$

$$I_{d,tot} = I_{d,Na,tot} + I_{d,K,tot} + I_{d,Cl,tot} \quad (1.4.4)$$

where $I_{s,Na,tot}$, $I_{s,K,tot}$, $I_{s,Cl,tot}$ are the total ionic currents of sodium ,potassium and chlorine ions of the soma respectively and $I_{d,Na,tot}$, $I_{d,K,tot}$, $I_{d,Cl,tot}$ are the total ionic currents of sodium ,potassium and chlorine ions of the dendrite respectively. These cross ionic currents simulate the diffusion of ions from

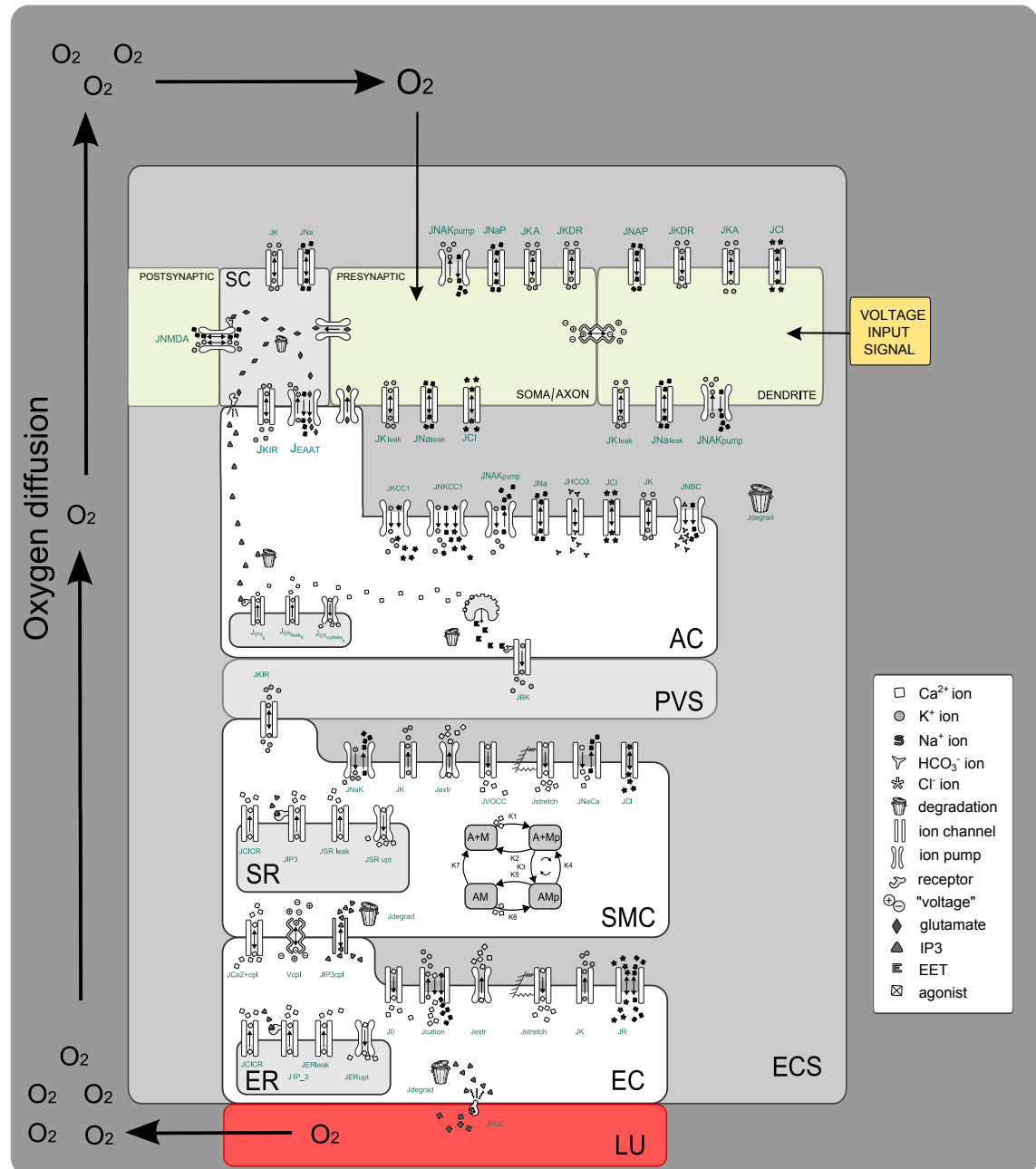


Figure 1.14: Overview of the complete neurovascular unit for version 2.0 using the new neuron/astrocyte model taken from [18]. NE-Neuron, SC-Synaptic cleft, AC-Astrocyte, PVS-Perivascular space, ECS- extracellular space, SMC-Smooth muscle cell, EC-Endothelial cell, LU-Lumen

the dendrite to the soma. Indeed in this particular model the "soma" is really the soma and the axon.

The somatic compartment total sodium current is given by $I_{s,Na,tot} = I_{s,Na,P} + I_{s,Na,leak} + I_{s,Na,pump}$ where $I_{s,Na,P}$ is the current through persistent-type sodium channels, $I_{s,Na,leak}$ is the current through sodium leak channels, $I_{s,Na,pump}$ is the sodium current through the sodium/potassium exchange pump. The dendritic compartment total potassium current is given by $I_{s,K,tot} = I_{s,K,DR} + I_{s,K,A} + I_{s,K,leak} + I_{s,K,pump}$ where $I_{s,K,DR}$ is the current through delayed rectifier type potassium channels, $I_{s,K,A}$ is the current through transient type potassium channels, $I_{s,K,leak}$ is the current through potassium leak channels, $I_{s,K,pump}$ is the potassium current through the sodium/potassium exchange pump. The dendritic compartment have all these channels in addition to NMDA(N-methyl-D-aspartate) channels which are permeable to sodium and potassium ions. There is evidence that glutamate is released from cells when extracellular potassium is elevated ([?]); ([?]) and high extracellular potassium enhances NMDA receptor activation ([?]). Hence, the glutamate-dependent depolarisation of the neuron is modelled as NMDA receptor activation. So, the NMDA channel current will be a function of both membrane potential and extracellular potassium. The cross-membrane currents of the voltage dependent ion channels are modelled using the Goldman-Hodgkin-Katz(GHK)equation

$$I_{ion,GHK} = m^p h^q \frac{g_{ion,GHK} F E_m [[ion]_i - \exp(\frac{-E_m}{\phi}) [ion]_e]}{\phi [1 - \exp(\frac{-E_m}{\phi})]} \quad (1.4.5)$$

where $g_{ion,GHK}$ is the maximal conductance value and permeability is absorbed into this parameter. The factors in the parameter $\phi = RT/F$ are R, the universal gas constant, T, the absolute temperature, and F, the Faraday constant. The conductance and concentration of the ions are ion and compartment specific. The parameters m and h are the ion specific activation and inactivation gating variables. The sodium, potassium and chlorine leak currents are calculated by Hodgkin-Huxley(HH) model given by

$$I_{ion,HH} = g_{ion,HH} (E_m - E_{ion}) \quad (1.4.6)$$

where $g_{ion,HH}$ is the constant conductance for the specific ion and E_{ion} is the Nernst potential for the specific ion. The Nernst potential is given by

$$E_{ion} = \frac{RT}{ZF} \log \frac{[ion]_e}{[ion]_i} \quad (1.4.7)$$

where Z is the valence of the ionic species, $[ion]_e$ is the concentration of the ion in the extracellular space and $[ion]_i$ is the concentration of the ion in the intracellular space.

$$\frac{1}{2R_a \delta_d^2} (E_{m,d} - E_{m,s}) \quad (1.4.8)$$

is the current moving from the dendrite to the soma (and along the axon to the presynaptic cleft). This current is established by a voltage variation in the

dendrite as a way of simulating a synaptic action potential from one synapse to another. Neuronal activation is made apparent by a Gaussian voltage profile input into the dendrite voltage equation for a specified time. This induces a current in the dendrite which via equation 1.4.24 allows the soma membrane voltage to change and induce potassium and glutamate efflux into the synaptic cleft.

Voltage dependent ion channels

The electrically excitable property of the neuron is simulated using the classical Hodgkin and Huxley kinetic description, ?? reference. This description consisted of an identification of the ionic species that carry the current, the steady state activation and inactivation curves for the current, and a measure of channel kinetics. They used peak conductances from voltage clamp experiments to estimate steady-state curves and the exponential rise or fall of the conductance to estimate kinetic properties. The model assumes each channel to have one or more independent gates , each of which are either in a open or closed state. All of its gates must be in a open state for the channel to be open. The variable conductance value is given by $g = g_{max}m^p h$. In this expression g_{max} is the maximal conductance of the channel, m and h are the fraction of activation and inactivation gates in the open state respectively. The rate at which the activation and inactivation gates open and close in response to the membrane potential are according to the equations

$$\frac{dm}{dt} = \alpha_m(V)(1 - m) - \beta_m(V)m \quad (1.4.9)$$

$$\frac{dh}{dt} = \alpha_h(V)(1 - h) - \beta_h(V)h \quad (1.4.10)$$

These equations state that the closed activation gates, (1-m), open at rate $\alpha_m(V)$, while the open activation gates, m, close at a rate $\beta_m(V)$. It is similar for the inactivation gates. The rate functions, $\alpha_m(V)$ and $\beta_m(V)$, are functions that depend on the voltage across the membrane. The forms of the functions α and β are usually determined through a mix of theoretical and empirical considerations and they are of the form

$$\alpha(V) = a_0 \exp\left(\frac{-\delta V}{s}\right) \quad (1.4.11)$$

$$\beta(V) = b_0 \exp\left(\frac{(1 - \delta)V}{s}\right) \quad (1.4.12)$$

where a_0 , b_0 , and δ are positive constants, with $0 \leq \delta < 1$. A gate that tends to open on depolarisation will have $s < 0$, while a gate that tends to open on hyperpolarisation will have $s > 0$. These exponential forms are modified to fit

the experimental data. The equation of the rate of change of activation gates may be rewritten as

$$\frac{dm}{dt} = \frac{m_\infty(V) - m}{\tau_m(V)} \quad (1.4.13)$$

where

$$m_\infty(V) = \frac{\alpha_m(V)}{\alpha_m(V) + \beta_m(V)} \quad (1.4.14)$$

and

$$\tau_m(V) = \frac{1}{\alpha_m + \beta_m(V)} \quad (1.4.15)$$

These expressions can be similarly written for inactivation gates. The functions $m_\infty(V)$ and $h_\infty(V)$ are called the steady-state activation and steady-state inactivation curves respectively. The values of m and h will get asymptotically close to the steady state if voltage is held constant for a sufficient length of time. The functions τ_m and τ_h are called the time constant curves of the activation and inactivation gates respectively and it describes the variation of the time constant with the membrane potential. Thus the varying response of different channels to membrane potential is modelled with the experimental data containing maximal conductances and rate functions of the activation and inactivation gates of the individual channels. The expressions used in the neuron model that describe the voltage-dependent rate functions are based on a model of hippocampal pyramidal cells described by Traub et al ([109]).

Ionic concentrations change in the neuronal components

The rates of change of ionic concentration in the soma and dendrite are due to the membrane currents and the exchange between soma and dendrites . The exchange between the somatic and dendritic compartments is modelled by a flux proportional to the difference between their ion concentrations. The equation describing the rate of change of ions in the soma is

$$\frac{\partial [ion]_{i,s}}{\partial t} = -\frac{A_s}{FV_s} I_{s,ion,tot} + \frac{D_{ion}(V_d + V_s)}{2\delta_d^2 V_s} ([ion]_{i,d} - [ion]_{i,s}) \quad (1.4.16)$$

The notation, D_{ion} , is the ion diffusion coefficient in aqueous solution taking into account tortuosity and volume fraction ([?]) and F is the Faraday constant. The quantities A_s and A_d are the surface areas of the soma and dendrite respectively in the total fixed volume given by the sum of the fixed somatic volume V_s , dendritic volume V_d , and extracellular volume, V_e . The equation describing the rate of change of ions in the dendrite is

$$\frac{\partial [ion]_{i,d}}{\partial t} = -\frac{A_d}{FV_d} I_{d,ion,tot} + \frac{D_{ion}(V_s + V_d)}{2\delta_d^2 V_d} ([ion]_{i,s} - [ion]_{i,d}) \quad (1.4.17)$$

The local rates of change of the extracellular space ions are due to the membrane currents and the buffering of potassium ions by glial cells. To ensure electro neutrality, the initial extracellular concentration of the anion Cl^- is chosen to be equal to the sum of the concentration of cations Na^+ and K^+ in the extracellular space. Also, the initial intracellular concentration of chloride is chosen in such a way that its Nernst potentials matched the resting membrane potential of -70 mV. The existence of immobile anions has been assumed in the soma and dendrites to achieve intracellular electro neutrality. Astrocyte, a type of glial cell, plays important roles in neurovascular coupling mechanism ([4]). One of the important roles of the astrocytes is the clearance of extracellular potassium ([?]). It is achieved through a variety of inward rectifying potassium channels. The buffering is also bolstered by the extreme polarity of the astrocyte cell membranes with membrane potential near the Nernst potential for potassium.

what is the nernst potential at this stage for potassium?

The equations describing the rate of change of ions in the extracellular compartment with the Chang model [18] is given by

$$\frac{\partial [ion]_e}{\partial t} = \frac{1}{f_e F} \left(\frac{A_s I_s, [ion], tot}{V_s} + \frac{A_d I_d, [ion], tot}{V_d} \right) + V_{buffer}(x, t) \quad (1.4.18)$$

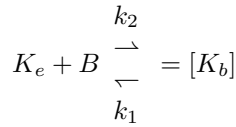
The extracellular space volume was defined as 15% of the intracellular space volume based on published data ([?]); ([?]). The differential equation governing the potassium buffering flux is given by

$$V_{buffer}(x, t) = -\frac{\partial B(x, t)}{\partial t} = \mu_+[K^+]_e B(x, t) \exp\left(\frac{[K^+]_e - 5.5}{-1.09}\right) - \mu_-(B_0 - B(x, t)) \quad (1.4.19)$$

where $B(mM)$ is the free buffer concentration, the rate constants $\mu_+ = \mu_- = 8.0 \times 10^{-6} ms^{-1}$ determine the speed at which potassium is buffered, and $B_0 = 200 mM$ is the effective total buffer concentration. The equation describes strong buffering of extracellular potassium for concentrations above 5.5 mM. The initial value of the free buffer concentration is set to maintain steady state when the extracellular potassium is at its resting value (3.5 mM). Here the extracellular space volume fraction is given by $f_e = V_e / (V_s + V_d)$.

We now know that this buffering term given by equation (1.4.19) is incorrect! Therefore we need to implement a correct term to ensure that the ECS potassium concentration $[K^+]_e$ remains at a reasonable level (about 3-10 mM) during normal excitation. [59] have implemented a neuron model based on the work of [63]. Their model investigates the role of buffering in cortical spreading depression. They make a significant point in assuming a closed system and reducing the number of dynamic variables along with defining a dynamic variable which simulates the "diffusion" of potassium into or out of the system. We cannot blindly copy this model as we do not necessarily

assume a constant concentration of ions within the total volume (i.e. ECS and ICS). However we can utilise their buffering model as shown below.



where K_b is the buffered potassium concentration, B the buffer, B^0 the total buffer with the relation $B^0 = K_e + B$, k_2 the forward buffering rate is a function of the extracellular potassium and given by

$$k_2 = \frac{\bar{k}_1}{1 + \exp\left(-\frac{(K_e - 15)}{1.09}\right)} \quad (1.4.20)$$

and the backward buffering rate k_1 is a constant $= 5.0 \times 10^{-5}$. (Very small!). \bar{k}_1 is a constant that normally has the same value as k_1 . We can therefore define a conservation equation for K_b .

$$\frac{dK_b}{dt} = k_2 K_e (B^0 - K_b) - k_1 K_b \quad (1.4.21)$$

[59] give an indication of the characteristic time scales and suggest that the forward buffering is of the order of 40 seconds whilst that of the backward rate is 5 hours!

redo buffering in ECS

1.4.3 Sodium-Potassium Exchange pump and their oxygen dependency

When an action potential is elicited, the sodium ions enter the cell, and potassium ions leave the cell. The primary role of Na+/K+ ATPase exchange pump in the neuronal membrane is to restore ionic concentrations to their homoeostatic state. The Na+/K+ ATPase pump is a transmembrane protein with two extracellular binding sites for potassium, three intracellular binding sites for sodium, and a single intracellular binding site for ATP. The pump moves out three intracellular sodium ions and two extracellular potassium ions against their electrochemical gradients and hence the need for energy. The pumps are fuelled by dephosphorylation of ATP (Adenosine triphosphate) in the cell and are given by



ATP is replenished by the reattachment of a phosphate ion to ADP(Adenosine diphosphate).The biochemical pathways through which ATP is generated is

powered by cellular respiration through both aerobic and anaerobic processes. Only about 5% of ATP production is independent of oxygen ([?]). Since the energy in the form of ATP is highly dependent on tissue oxygen concentration, the Na^+/K^+ ATPase exchange pump in the neuronal membrane is modelled as a variable dependent on the availability of oxygen. The potassium and sodium currents in the soma and dendrite are given by $I_{*,K,pump} = -2I_{*,pump}$ and $I_{*,Na,pump} = 3I_{*,pump}$, respectively. The total currents due to the sodium/potassium exchange pump in the soma and dendrite is given by

$$I_{*,pump} = I_{max} \gamma_{*,pump,1} \gamma_{*,pump,2} \quad (1.4.23)$$

where

$$\gamma_{*,pump,1}([K^+]_e, [Na^+]_i, *) = \left(1 + \frac{[K^+]_{e,0}}{[K^+]_e}\right)^{-2} \left(1 + \frac{[Na^+]_{i,0}}{[Na^+]_{i,*}}\right)^{-3} \quad (1.4.24)$$

This particular pump is crucial in simulations as it effectively determines the extracellular potassium concentration. On activation the neuron exudes K^+ into the ECS so if the exchange pump activity rate is high enough then the potassium stays at a reasonable level (of the order of 8 mM) pumping K^+ back into the neuron by exchanging Na^+ .

Simulation of the BOLD response

Elshin's work uses the model of Chang et al [18] and links it with NVU version 1.0 (and probably version 1.1). The output from this model allows for analysis of the time-dependent behaviour of both CBF (cerebral blood flow) and $CMRO_2$ the metabolic rate of oxygen consumption. Buxton et al [16] have developed a simple model for BOLD response based on assumed functional forms for CBF and $CMRO_2$. They utilise a "balloon" model which evaluates the CBV (cerebral blood volume) $v(t)$ and the mass conservation of deoxygenated blood $q(t)$ such that

$$\frac{dq}{dt} = \frac{1}{\tau_{MTT}} \left[f(t) \frac{E(t)}{E_0} - \frac{q(t)}{v(t)} f_{out}(v, t) \right] \quad (1.4.25)$$

$$\frac{dv}{dt} = \frac{1}{\tau_{MTT}} [f(t) - f_{out}(v, t)] \quad (1.4.26)$$

here τ_{MTT} is the characteristic mean transit time through the balloon at rest, $f(t)$ is the CBF, $E(t)$ the oxygen extraction fraction with E_0 the resting value for extraction fraction, F_{out} is the outflow from the balloon and is given by

$$f_{out} = v^{\frac{1}{\alpha}} + \tau \frac{dv}{dt} \quad (1.4.27)$$

Hence the output from Elshin's model can replicate the time-dependent behaviour of both q and v and in doing so simulate the BOLD signal given by

Buxton et al [16] as

$$\frac{\delta S}{S_0} = A (1 - f^{\alpha-\beta} m^\beta) \quad (1.4.28)$$

with $m = \frac{E}{E_0} f$, the normalised metabolic rate of oxygen consumption.

1.4.4 version 2.1

version 2.0 + neuron Ca²⁺ This model is that funded by the CMRF. Astrocytic and neuronal Ca²⁺ can be validated by work from Owen Jones at Otago Univ.

1.4.5 version 2.2:

version 2.1 + version 1.2 whic is essentially the introduction of nitric oxide pathway

NOT YET IMPLEMENTED

1.4.6 Integration with the model of Cloutier [21]

Equation 1.4.24 describes the action of the pump dependent on the initial concentration of extracellular potassium and intracellular sodium concentrations. The second pump represents the oxygen dependent production of ATP by the mitochondria [21?] and it takes the form

$$\gamma_{*,pump,2}([O_2]) = 2 \left(1 + \frac{[O_2]_0}{(1-\alpha)[O_2] + \alpha[O_2]_0} \right)^{-1} \quad (1.4.29)$$

where $[O_2]$ is the tissue oxygen concentration and $[O_2]_0$ is the initial equilibrium value of oxygen concentration. This expression indicates that the pumping rate will be reduced whenever there is a decrease of the oxygen level in the tissue.

proper oxygen model that fits with Cloutier is crucial see section 2.2.1 and section 1.4

1.4.7 Mitochondrial modelling

It is clear that with the Cloutier model [21] the mitochondrial function is modelled relatively simply by an input of oxygen, [ADP] and a resulting rate of change of [NADH] to produce [ATP]. A more complex model developed by Beard [11] suggests that we might be able to combine Cloutier and Beard together. **HOWEVER** this would increase the complexity, number of o.d.e.s and resulting parameters to a large, probably unsustainable number. Hence we will need to look closely at Beard [11] to develop a *black-box* approach which fits nicely with Cloutier.

Note that there is a correction to [11] that being [12]. Here the table of parameters has a number of important changes to values.

Or conversely look at Cloutier as a *black-box* and introduce Beard as the main model.

black-box Beard and link to Cloutier or black-box Cloutier and link to Beard

. Although not a modelling paper [101] provide some good background on mitochondrial membrane potential during reactive oxygen species generation. This paper should be read in conjunction with [?]. An excellent review paper on Mitochondria, endothelial cell function and vascular diseases is given by Tang et al [106] Research indicates that with Alzheimer's disease there exists reduced activity of α -ketoglutarate dehydrogenase complex (KGDHC). Work by Berndt et al [14] through a complex model simulates the relationship between reduced KGDHC and mitochondrial ATP production, redox state, transmembrane potential, and generation of ROS by the respiratory chain. **The simulation of ROS has particular importance.**

email sasha.bulik@charite.de for the code

look at integrating mitochondrial models into a single model linked with NVU

1.4.8 integration of Cloutier model into version 2.1?

Work has been ongoing into developing a more physiological neuron and astrocyte model. This has been based on the work by Cloutier et al [21]. Figure 1.15 shows the pathways that will become part of the full model. Why do we need

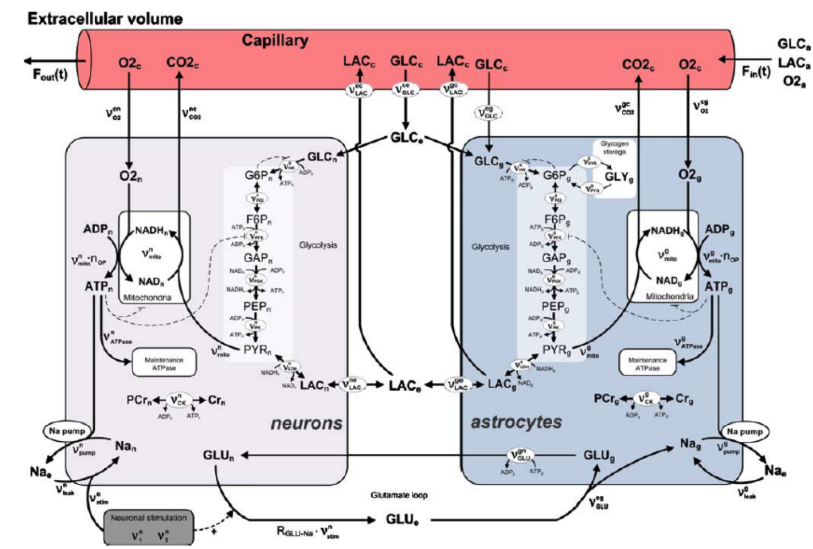


Figure 1.15: Overview of the complete Model due to Cloutier et al [21].

to do develop the model to this level of complexity and can we ever validate it ?

The answer to the second question is that we validate each module then assume the full model is also validated. The first question requires some explanation. From a mathematical perspective we would wish to make the model as simple as possible to mathematically and numerically analyse the dynamics etc. However the majority of funding for such research does not come from the mathematical community but from the biological and clinical funding bodies. It is therefore crucial that the model shows physiological correctness and that experiments in the numerical domain can explain those experiments in the "in vivo" and "in vitro" domains.

1.5 Neuro-vascular Simulator

In order to develop NVU simulation code that works both in a Matlab environment and parBRAIN the group had considerable problems with bugs that came about with trying to rewrite Matlab code in C. The group (led by Kathi and Kon) devised a python code which took .ini files as input and provided exact copies of functional code in both Matlab and C thereby alleviating the problem with porting bugs. A description of the NVS (as it is known) is given in an appendix.

Chapter 2

Parallel Implementation of NVU: parBRAIN

2.1 parBrain (version 0)

This section provides details and future trends for the parallelisation of NVU where the neurovascular coupling model is integrated into a tissue slice decomposed into tissue blocks. Each block contains an adaptive perfusing arteriole that is regulated by the NVU model.

2.1.1 parallel NVU code and Non-dimensionalisation

The NVU model (version 1.0 and soon to be version 1.1) has been integrated into an H-tree environment which allows for scalable parallel simulations of a large number of tissue blocks. This software is termed **parBrain**. An H-tree is a space filling tree such that in the case of simulating cortical perfusion each leaf of the tree models a penetrating arteriole into the cortex. Each leaf is dynamic since its time-dependent state is governed by the NVU output as shown above. Figure 2.1 shows the basic make-up of the environment.

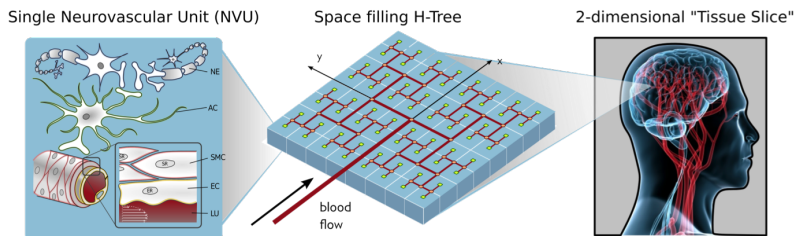


Figure 2.1: Overview of the H-tree integrated with NVU units.

2.1.2 scaling results for the parallel H-tree

These results have been evaluated using version 1.0 of the envy-you code. It is noted that the wall clock time is substantial to simulate 200 physiological seconds compared to a non-parallel Matlab version that simulates just a single NVU. For the parallel version to scale properly then the time taken to simulate a single NVU should be roughly the same for n cores to simulate n NVUs. As can be seen in the Figures that this is in fact the case. However, the time for each simulation is excessive, the reason for this is the use of a home-grown implicit Euler solver. Even though, using Newton iteration, the time step sizes should be relatively large it still takes extremely small steps. This may be due to the number of reasons, possibly the differing time-scales of the ion channels or the "stiffness" of the resulting equations. Non-dimensionalisation will certainly allow us to examine the relative sizes of components of the equations. However great care must be taken since Sneyd et al

need to find this reference

have shown that even small elements which one would normally ignore (due to their relative size) can dramatically alter the dynamics of the full system.

Work will continue on developing the parallel code (by Richard Brown at

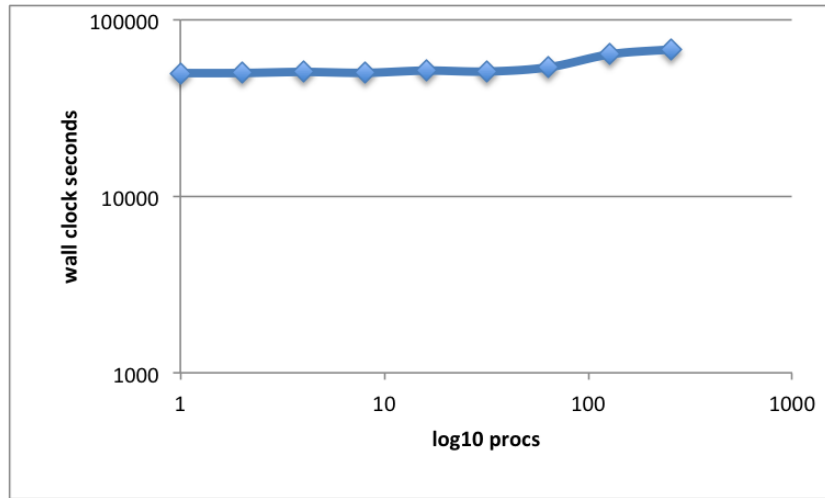


Figure 2.2: parBrain Weak Scaling.

Massey, who wrote the original parallel implementation) for new ode solvers that can adapt to the varying timescales. In addition the **parBrain** model will be continually updated by new versions of the NVU model. Initially the group will look to non-dimensionalise the envy-you version 1.0 that is used in **parBrain**.

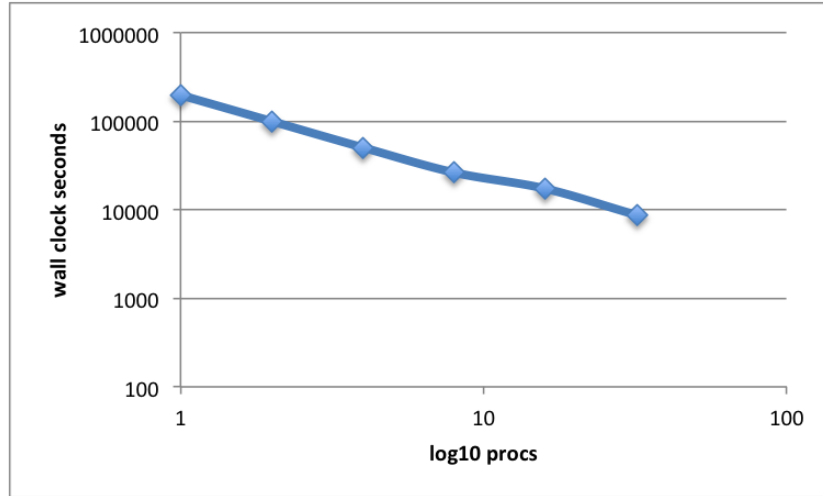


Figure 2.3: parBrain strong scaling.

2.1.3 Diffusion across tissue blocks

At present the tissue blocks are independent even though they represent a "continuous" tissue. Hence the parallel model has to simulate the diffusion of ions through the tissue. This is not a trivial exercise since it will require a considerable increase in communication between processor cores. However due to the way in which the tissue slice is decomposed the communication will be "local". **diffusion of extracellular $[K^+]$ _e has been successfully implemented** What do we need to diffuse, in terms of ions and messenger molecules, across the tissue block boundaries? Extracellular K^+ is certainly important due to its crucial part played in cortical spreading depression, whilst Ca^{2+} in the SR/ER would clearly not diffuse. Na^+ will need to be diffused as this has an effect on the K^+Na^+ ATPase pump on the neuron membrane. Ions and glutamate effluxed into the synaptic space would not be diffused as it is assumed that the synaptic space is not part of the extracellular space. **at present only K^+ is diffused see Figure 2.4 and connection from ECS to PVS is now NOT USED.**

Paper by [13] provides an insight into the diffusion and advection in complex networks. They impose a capillary network composed of axially aligned capillary segments joined in a random fashion. An hexagonal grid is used to find steady state concentration profiles within the tissue. Fickian diffusion (Laplacian operator) is modelled with an approximation on the hexagonal grid. Significant under-relaxation is needed for convergence. However the paper does give important insights into how the parBrain code can be developed for diffusion across tissue boundaries.

[79] model gap junctions in astrocytic networks simulating Ca^{2+} waves from cell to cell and this will have consequence when we come to look at how ions

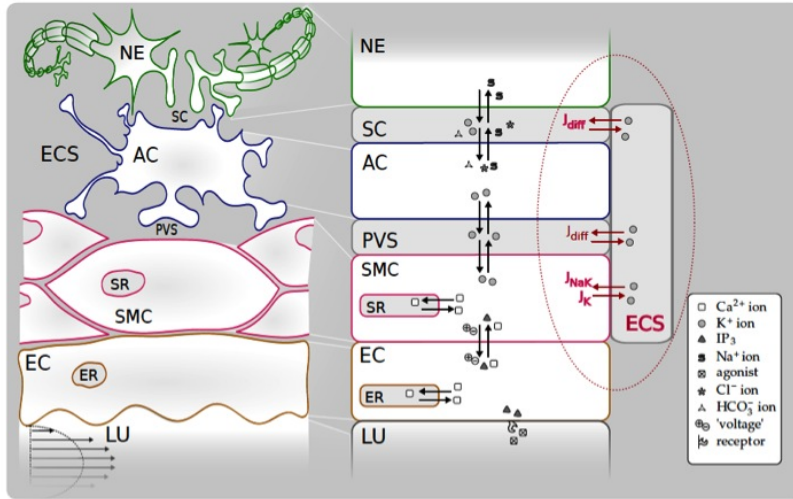


Figure 2.4: sketch of K^+ diffusion from ECS to SC, PVS and SMC.

diffuse across tissue boundaries in the parallel code.

2.1.4 Capillary models and their integration with NVU

At present the NVU model terminates with a perfusing arteriole. It is assumed that the oxygen flow into a tissue block is distributed instantaneously and homogeneously into the cerebral tissue. This is clearly not the case. Work on capillary perfusion has been done by a variety of research groups and the group at Canterbury has published a relatively state-of-the-art model [100]. It is unclear how this model can be integrated into either envy-you version 1.1 or parBrain. However the input to the Safaeian model is a simple flow inlet which could be the perfusing arteriole. **is this level of detail necessary? Does it help in determining the cerebral function? can it provide additional information for integration into the NTS system?** Also see the work (noted above) in section 2.2.1.

”To Pericyte or not to Pericyte”? , that is the question

Are pericytes important in determining neurovascular coupling? Papers seem to contradict each other. The first by [?] and further exemplified by the same group [53] promotes the idea that pericytes modulate capillary diameter in response to neural activity (glutamate release produces messengers that relax pericytes) and infer that neurovascular regulation at the capillary level is pericyte dominant (see also [?]). In addition they state that capillaries dilate before perfusing arterioles hence producing over 80 % of blood flow increase. On the other hand [39] provides evidence for the opposite.

The paper by Hill et al [58] clearly indicates that pericytes do NOT have contractile properties. We therefore do not need to integrate pericytes into the model at this time.

2.2 Integration of NVU with the (IBM) Neural Tissue Simulator

the relationship with IBM has gone very silent. We do not expect this to be rejuvenated any time soon.

Recently the brain group has been in negotiation with IBM to integrate the NVU model with the Neural Tissue Simulator (NTS), under the leadership of James Kozloski [71],[86] and an internal IBM document [72]. This software tool extends requirements and constraints of previous neuronal and neural circuit simulation methods, creating a tissue coordinate system. They have developed a novel tissue volume decomposition, and a hybrid branched cable equation solver. The decomposition divides the simulation into regular tissue blocks and distributes them on a parallel multithreaded machine (in this case a Blue Gene/P). The solver computes activation and functionality of neurons that have been divided arbitrarily across blocks. They demonstrate thread, strong, and weak scaling of the approach on a machine with more than 4000 nodes and up to four threads per node. Scaling synapses to physiological numbers had little effect on performance, since the decomposition approach generates synapses that are almost always computed locally. The largest simulation included in the scaling results comprised 1 million neurons, 1 billion compartments, and 10 billion conductance-based synapses and gap junctions. [71][72] discusses the implications of the ultrascalable Neural Tissue Simulator, and with their results estimate requirements for a simulation at the scale of a human brain.

this project has had to be put back for at least a year

2.2.1 Transport across the BBB

[26] provide a substantially complex model of transport (gas exchange) across the blood-tissue barrier. The model utilises four regions (RBC, plasma, interstitial fluid and parenchymal cell) .

Spatial profiles are given for a number of variables as a function of blood flow including pH, O_2 consumption and CO_2 production. The spatial independent variable was chosen to represent a 0.1 cm component of a capillary. Radial diffusion is treated an instantaneous given the small distance travelled from lumen across the tissue boundary. Axial diffusion is simulated. Boundary conditions for concentrations at $x = 0$ are assumed constant. However for our purposes we do not need axial profiles in a capillary but a spatially averaged value that allows us to estimate the concentrations of O_2 etc in the tissue. This would probably help with the work

can we use this, by implementing a spatially averaged value of concentrations in the NVU model?

2.2.2 Draft NVU model for parBRAIN

We show below in Figure 2.5 a draft sketch of how the NVU may be used in parBRAIN by linking (nearest neighbour) NVUs. Notice that we need to make clear as to whether we have two or just a single extracellular space (ECS). There are ten compartments

1. synaptic cleft
2. Astrocyte
3. Dendrite
4. Soma/Axon
5. Extracellular Space i)
6. Extracellular Space ii)
7. perivascular space PVS
8. smooth muscle cell SMC
9. endothelial cell EC
10. Lumen (blood flow)

Compare Figure 2.5 with 2.4. Is this the same topology ?

Figure 2.6 indicates a possible variation to the parBRAIN model. For this case in contrast to the diffusion where nearest neighbour connection is utilised to simulate diffusion we can introduce a more complex connectivity, not for ion transport, but for connecting outputs from the axon to the input (post synaptic dendrite) of each NVU model. **What does this simulate ?**. This might simulate connections of certain types of neurons to those which are geographically distant yet over the length scale of the vasculature is not necessarily distant. **Maybe the basal ganglia connectivity?.**

2.3 Some clinical models

The main question here is : Is the present model capable of investigating certain clinical phenomena?

Basic Unit for parBRAIN.jpg

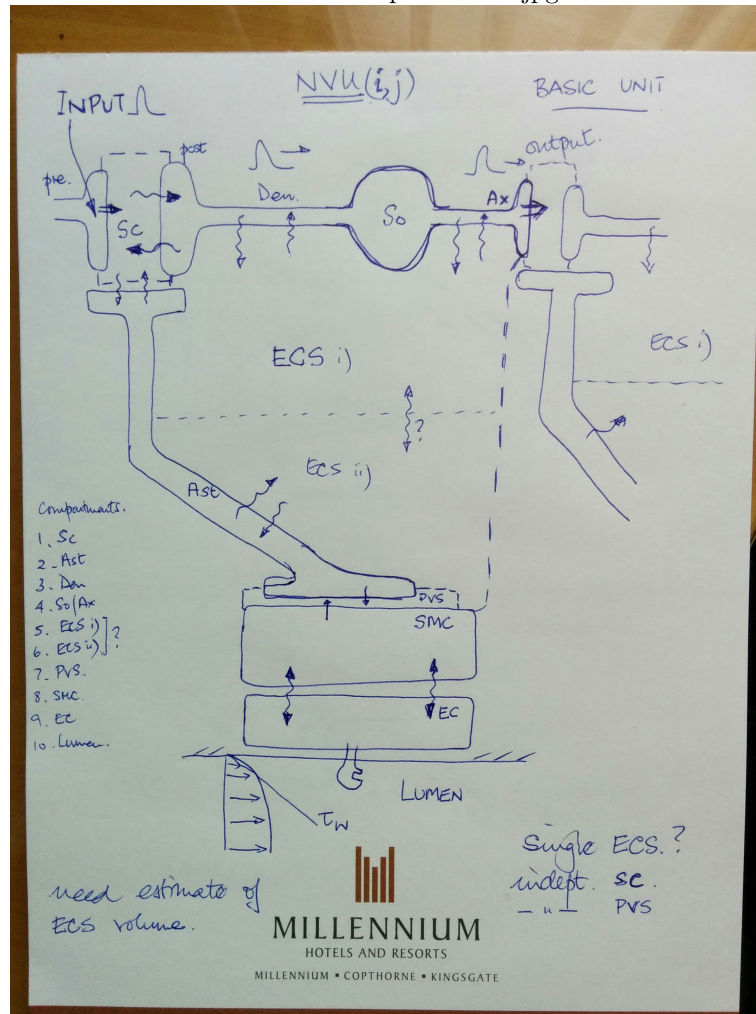


Figure 2.5: draft sketch of basic NVU with possible use in parBRAIN

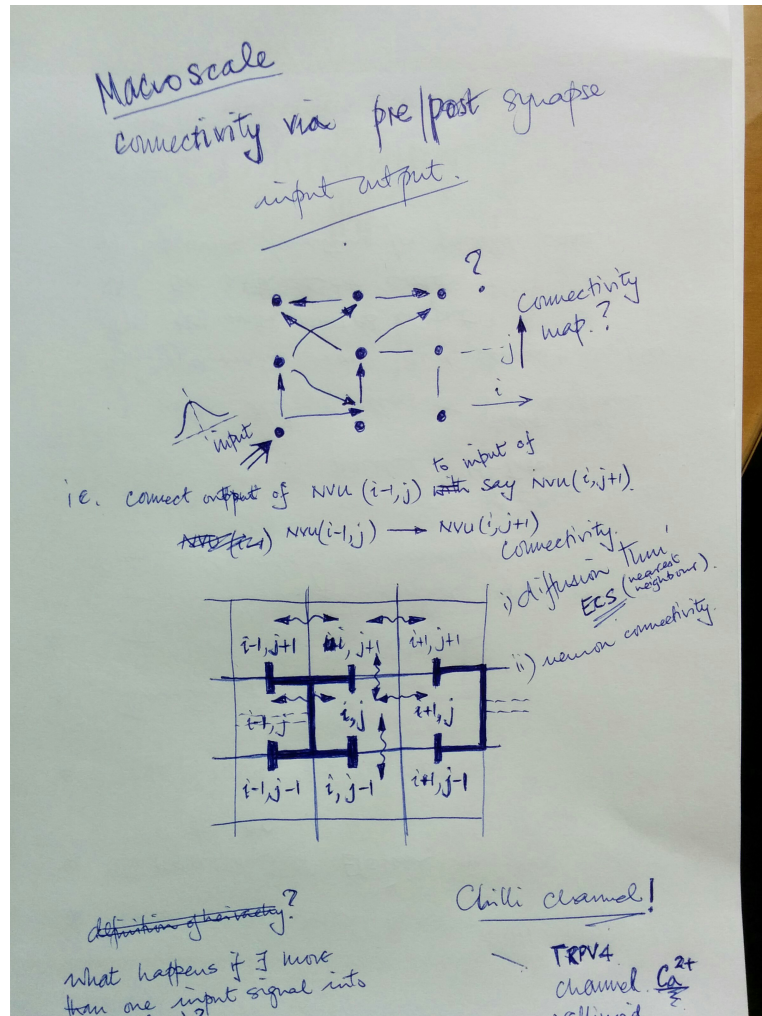


Figure 2.6: draft sketch of basic NVU with possible use in parBRAIN

2.3.1 Cortical Spreading Depression (CSD), Subarachnoid hemorrhage (SAH) and traumatic brain injury (TBI)

We look at the condition of subarachnoid hemorrhage since it seems that ECS K^+ has a particularly important role to play in determining the continued perfusion of ischæmic cerebral tissue this is exemplified by the perspective editorial in Nature Medicine by Lo [81]. [33] reviews the role of spreading depression and ischaemia in neurological diseases. The review puts forward a number of interesting phenomena which our model may well be able to simulate. In a substantial number of cases cortical spreading depression (CSD) occurs which can support several important physiological states. Shin et al [103] present data showing anoxic depolarisation cause vasoconstriction and reduce CBF in the ischæmic cortex strengthening the argument for modelling.

1. During CSD neurotransmitters such as GABA, glutamate are released in high concentrations whereby sustained cation influx occurs enhancing depolarisation. These high concentrations of glutamate signal vascular smooth muscle cells through a variety of pathways including arachidonic acid.
2. metabolism and energy demand are increased
3. CSD induces a rise in regional CBF (spreading hyperæmia) however despite this pockets of ischæmic tissue can occur. the increased rate of metabolism is not fully matched by the increase in rCBF.
4. tissue ATP falls, glucose concentration increases substantially along with the release of lactate and ECS pH falls.
5. basal K^+ increases during SAH with a consequential shift from spreading hyperæmia to spreading ischæmia
6. basal NO decreases since it is scavenged by the increased haemoglobin due to the haemorrhage and possibly the uncoupling of eNOS along with rho kinase.
7. see Figure 4 in [33]
8. **Lisa's work with the [21] model is now important along with Elshin's new neuron model**

[70] reviews the current state of effects of SAH on NVC. With the increase of K^+ and extravascular haemoglobin (causing reduced NO) dilation (see [32] for experimental evidence) is shifted to constriction which reduces blood flow and causes further ischæmia to an already deprived cerebral area. The authors state that increased K^+ causes a switch between dilation to constriction and of course we can already model this. They suggest that inversion of neurovascular coupling after SAH is due to increased basal BK channel activity and increased K^+

in the PVS. There is also experimental evidence given in [69] noting especially Figures 5 and 7.

[25] provides experimental evidence for the role of glial KIR channels and Na^+/glcK -pump in regulating ECS K^+ (in the rat hippocampus). They state that K^+ dynamics are independent of the neuronal membrane potential but are a function of the "balance" between extruded K^+ by those neurons which are firing and the K^+ buffered by the glial mechanism. This is important in determining the correct ECS K^+ crucial for modelling SAH etc. A good explanation of uncontrolled depolarisation of neurons following stroke or brain ischaemia is given in [111].

The work of [95] gives evidence concerning the increase in oxygen consumption (by approx 71 %) and surprisingly an increase of CBF by approx 238 % which they state impaired NVC after CSD. In the following 2 hours the authors suggested impaired NVC by looking at the local field potential (LFP) versus CBF. Early work by [89] provides evidence of pH changes during CSD and cerebral ischaemia caused they hypothesise by hyperpolarisation. As cited above [79] by modelling astrocytic networks simulate the consequence of CSD-triggered Ca^{2+} .

2.3.2 vasomotion

It seems clear that vasomotion plays a part in a number of pathologies. Evidence, although scarce, does indicate that neuronal, glial and VSMC Ca^{2+} dynamics can provide the environment for vasomotion to occur. parBrain can simulate this condition by a number of ways. Firstly the concentration of ATP can increase and in doing so induce IP_3 into the cytosol mediating Ca^{2+} efflux from the ER and inducing vasomotion or the concentration of ATP could decrease and by the same pathway produce vasomotion. This all depends on the "normal" concentration of ATP in the cerebral tissue (a value about which we know virtually nothing!!).

[107] indicates that ischaemia (such as stroke) open gap junctions between neurons, the Px1 channel. This channel opening may result in an efflux of ATP and glucose resulting in a decrease in the recovery rate from the ischaemic insult. In addition the release of ATP into the ECS would induce possible oscillations of Ca^{2+} in the SMC cytosol and thereby providing an environment for vasomotion. At the moment ATP only exists as an effective influx of IP_3 into the EC. We would therefore need to look at diffusing ATP in the ECS (see section Priorities)

2.3.3 The COX-1 pathway for neurovascular coupling

see section 3 with the work of Lecrux and Hamel [76]. Having spoken with Edith Hamel (in June 2016) she emphasised that this pathway seemed from experiment to be very important.

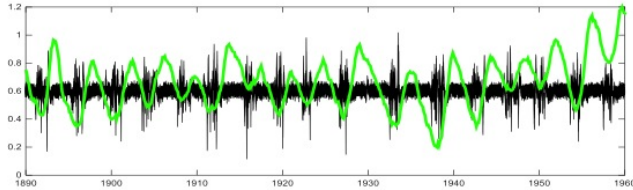


Figure 2.7: experimental data showing relationship between blood volume(green) and neuronal activity (black) from Berwick lab without vasomotion

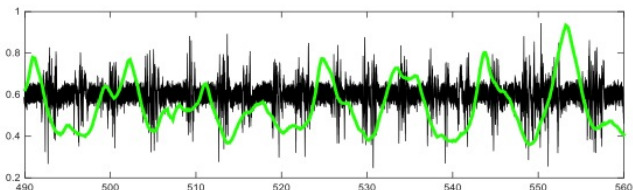


Figure 2.8: experimental data showing relationship between blood volume(green) and neuronal activity (black) from Berwick lab with vasomotion

2.4 Experimental Validation

- we have started a collaboration with Jason Berwick in Sheffield (UK). Dr Berwick's lab has the ability to measure (simultaneously) blood volume and neuronal activity. Figure 2.7 shows the time-dependent behaviour of blood volume (green) and neuronal activation (black) whilst Figure 2.8 shows the same variables but this time the vascular undergoes vasomotion. **Quote from Jason Berwick** "no stimulation in it - it was spontaneous neural and hemodynamic data over 2100s. Whats nice about the 101214 is that the spontaneous neural activity is in so called burst-suppression mode. it looks like a stimulation every 4 seconds or so but it is similar to a stage of sleep in the anaesthetised rat. After we have corrected blood pressure with phenylephrine each burst of neural is accompanied by an increase of blood volume (ie normal neurovascular coupling").

Figure 2.9 shows the numerical simulation of blood volume (which is represented by radius change) and neuronal activity. This should be compared with Figures 2.7 and 2.8. For this case the neuron model was Ostby. parBrain will be able to model these scenarios when the neuron model of Chang et al [18] is fully implemented. In addition we will need to ascertain the various conditions under which vasomotion can be simulated.

- we should look more closely at the work of Bai et al with respect to the TRPV4 channel and its relationship with Alzheimers [5], [6]

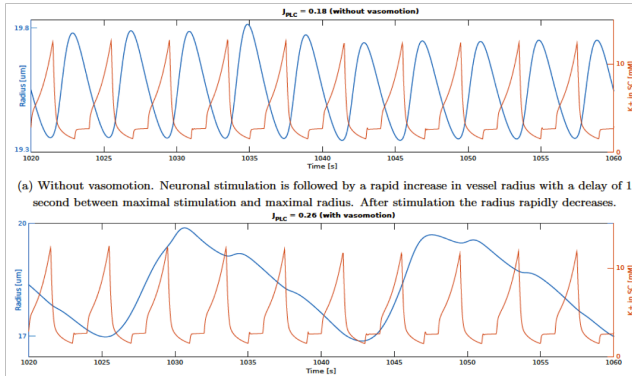


Figure 2.9: numerical simulaiton of no vasomotion and with vasomotion

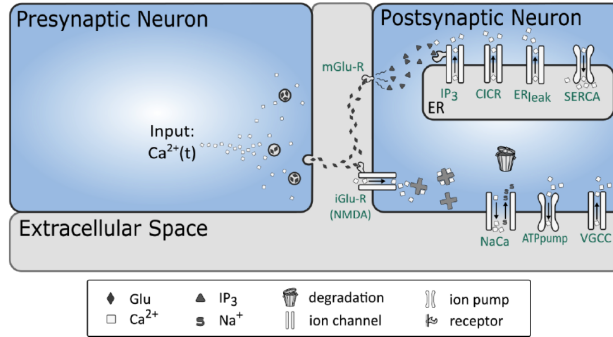


Figure 2.10: Neuronal Calcium model

- there is a small but important piece of validation with the work by Mauban et al [84]. The paper provides a relationship between calcium concentration in the SMC with variation in diameter of the perfusing arteriole (see Figure 4 in [84]).
- investigate work of Edith Hamel see <https://www.mcgill.ca/neuro/research/researchers/hamel>
- investigate the published work of the Hillman lab at Columbia see http://orion.bme.columbia.edu/~hillman/brain_imaging.html.
- work with KC Brennan : *in vivo* cortical spreading depression (Salt Lake, Utah). We have now obtained mouse neuronal Ca^{2+} data from KC and this is being used to compare with the numerical model development by Tim vanGinkel. The basic model sketch is shown in Figure 2.10 whilst the results of the model (blue trace) is shown in Figure 2.11.
- look at paper by Andrews et al [3] and [2] for experimental evidence on endothelial NO production.

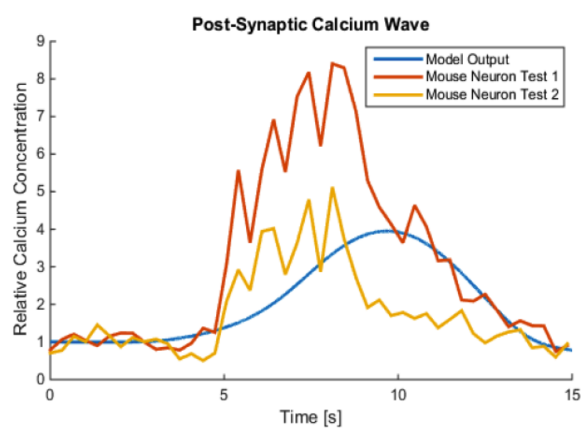


Figure 2.11: comparison of numerical model (blue) with two neuronal calcium profiles from KC Brennan mouse experiments

Chapter 3

Literature review notes

Amiri et al [1] using a Morris Lecar model of a neuron investigate neural synchronisation along with the functional contribution of astrocytes in neuronal synchrony using computer simulations and field potential recordings. The structure is based on the CA1 hippocampal area. Models show that astrocytes are able to change the threshold value of transition from synchrony to asynchronous behaviour. The model consists of both pyramidal and inhibitory interneurons. Astrocytes are connected to both pyramidal and interneurons. This particular paper may have some important information when looking at the role of ATP production from astrocytes and how this affects the LTP and LDP of neurons.

Lecrux and Hamel [76] review neurovascular coupling in brain function and disease. They suggest that the main pathway is via COX-1 and the association of GABA interneurons along with astrocytes form the relationship with Glutamatergic pyramidal neurons. They state that NO is NOT a primary mediator of the CBF response to neuronal stimulation but rather a permissive factor required for vasodilation by other pathways. In addition there seems to be clear evidence of the role of EETs in functional hyperaemia (this is via the arachidonic acid pathway) and that EETS my also act in a paracrine fashion by enhacning astricytic Ca^{2+} leading to the opening of Ca^{2+} sensitive K^+ channels. Finally they state that increases in perivascular K^+ can induce vasodilation which supports our current model. It is therefore clear that we should look at the COX-1 pathway as well as K^+ . Lecrux and Hamel also write about the possible relationship between neurovascular coupling and Alzheimers; indeed they mention that some authors consider AD to be a vascular disease [115].

look at GABA interneurons and the glutamatergic pyramidal neurons forming a COX-1 type pathway via AA and EETs. In contrast to the K^+ pathway that we currently support.

[54] shows further evidence of the relationship between interneurons via GABA and functional hyperaemia.

Zhang et al [114] have proposed via their experiments that endothelial sited TRPV4 channels mediate the dilation of cerebral arteries and that APP mice have impaired TRPV4 function. They induced TRPV4 opening via GSK (a TRPV4 channel opener) and showed that when the artery was denuded of the endothelium the dilation was eliminated. However this does not prove that astrocytic nor SMC TRPV4 do not mediate neurovascular coupling since these particular channels may only be functional under mechanical stress (stretching due to dilation) and Zhang et al did not test for this and astrocytic TRPV4 channels may have different activations as opposed to GSK. It is clear that we need to test these proposals in our model.

In contrast work by [87] shows that TRPV4 channels in the endfeet of astrocytes have a significant influence on constriction and dilation of the associated arterioles. They propose that the pathway involves the phospholipase A₂ arachidonic acid pathway and 20-HETE production causing SMC constriction.

The abstract states

Brain perfusion is tightly coupled to neuronal activity, is commonly used to monitor normal or pathological brain function, and is a direct reflection of the interactions that occur between neuronal signals and blood vessels. Cerebral blood vessels at the surface and within the brain are surrounded by nerve fibers that originate, respectively, from peripheral nerve ganglia and intrinsic brain neurons. Although of different origin and targeting distinct vascular beds, these "perivascular nerves" fulfill similar roles related to cerebrovascular functions, a major one being to regulate their tone and, therein, brain perfusion. This utmost function, which underlies the signals used in functional neuroimaging techniques and which can be jeopardized in pathologies such as Alzheimer's disease, stroke, and migraine headache, is thus regulated at several levels. Recently, new insights into our understanding of how neural input regulate cerebrovascular tone resulted in the rediscovery of the functional "neurovascular unit." These remarkable advances suggest that neuron-driven changes in vascular tone result from interactions that involve all components of the neurovascular unit, transducing neuronal signals into vasoconstrictor responses not only through direct interaction between neurons and vessels but also indirectly via the perivascular astrocytes. Neurovascular coupling is thus determined by chemical signals released from activated perivascular nerves and astrocytes that alter vascular tone to locally adjust perfusion to the spatial and temporal changes in brain activity.

in addition they state

Recently, in cortical and hippocampal brain slices, it was evidenced that application of norepinephrine triggers increases in intracellular Ca²⁺

concentrations ($[Ca^{2+}]_i$) in astrocytes and perivascular astrocytic end-feet and that this response elicited constriction of the microarterioles on which the end-feet abutted [87]. Furthermore, the authors were able to show that the contraction was mediated by 20-HETE, a cytochrome P450A derivative of arachidonic acid. However, other studies in cortical brain slices showed that a rise in astrocytic $[Ca^{2+}]_i$ after increased neuronal activity by electrical stimulation [41] or synaptically released glutamate [116] induced dilatations of cortical arterioles. In the latter study, the vasoactive signaling molecule corresponded to a cyclooxygenase product of arachidonic acid, likely PGE2, but could not be unequivocally demonstrated. Furthermore, it was suggested by Filosa and colleagues [41] that suppression of $[Ca^{2+}]_i$ oscillations and accompanying vasomotion in microarterioles, possibly due to smooth muscle hyperpolarization, was involved in coupling local perfusion to increased neuronal activity. Despite apparent discrepancies between findings of microvascular contraction and dilatation mediated by changes in astrocytic Ca^{2+} , likely because of different experimental paradigms and the use or not of preconstricted vessels in the slices, these studies emphasize the importance of further assessing this newly identified intermediary role of astrocytes in transducing neuronal signals into vaso-motor responses [56] [104] and whether or not the endothelium is required for their vasomotor effects [88]. Furthermore, as can be appreciated, several recent studies have used brain slices to investigate the role of astrocytes or neurons (see LOCAL INTERNEURONS) in the regulation of microvascular tone. Although limited by the fact that brain slices are maintained in artificial conditions in which vessels are not pressurized and do not have intraluminal flow, it is unarguable that such preparations, in which neuronal glial vascular interactions are preserved and can be assessed in a controlled manner, offer an additional means to isolated microvessels and whole animal experiments for investigating the microcirculation.

[105] proposes that hypoxia facilitates Alzheimer's pathology by upregulating BACE1 gene expression. Figure 3.1 shows the basic hypothesis which was the kernel of an (unsuccessful) HRC grant in 2013. **This particular area of work could be a high priority for our group.**

Rejuvinate the BACE1/hypoxic hypothesis for another HRC grant application

[7] provides a model of brain circulation and importantly energy metabolism. Their model was used to investigate and compare with NIRS signals (oxy-hemoglobin concentrations). The model for functional hyperaemia is relatively simple compared to our model. However the energy consumption model is worth looking at. Equations for the Banaji model can be found at [8]

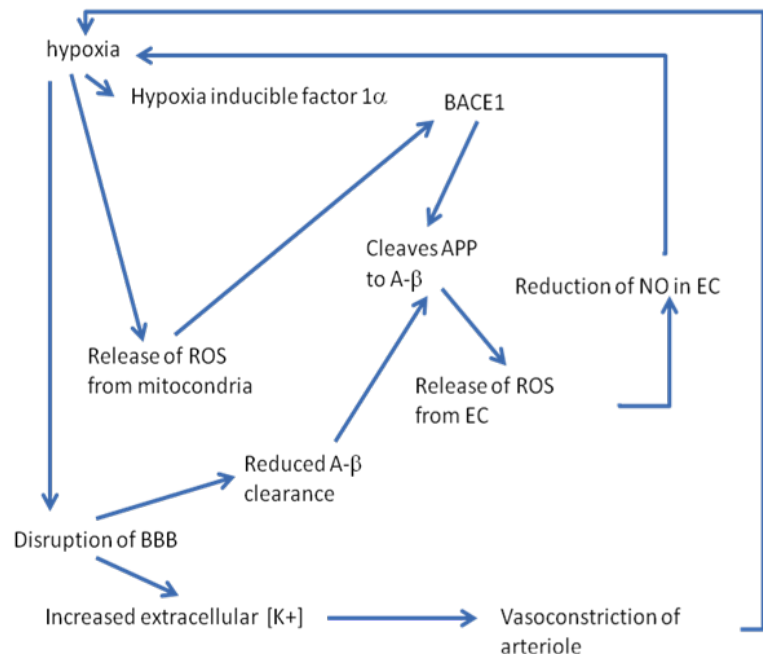


Figure 3.1: Sketch of hypothesis for hypoxic mediated production of ROS etc.

investigate energy model of mitochondrial oxygen consumption of [7]
perhaps we should compare with the model of [21]

[80] shows through experimentation that hypoxia induces an intracellular Ca^{2+} rise and that ROS is the key indicator of hypoxic vasoconstriction. The Ca^{2+} rise is mediated by a reduction in the FK506 binding protein (an inhibitor of RyR). The experiments are done on pulmonary arteries and it is yet to be shown as to whether this particular phenomenon occurs in cerebral arteries. Again this could be linked to the work on the BACE1 expression.

[94] provides experimental evidence of neurovascular coupling during cortical spreading depression. The group defines a capillary transit time heterogeneity (CTH) which looks at the variation in transit times for RBCs passing through the capillary bed. They state that CTH reduces oxygen extraction efficacy. It is expected (according to their hypothesis) that reduction in CTH would increase oxygen efficient extraction during functional hyperaemia. They state that the recent study by [53] indicates control of CBF and CTH is done via pericytes. However a more recent publication by [58] indicates that pericytes have no contractile ability and do not participate in functional hyperaemia. Although this paper by Ostergaard provides experimental evidence it does not in any way support the physiological phenomena that clearly occurs during metabolic activation and subsequent increase in CBF.

The clinical group of Ostergaard from Aarhus seem to attribute all phenomena (including BOLD signals which they refer to another group) to CTH. In reality this is a somewhat "blinkered" view to say the least.

[73] provides an excellent review of calcium dyshomeostasis (a perturbation away from the cellular ionic equilibrium) and intracellular signalling in Alzheimer's disease.

Chapter 4

New projects

4.1 Tonic Control of CBF

The control of cerebral blood flow to the tissue has been up to now concentrated on the "phasic" component of neurovascular coupling. That is the almost instantaneous contraction/dilation of the perfusing arterioles and the consequential increase of nutrients to the neurons and surrounding cells. However experiments have now shown [10] that inhibiting NAAG peptidase (an enzyme that hydrolyses NAAG) produced a prolonged reduction in global cerebral blood flow but with little or now effect on physical activity. NAAG (N-acetylaspartyglutamate) is produced by neurons and is slowly released into the ECS. It has been found that NAAG is selective for the mGluR3 receptor. This docking of NAAG onto mGluR3 releases glutamate into the cytosol of the astrocyte and subsequently produces COX-1 [98]. This in turn produces prostaglandins which provide a dilatory effect on the surrounding SMC of the perfusing arteriole **Can't find this reference Adv. Exptl. Med. and Biol. 576: 95-112.**

Figure 4.1 shows a sketch of the mechanisms for the mGluR3 . Neuron plasma membrane depolarisation with or without synaptic signalling can trigger NAAG release. In addition the catabolic reduciton of NAAG can influence blood flow be releasing Glu and inducing vascular relaxation. Baslow and Guilfoyle [9] indicates that NAAG is released in to the ECS at a rate of about 6 % per hour (not sure what the percentage is anyway ! but is crucially linked to the individual rate of glucose oxidation. This could possibly be modelled by the non ATP part of the Na/K ATPase pump in the neuron) targeted by the mGluR3 and hence produce GLu into the cytosol with secondary messangers COX-1 and prostaglandins. This affects both astrocyte and SMC dynamics [117]. [116] showed that activation of isolated astrocyte-arteriole preparations resulted in a **slow increase** in arteriolar radius.

So why is this so important?

Cerebral tissue , especially neurons have a requirement for a basal level of nutrient flow. Any increase in neuronal activity requires additional nutrients and this is essentially neurovascular coupling that we all know and love. However, the basal level is clearly important as a long-term energy supply such as maintaining basic metabolic reactions, transport of amino acids and the maintenance of osmotic pressure in the cell. This has been seen in blocking specific pathways to decrease blood flow and then inducing neuron firing to provide the need of nutrients such as glucose (Glc) [98]. The release of COX-1 and the production of prostaglandins can induce a hyperaemic response [91] and the authors conclude that secondary messengers of COX-1 were "critical in maintaining resting cerebro-vascular tone.

We must be careful here because as [78] shows that the hyperemic response to BF stimulation was largely mediated by glutamate released from activated pyramidal cells and by vasoactive EETs (which as we know mediate the astrocytic end-foot BK channel), likely originating from activated astrocytes and not via the cyclo-oxygenase COX-2 pathway. But COX-2 pathway was involved in neurovascular coupling for pyramidal neurons [77]. This is in contrast to the following work of [78]. These are confusing publications , however [4] indicates a possible clear set of pathways. In this case neurons provide nitric oxide and prostaglandins (PG) which dilate SMC whilst astrocytic Ca^{2+} from mGLuR5 receptors provides secondary messengers arachidonic acid (AA) to provide PG, EETs and increased K^+ to dilate SMC . The diffusion of AA across to the SMC can induce the production of 20-HETE a vasoconstrictor. We know how EET mediate BK channels and increase PVS K^+ but we do not know yet how PG can induce dilation of SMCs. Attwell [4] makes it clear that COX-1 is the main mediator of vasodilation from the astrocyte with COX-2 in a pathological case.

Our main take home message from this is to concentrate (sorry about the pun!) on COX-1 pathway via AA which produces EET, PG and increase opening of the BK channel and the use of NAAG [9] to provide a basal level of arteriolar tone.

So what's the difference between COX-1 and COX-2 pathways ?

4.2 ATP/Astrocyte messaging from dendrite to dendrite: An intercellular model of heterosynaptic metaplasticity

This is the start of notes for a new project involving the Owen Jones/Cliff Abraham's lab.

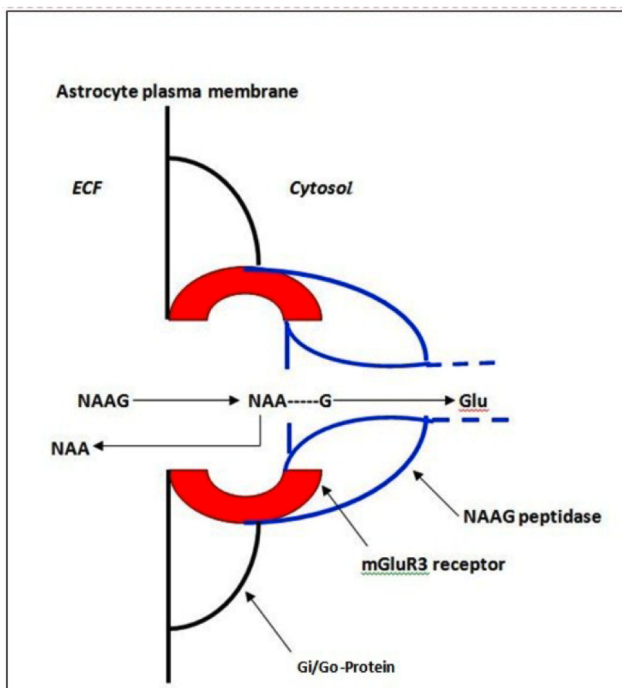


Figure 4.1: Sketch of NAAG mGluR3 mechanism. Taken from [?]

There is substantial evidence of non-transporter mediated neuron-astrocyte communication. Early reports showed glutamate or GABA-mediated currents in cultured astrocytes (Bowman and Kimelberg, 1984; Hsli, Andrs, and Hsli, 1979; Kettenmann, Backus, and Schachner, 1984). Functional neurotransmitter receptors have since been found on astrocytes; among them are AMPARs (Seifert and Steinhuser, 1995), NMDARs (A. Serrano, Robitaille, and Lacaille, 2008), mGluRs (Nicoletti, et al., 1990), mAChRs (Ulas, 1988), ARs (Porter and McCarthy, 1995) and P2Rs (Neary and Zhu, 1994). However, receptor expression varies with astrocyte subtype (Matthias, et al., 2003; A. Serrano, et al., 2008) and development (Cai, Schools, and Kimelberg, 2000; Seifert, Zhou, and Steinhauser, 1997; Sun, et al., 2013).

Astrocytes respond to iGluR and mGluR activation with, respectively, rapid influx and intracellular release of Ca²⁺ (Cornell-Bell, Finkbeiner, Cooper, and Smith, 1990; Glaum, Holzwarth, and Miller, 1990). Cytosolic Ca²⁺ signals spread within and between astrocytes as Ca²⁺ waves, allowing long-range communication within cell networks. These waves require the formation of IP₃ (Leybaert, Paemeleire, Strahonja, and Sanderson, 1998), and are also triggered by acetylcholine (Araque, Martn, Perea, Arellano, and Buo, 2002), adenosine and ATP (Porter and McCarthy, 1996), GABA (Fraser, et al., 1995) and mechanical stimulation (Charles, Merrill, Dirksen, and Sanderson, 1991). They may also appear spontaneously (Nett, Oloff, and McCarthy, 2002; Parri and Crunelli, 2001). Evoked astrocytic Ca²⁺ signals are highly plastic. They are augmented or depressed by varying patterns of synaptic stimulation (Perea and Araque, 2005), and display lasting increases in frequency with repeated generation (Pasti, Pozzan, and Carmignoto, 1995; Pasti, Volterra, Pozzan, and Carmignoto, 1997). Further, astrocytic A2BRs trigger widespread and sustained generation of asynchronous Ca²⁺ events lasting ≤ 20 min (Kawamura and Kawamura, 2011).

The nature of astrocyte-astrocyte Ca²⁺ signaling has been heavily debated. These signals were first thought to spread via GJNs (Enkvist and McCarthy, 1992). Astrocytes are extensively coupled via GJNs comprised of opposed connexin43 (Cx43) hemichannels (Giaume, et al., 1991; Yamamoto, Ochalski, Hertzberg, and Nagy, 1990), which allow passage of small molecules such as Ca²⁺ and IP₃ (Saez, Connor, Spray, and Bennett, 1989). Inter-astrocytic signaling via GJNs is enhanced in an activity-dependent manner (Enkvist and McCarthy, 1994; Rouach, Glowinski, and Giaume, 2000), and is bidirectionally regulated via channel phosphorylation by serine-threonine kinases (Kwak, et al., 1995; Sez, Martnez, Braes, and Gonzlez, 1998; Shah, Martinez, and Fletcher, 2002). However, cultured astrocytes display intercellular Ca²⁺ waves even when not coupled by GJNs (Hassinger, Guthrie, Atkinson, Bennett, and Kater, 1996). The extent of Ca²⁺ wave propagation is also independent of GJN coupling (Blomstrand, berg, Eriksson, Hansson, and Rnnbck, 1999). Further,

these waves are visible in Cx43-KO mutant mice (Suadicani, Brosnan, and Scemes, 2006).

An extracellular mode of communication between astrocytes has been identified. Ca^{2+} signaling between astrocytes is inhibited by blockers of purinergic receptors or by ectonucleotidases (Cotrina, Lin, and Nedergaard, 1998; Guthrie, et al., 1999). Previous reports of gap-junctional contribution to this process may be due to the inhibitory actions of GJN antagonists on P2X7Rs or connexin hemichannels, a trigger (Suadicani, et al., 2006) or source (Cotrina, Lin, Alves-Rodrigues, et al., 1998) of astrocytic ATP release, respectively. Importantly, ATP triggers further ATP release from neighbouring astrocytes (C. M. Anderson, Bergher, and Swanson, 2004). ATP can therefore trigger regenerative Ca^{2+} signals within the astrocytic network. As a caveat, GJNs may still be sufficient, if not essential, for mediating Ca^{2+} waves, as purine and GJN mediated Ca^{2+} waves can operate in tandem in culture (Paemeleire, et al., 2000).

Taken together, the results of the experiments in this thesis can be combined into a plausible explanation of how neurons and astrocytes generate temporally and spatially widespread metaplasticity in CA1 (Fig 4.2). The results implicate M1-AChRs as a likely trigger of the signalling cascade culminating in metaplasticity, whether via Gq-coupled Ca^{2+} release or by facilitated firing. It is also likely that M1-AChRs are responsible through either of these mechanisms for recruitment of astrocytes in SO. A parsimonious explanation of purinergic involvement is that astrocytes respond to activation by releasing ATP, which triggers widespread signalling within the astrocytic network. This signalling could be accomplished via GJNs, but given the limited evidence for purely GJN-mediated communication between astrocytes, it is more likely that connexins, in the form of hemichannels, in fact serve as the source of released ATP. From here, ATP is hydrolysed extracellularly to adenosine which acts on A2BRs. Given the canonical actions of A2BR-mediated neuronal signalling, it is probable that the relevant receptors are on astrocytes. Further, given that BAY 60-6583 could prime SR synapses even when ejected into SO, it is plausible that A2BRs are the trigger of widespread intercellular communication, perhaps via the same mechanism described by Kawamura and Kawamura. The consequences of activating astrocytic A2BRs (namely, cytokine release) also provide a candidate mechanism for ultimately inhibiting LTP. Several components of this model are yet to be validated; however they provide testable hypotheses for further experimentation. Thus, a complete mechanistic explanation of heterosynaptic metaplasticity in CA1 is obtainable from the model.

In Figure 4.2 we have the following definitions.

- SO = stratum Oriens (contains the basal dendrites)
- SP = stratum Pyramidale (contains the cell bodies of pyramidal cells)
- SR = stratum Radiatum (contains the apical dendrites)

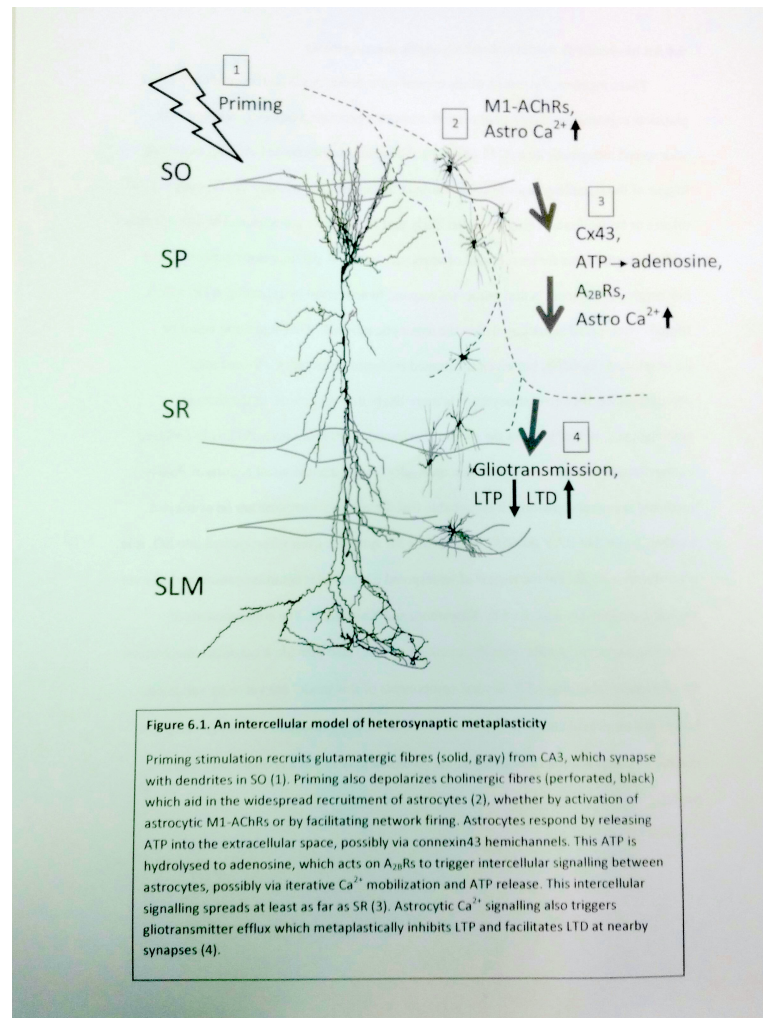


Figure 4.2: Sketch of heterosynaptic metaplasticity

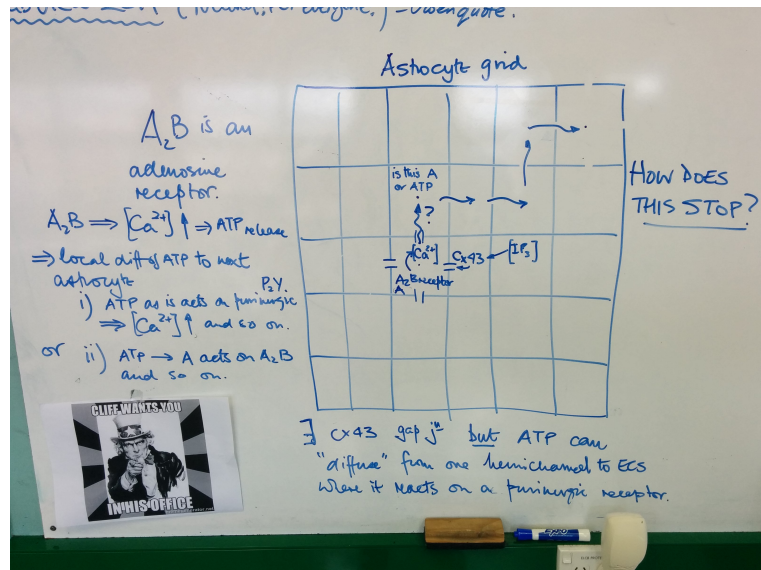


Figure 4.3: Sketch of possible communication of

– SLM = stratum Lacunosum Moleculare (contains the tuft dendrites)

At some point in the cortical tissue an A_2B receptor is activated by ATP. This mediates an increase in cytosolic Ca^{2+} , this in turn increases ATP production from the cell and ATP then diffuses to the neighbouring tissue. The pathway now has two possibilities.

1. ATP acts on a purinergic receptor P2Y and releases Ca^{2+} which continues the path
2. ATP acts on an A_2B receptor and the path is continued

We intend to utilise version 2.* with parBRAIN to simulate this effect. A sketch is given in Figure 4.3. Our reason for using version 2.* is because we will need to diffuse ATP through the ECS (which all versions 1.* do not have). The version 2.*/parBRAIN code will need to have the ability to connect any variable within a subdomain with any other subdomain. At present parBRAIN can diffuse through the PVS (which is not physiologically realistic).

Figure 4.4 is taken from [67] and shows a schematic of the purinergic autocrine/paracrine regulation of Ca^{2+} dynamics. However the authors seem to concentrate on the perceived increase in (what look like from the data) random oscillations and frequencies. There is a large increase in (what they call) transient Ca^{2+} following ATP injection onto the brain slice. The so called oscillations do seem to be random and may possibly be just Ca^{2+} "puffs" released from the ER stores. But the main point to be taken

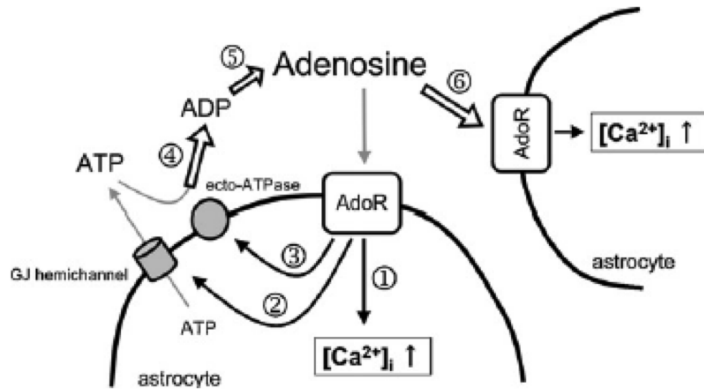


Figure 4.4: schematic of the purinergic autocrine/paracrine regulation of Ca^{2+} dynamics

from this is that on injection of ATP the Ca^{2+} increases and subsequently releases more ATP from the cell via CBX (carbenoxolone)-sensitive gap junction hemichannels. Mediated by the increase in ecto-ATPase via PKC activation the ATP is dephosphorylated to adenosine which then diffuses to an adenosine receptor (AdoR) on a different astrocyte which repeats the process and so on. carbenoxolone is an effective blocker of gap junctions.

One of the issues here is that we do not have as much data as we would like to provide the parameter values for the pathway suggested in Figure 4.4. We will need to dig deep into the paper of [67] and ask questions of Owen and Cliff.

We do have a possible problem here since the neuron compartment model of ELshin uses the entire neuron in the compartment ; meaning that there are parameters for the the resistance and half-length of the dendritic tree. So if we wish to use the compartments as sub-domains that cover a single pyramidal neuron then we will need to look carefully at the neuron model in each sub-domain. Rather than one neuron in a single sub-domain as is the case at present we will need to "split" the neuron" across the entire domain.

4.2.1 Algorithm development

In order to simulate the diffusion of adenosine in the cerebral tissue the neuron dendrites and soma need to be mapped across the subdomains of the computational tissue slice. So each subdomain holds a section of the dendrite or axon. Then a discrete version of the neuron model equations is needed. As we shall see we can utilise this discrete methodology to our advantage. We need to solve for the membrane potential E_m governed by the partial equation which is similar to 1.4.1 and 1.4.2 but has the full

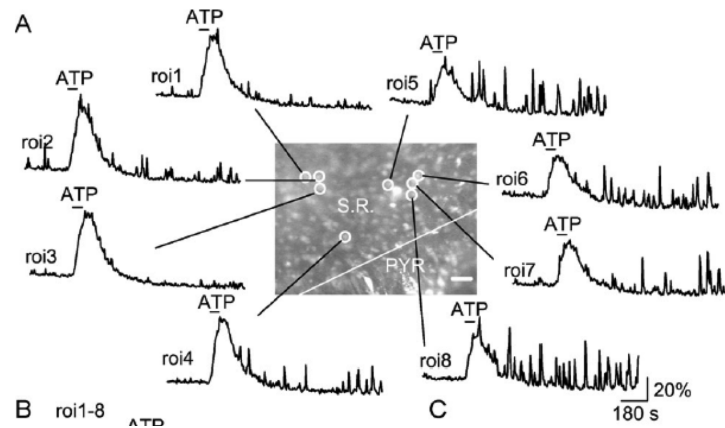


Figure 4.5: time dependent profiles for 8 rois of Ca^{2+} dynamics taken from [67]

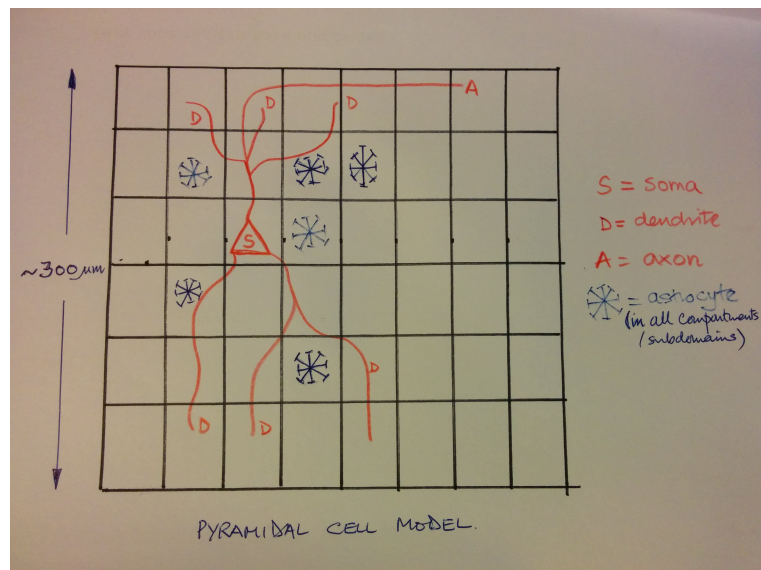


Figure 4.6: schematic of a pyramidal cell mapped onto a tissue slice with associated astrocytes

diffusion format rather than a linear gradient approximation

$$C_m \frac{\partial E_m}{\partial t} = -I_{s,tot} + \frac{1}{2R_a} \frac{\partial E_m}{\partial x^2} \quad (4.2.1)$$

and the ion concentration along the dendrite and axon/soma projections

$$\frac{\partial [ion]_{cyto,i}}{\partial t} = -\frac{A_s}{FV_s} I_{s,i,tot} + \frac{D_{ion}(V_d + V_s)}{2V_s} \frac{\partial [ion]_{cyto,i}}{\partial x^2} \quad (4.2.2)$$

for each ion species i. We discretise the equations in a number of ways depending on the form of the ionic currents. For linear Hodgkin Huxley forms then we use a similar manner to that found in the book by Gabiani and Cox (Mathematics for Neuroscientists, Academic Press, 2010). When this works we will then use the more robust but more complex algorithm of Wagner and Kozloski [71]. Finally we will utilise the Goldman/Hodgkin/Katz ionic current equations (which are inherently non-linear). As noted in section 1.4.2 we also need to solve for the ion concentrations and the associated activation variables m and h. Their equations are given below as

$$\frac{dm}{dt} = \alpha_m(V)(1 - m) - \beta_m(V)m \quad (4.2.3)$$

$$\frac{dh}{dt} = \alpha_h(V)(1 - h) - \beta_h(V)h \quad (4.2.4)$$

These equations state that the closed activation gates, (1-m), open at rate $\alpha_m(V)$, while the open activation gates, m, close at a rate $\beta_m(V)$. It is similar for the inactivation gates. The rate functions, $\alpha_m(V)$ and $\beta_m(V)$, are functions that depend on the voltage across the membrane. The forms of the functions α and β are usually determined through a mix of theoretical and empirical considerations and they are of the form

$$\alpha(V) = a_0 \exp\left(\frac{-\delta V}{s}\right) \quad (4.2.5)$$

$$\beta(V) = b_0 \exp\left(\frac{(1 - \delta)V}{s}\right) \quad (4.2.6)$$

where a_0 , b_0 , and δ are positive constants, with $0 \leq \delta \leq 1$. A gate that tends to open on depolarisation will have $s < 0$, while a gate that tends to open on hyperpolarisation will have $s > 0$. These exponential forms are modified to fit the experimental data. The equation of the rate of change of activation gates may be rewritten as

$$\frac{dm}{dt} = \frac{m_\infty(V) - m}{\tau_m(V)} \quad (4.2.7)$$

where

$$m_\infty(V) = \frac{\alpha_m(V)}{\alpha_m(V) + \beta_m(V)} \quad (4.2.8)$$

and

$$\tau_m(V) = \frac{1}{\alpha_m + \beta_m(V)} \quad (4.2.9)$$

We should also define the appropriate boundary conditions at the ends of the axon/dendrite such that

$$\frac{\partial E_m}{\partial x} = (0, t) = \frac{\partial E_m}{\partial x}(L, t) \quad (4.2.10)$$

and that things begin at rest so that

$$E_m(x, 0) = E_{m,r}, \quad m(x, 0) = m_{inf}(E_{m,r}), \quad h(x, 0) = H_{inf}(E_{m,r}), \quad n(x, 0) = n_{inf}(E_{m,r}). \quad (4.2.11)$$

Suppose that the entire length of the neuron is of length, L. Then we choose $N_x = \frac{L}{dx}$ compartments and a specific timestep dt. Variables are evaluated on the associated space-time grid such that

$$E_{m,i}^j \approx E_m((i - 1/2)dx, (j - 1)dt) \quad (4.2.12)$$

$$m_i^j \approx m((i - 1/2)dx, (j - 1)dt) \quad (4.2.13)$$

$$ion_i^j \approx ion((i - 1/2)dx, (j - 1)dt) \quad (4.2.14)$$

$$i = 1, \dots, N_x, \quad j = 1, \dots, N_t \quad (4.2.15)$$

We now need to discretise the gate variables m and h. This is achieved with a trapezoidal approximation so that equations ?? and ?? can be written as

$$m_i^j - m_i^{j-1} = \alpha_m(E_m^{j-1})dt - (\alpha_m(E_m^{j-1}) + \beta_m(E_m^{j-1}))(m_i^j + m_i^{j-1})dt/2 \quad (4.2.16)$$

and simplified as

$$m_i^j = \frac{(1/dt - (\alpha_m(E_m^{j-1}) + \beta_m(E_m^{j-1}))/2)m_i^{j-1} + \alpha_m(E_m^{j-1})}{1/dt + (\alpha_m(E_m^{j-1}) + \beta_m(E_m^{j-1}))/2} \quad (4.2.17)$$

this is repeated for the gating variable h.

There is a simpler notation where we use the format of

$$\frac{dm_i}{dt} = \frac{m_{i,inf}(E_m(t)) - m_i(t)}{\tau_m(E_m(t))} \quad (4.2.18)$$

so that the discretised equation for m becomes

$$m_i^j = \frac{(2\tau_m(E_m^{j-1}) - dt)m_i^{j-1} + 2m_{i,inf}(E_m^{j-1})dt}{2\tau_m(E_m^{j-1} + dt)} \quad (4.2.19)$$

with a similar equation for h. We now discretise the equations for membrane potential E_m 4.2.1 and the various ion concentrations 4.2.2. We collect the compartmental terms into vectors such that

$$\mathbf{E}_m = (E_{m,1}^j, E_{m,2}^j, \dots, E_{m,N_x}^j)^T \quad (4.2.20)$$

$$\mathbf{ion}_k^j = (ion_{k,1}^j, ion_{k,2}^j, \dots, ion_{k,N_x}^j)^T \quad (4.2.21)$$

Following the form given in by Gabbiani and Cox (Mathematics for Neuroscientists, Academic Press, 2010, pages 120, 121) then

$$C_m \frac{\mathbf{E}_m^{j-1/2} - \mathbf{E}_m^{j-1}}{dt/2} = G_a \mathbf{S} \quad \mathbf{E}_m^{j-1/2} - I_{total}(\mathbf{E}_m^{j-1/2}) + I_{stim} \quad (4.2.22)$$

$$\frac{\mathbf{ion}_k^{j-1/2} - \mathbf{ion}_k^{j-1}}{dt/2} = D \mathbf{S} \quad \mathbf{ion}_k^{j-1/2} - \frac{2}{Fa} I_{total}(\mathbf{E}_m^{j-1/2}) \quad (4.2.23)$$

where a is the area of the dendrite/axon and \mathbf{S} is the standard difference matrix for diffusion. We can write this as a linear system for $\mathbf{E}_m^{j-1/2}$ and $\mathbf{ion}_k^{j-1/2}$.

$$(diag((\mathbf{d}_{E_m}^j + 2C_m/dt) + G_a \mathbf{S}) \mathbf{E}_m^{j-1/2} = (2C_m/dt) \mathbf{E}_m^{j-1} + \mathbf{f}_{E_m}^j \quad (4.2.24)$$

$$(diag((\mathbf{d}_{ion}^j + 2/dt) + D \mathbf{S}) \mathbf{ion}^{j-1/2} = (2/dt) \mathbf{ion}^{j-1} + \mathbf{f}_{ion}^j \quad (4.2.25)$$

where the elements of $\mathbf{d}_{E_m}^j$ and \mathbf{d}_{ion}^j are functions of $E_m^{j-1/2}$ and those of $\mathbf{f}_{E_m}^j$ and \mathbf{f}_{ion}^j are constant functions.

Finally we update both \mathbf{E}_m and \mathbf{ion} using

$$\mathbf{E}_m^j = 2\mathbf{E}_m^{j-1/2} - \mathbf{E}_m^{j-1} \quad (4.2.26)$$

$$\mathbf{ion}^j = 2\mathbf{ion}^{j-1/2} - \mathbf{ion}^{j-1} \quad (4.2.27)$$

We should note that equation 4.2.24 is non-linear since the active ion currents are non-linear and are functions of the unknown $E_m^{j-1/2}$. Due to the active form of the Goldman/Hodgkin/Katz ion current given by

$$I_{GHK} = m^p h^q \frac{g_{ion} F E_m [[ion]_{cyto} - e^{(-\frac{E_m}{\phi})} [ion]_{ext}]}{\phi [1 - e^{(-\frac{E_m}{\phi})}]} \quad (4.2.28)$$

Hence they would therefore require an iterative scheme. However the equation is of parabolic form and can be solved using an iterative scheme. The passive leak currents are in the linear form of Hodgkin-Huxley given by $I_{k,HH} = g_{HH}(E_m - E_k)$ for the ion species k. We show the method of solution from discretising the equations 4.2.24 in the following format

$$E_{m,i}^{j-1/2} \left[1 + \frac{2\delta t G_a}{C_m(\delta x)^2} \right] - \frac{G_a \delta t}{C_m(\delta x)^2} [E_{m,i+1}^{j-1/2} + E_{m,i-1}^{j-1/2}] - \frac{\delta t}{C_m} I_l(E_{m,i}^{j-1/2}) = \frac{\delta t}{C_m} [I_n(E_{m,i}^j)] + E_{m,i}^j \quad i = 1, \dots, N_x \quad (4.2.29)$$

and for each ion species k,

$$ion_{k,i}^{j-1/2} \left[1 + \frac{2\delta t D}{(\delta x)^2} \right] - \frac{D \delta t}{(\delta x)^2} [ion_{k,i+1}^{j-1/2} + ion_{k,i-1}^{j-1/2}] - \delta t I_l(ion_{k,i}^{j-1/2}) = \delta t [I_n(ion_{k,i}^j)] + ion_{k,i}^j \quad i = 1, \dots, N_x \quad (4.2.30)$$

Here I_l and I_n are the linear and non-linear parts of the ion current respectively. To solve this matrix system we iterate at each time step due to the non-linear currents. For this case we choose a starting membrane potential E_{m_0} and set of ionic species \mathbf{ion}_0 . These are then used in the non-linear current $I_n(E_{m_0}, \mathbf{ion}_0^j)$. We then solve for $E_{m,i}^{j-1/2}$ and $ion_{k,i}^{j-1/2}$. We use this value in the non-linear part of the discretised equations and again solve for $ion_{k,i}^{j-1/2}$ etc until there is no change in either $ion_{k,i}^{j-1/2}$ or $E_{m,i}^{j-1/2}$. To complete the full Crank-Nicolson step we then update as follows

$$\mathbf{E}_m^j = 2\mathbf{E}_m^{j-1/2} - \mathbf{E}_m^{j-1} \quad (4.2.31)$$

$$\mathbf{ion}_k^j = 2\mathbf{ion}_k^{j-1/2} - \mathbf{ion}_k^{j-1} \quad (4.2.32)$$

Finally we need to specify an equation for the ionic concentration in the extracellular space.

$$\frac{\partial \mathbf{ion}_{k,e}}{\partial t} = D_e \frac{\partial^2 \mathbf{ion}_{k,e}}{\partial x^2} + \frac{2}{F f_e} I_{total}(\mathbf{E}_m) \quad (4.2.33)$$

f_e is the volume fraction of the extracellular space (approximately 15%). The discretised equation becomes

$$\frac{\mathbf{ion}_{k,e}^{j-1/2} - \mathbf{ion}_{k,e}^{j-1}}{dt/2} = D_e \mathbf{S} \cdot \mathbf{ion}_{k,e}^{j-1/2} + \frac{2}{F} I_{total}(\mathbf{E}_m^{j-1/2}) \quad (4.2.34)$$

The time step is then incremented and the inner iteration is started anew. The neuron model developed above now needs to be embedded into a slice of tissue in a similar manner to that used in parBRAIN see Chapter 2. How do we do this?

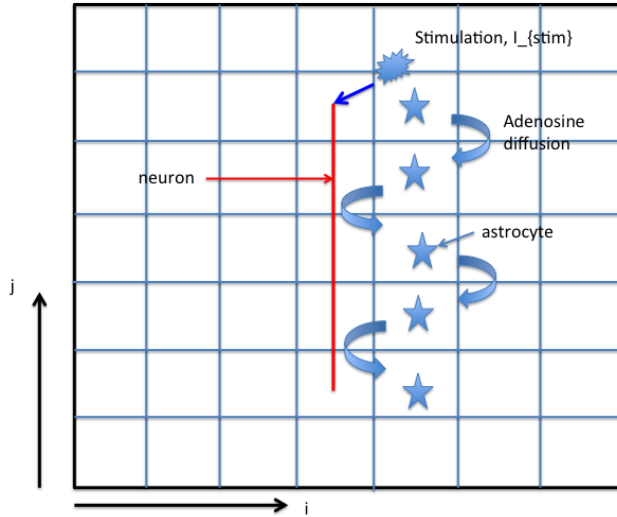


Figure 4.7: sketch of the simple neuron embedded into the tissue slice , showing the anticipated diffusion of adenosine from astrocyte to astrocyte

neuron in tissue slice

As a first attempt we simplify the geometry of the neuron such that it has a linear form, i.e. that it is a simple active uniform cable. This is shown in Figure ???. We will extend this to the full dendritic tree at a later stage.

The normal size of the tissue slice when implementing an NVU coupled problem is of the order of millimeters. However a pyramidal neuron for instance is of the order of length $300\text{-}500 \mu\text{m}$. In addition the discretised uniform cable would normally have approximately hundreds of compartments. This means that the neuron would only cross a few tissue slice subdomains. In fact on the basis of modelling dimensions from [?] a tissue slice that has 64 subdomains per side and the length of the tissue slice is 25.6 mm, then each subdomain is only $400 \mu\text{m}$ wide. Enough for a single neuron. Astrocytes, although have small cell bodies have a long extensions (pseudo-pods) so it is difficult to estimate their exact size. However I suspect that they can reach from one end of a neuron to another.

For the moment we treat the astrocytes as being small enough to have one in each subdomain and each subdomain has a characteristic length of the order of δx (the discretised length for the neuron model). We go back to the Figure ?? and investigate the best way to utilise the parBRAIN parallel code to solve the neuron model along with diffusion of adenosine/ATP from astrocyte to astrocyte.

Chapter 5

Priorities

5.1 Priority List

Make sure any changes to single NVU are implemented into current version of parBrain

1. success in parBrain version 2.0 . This should be made master code in GitHub.
2. diffusion into the PVS is not needed as the space is small and is effectively hidden in the arterial submatrix.
3. inclusion of TRPV4 channel in astrocyte/SMC (version 2.0 parBrain) see paper by Zhang et al [114], [87] and in the section 3.
4. inclusion of TRPV4 channels in EC compartment (again as above see [114]).
5. inclusion of Ca^{2+} in neuron of parBrain version 2.0
6. investigation of induction of vasomotion and comparison with Berwick data
7. investigation of COX-1 pathway (possibility for Tim vG ?)

Bibliography

- [1] Mahmood Amiri, Narges HosseiniMardi, Fariba Bahrami, and Mahyar Janahmadi. Astrocyte- neuron interaction as a mechanism responsible for generation of neural synchrony: A study based on modeling and experiments. *Journal of Computational Neuroscience*, 34(3):489–504, 2013. ISSN 09295313. doi: 10.1007/s10827-012-0432-6.
- [2] Allison M Andrews, Dov Jaron, Donald G Buerk, Patrick L Kirby, and Kenneth a Barbee. Direct, real-time measurement of shear stress-induced nitric oxide produced from endothelial cells in vitro. *Nitric oxide : biology and chemistry / official journal of the Nitric Oxide Society*, 23(4):335–42, dec 2010. ISSN 1089-8611. doi: 10.1016/j.niox.2010.08.003. URL <http://www.pubmedcentral.nih.gov/articlerender.fcgi?artid=2965060&tool=pmcentrez&rendertype=abstract>.
- [3] Allison M. Andrews, Dov Jaron, Donald G. Buerk, and Kenneth a. Barbee. Shear Stress-Induced NO Production is Dependent on ATP Autocrine Signaling and Capacitative Calcium Entry. *Cellular and Molecular Bioengineering*, aug 2014. ISSN 1865-5025. doi: 10.1007/s12195-014-0351-x. URL <http://link.springer.com/10.1007/s12195-014-0351-x>.
- [4] D Attwell, Am Buchan, S Charpak, M Lauritzen, Ba MacVicar, and Ea Newman. Glial and neuronal control of brain blood flow. *Nature*, 468:232–241, 2010. ISSN 0028-0836. doi: 10.1038/nature09613. URL <http://discovery.ucl.ac.uk/402070/>.
- [5] Ji Zhong Bai and Janusz Lipski. Differential expression of TRPM2 and TRPV4 channels and their potential role in oxidative stress-induced cell death in organotypic hippocampal culture. *NeuroToxicology*, 31(2):204–214, 2010. ISSN 0161813X. doi: 10.1016/j.neuro.2010.01.001. URL <http://dx.doi.org/10.1016/j.neuro.2010.01.001>.
- [6] Ji Zhong Bai and Janusz Lipski. Involvement of TRPV4 channels in Abeta40-induced hippocampal cell death and astrocytic Ca²⁺ signalling. *NeuroToxicology*, 41(JANUARY 2014):64–72, 2014. ISSN 0161813X. doi: 10.1016/j.neuro.2014.01.001.

- [7] Murad Banaji, Alfred Mallet, Clare E. Elwell, Peter Nicholls, and Chris E. Cooper. A model of brain circulation and metabolism: NIRS signal changes during physiological challenges. *PLoS Computational Biology*, 4(11), 2008. ISSN 1553734X. doi: 10.1371/journal.pcbi.1000212.
- [8] Murad Banaji, Alfred Mallet, Clare E. Elwell, Peter Nicholls, and Chris E. Cooper. Supplementary material for A model of brain circulation and metabolism . *PLoS Computational Biology*, 4(11):A1–A26, 2008.
- [9] M H Baslow and D N Guilfoyle. JOURNAL OF GLYCOMICS AND METABOLISM ISSN NO : Coming Soon. (1):1–12.
- [10] M H Baslow, V V Dyakin, K L Nowak, B L Hungund, and D N Guilfoyle. 2-PMPA, a NAAG Peptidase Inhibitor, Attenuates Magnetic Resonance BOLD Signals in Brain of Anesthetized Mice. *Journal of molecular neuroscience : MN*, 26(3):1–16, 2005.
- [11] Daniel a Beard. A biophysical model of the mitochondrial respiratory system and oxidative phosphorylation. *PLoS computational biology*, 1(4):e36, sep 2005. ISSN 1553-7358. doi: 10.1371/journal.pcbi.0010036. URL <http://www.ncbi.nlm.nih.gov/article/abstract.fcgi?artid=1201326&tool=pmcentrez&rendertype=abstract>.
- [12] Daniel a. Beard. Correction: A Biophysical Model of the Mitochondrial Respiratory System and Oxidative Phosphorylation. *PLoS Computational Biology*, 2(1):e8, 2006. ISSN 1553-734X. doi: 10.1371/journal.pcbi.0020008. URL <http://dx.plos.org/10.1371/journal.pcbi.0020008>.
- [13] Daniel a. Beard and James B. Bassingthwaigte. Modeling Advection and Diffusion of Oxygen in Complex Vascular Networks. *Annals of Biomedical Engineering*, 29(4):298–310, apr 2001. ISSN 0090-6964. doi: 10.1114/1.1359450. URL <http://link.springer.com/10.1114/1.1359450>.
- [14] Nikolaus Berndt, Sascha Bulik, and Hermann-Georg Holzhütter. Kinetic Modeling of the Mitochondrial Energy Metabolism of Neuronal Cells: The Impact of Reduced α -Ketoglutarate Dehydrogenase Activities on ATP Production and Generation of Reactive Oxygen Species. *International journal of cell biology*, 2012: 757594, jan 2012. ISSN 1687-8884. doi: 10.1155/2012/757594. URL <http://www.ncbi.nlm.nih.gov/article/abstract.fcgi?artid=3376505&tool=pmcentrez&rendertype=abstract>.
- [15] D S Bredt. Nitric oxide signaling specificity - the heart of the problem. *Journal of cell science*, 116(Pt 1):9–15., 2003. ISSN 00219533. doi: 10.1242/jcs.00183. URL [http://www.google.com/search?client=safari&rls=en-us&q=Nitric+oxide+signaling+specificity+the+heart+of+the+problem&ie=UTF-8&oe=UTF-8\\$&delimiter"026E30F\\$npapers2://publication/uuid/28C11E92-B6F7-4F10-896B-C1467459F0D1](http://www.google.com/search?client=safari&rls=en-us&q=Nitric+oxide+signaling+specificity+the+heart+of+the+problem&ie=UTF-8&oe=UTF-8$&delimiter).

- [16] R. B. Buxton, Kâmil Uluda, David J Dubowitz, and Thomas T Liu. Modeling the hemodynamic response to brain activation. *NeuroImage*, 23 Suppl 1:S220–33, jan 2004. ISSN 1053-8119. doi: 10.1016/j.neuroimage.2004.07.013. URL <http://www.ncbi.nlm.nih.gov/pubmed/15501093>.
- [17] G Carmignoto, L Pasti, and T Pozzan. On the role of voltage-dependent calcium channels in calcium signaling of astrocytes in situ. *The Journal of neuroscience : the official journal of the Society for Neuroscience*, 18 (12):4637–4645, 1998. ISSN 0270-6474.
- [18] Joshua C. Chang, Kevin C. Brennan, Dongdong He, Huaxiong Huang, Robert M. Miura, Phillip L. Wilson, and Jonathan J. Wylie. A Mathematical Model of the Metabolic and Perfusion Effects on Cortical Spreading Depression. *PLoS ONE*, 8(8):1–9, 2013. ISSN 19326203. doi: 10.1371/journal.pone.0070469.
- [19] Kejing Chen and Aleksander S. Popel. Theoretical analysis of biochemical pathways of nitric oxide release from vascular endothelial cells. *Free Radical Biology and Medicine*, 41(4):668–680, 2006. ISSN 08915849. doi: 10.1016/j.freeradbiomed.2006.05.009.
- [20] Kejing Chen and Aleksander S. Popel. Vascular and perivascular nitric oxide release and transport: Biochemical pathways of neuronal nitric oxide synthase (NOS1) and endothelial nitric oxide synthase (NOS3). *Free Radical Biology and Medicine*, 42(6):811–822, 2007. ISSN 08915849. doi: 10.1016/j.freeradbiomed.2006.12.007.
- [21] Mathieu Cloutier, Fiachra B Bolger, John P Lowry, and Peter Wellstead. An integrative dynamic model of brain energy metabolism using in vivo neurochemical measurements. *Journal of computational neuroscience*, 27 (3):391–414, dec 2009. ISSN 1573-6873. doi: 10.1007/s10827-009-0152-8. URL <http://www.ncbi.nlm.nih.gov/pubmed/19396534>.
- [22] A Comerford, Michael J Plank, and T David. Endothelial Nitric Oxide Synthase and Calcium Production in Arterial Geometries: an Integrated Fluid Mechanics/Cell Model. *Journal of Biomechanical Engineering*, 130 (13):011010–1–13, 2008. ISSN 01480731. doi: 10.1115/1.2838026.
- [23] P Condorelli and S C George. In vivo control of soluble guanylate cyclase activation by nitric oxide: a kinetic analysis. *Biophys J*, 80(5):2110–2119, 2001. ISSN 0006-3495. doi: 10.1016/S0006-3495(01)76184-X.
- [24] T H Crouch and C B Klee. Positive cooperative binding of calcium to bovine brain calmodulin. *Biochemistry*, 19(16):3692–3698, 1980. ISSN 0006-2960.
- [25] Raimondo D D'Ambrosio, David S Gordon, H Richard Winn, Canan Doganli, Kasper Kjaer-sorensen, Christopher Knoeckel, Hans Christian Beck, Randel Nyengaard, Bent Honoré, Poul Nissen, Angeles Ribera, and Claus

Oxvig. Differential Role of KIR Channel and Na⁺ / K⁺-Pump in the Regulation of Extracellular K⁺ in Rat Hippocampus Differential Role of KIR Channel and Na⁺ / K⁺-Pump in the Regulation of Extracellular K in Rat Hippocampus. *Journal of neurophysiology*, pages 87–102, 2002.

- [26] Ranjan K Dash and James B Bassingthwaighe. Simultaneous blood-tissue exchange of oxygen, carbon dioxide, bicarbonate, and hydrogen ion. *Annals of biomedical engineering*, 34(7):1129–48, jul 2006. ISSN 0090-6964. doi: 10.1007/s10439-005-9066-4. URL <http://www.ncbi.nlm.nih.gov/article/fcgi?artid=4232240&tool=pmcentrez&rendertype=abstract>.
- [27] Tim David. Wall Shear Stress Modulation of ATP/ADP Concentration at the Endothelium. *Annals of Biomedical Engineering*, 31(10):1231–1237, nov 2003. ISSN 0090-6964. doi: 10.1114/1.1615574. URL <http://link.springer.com/10.1114/1.1615574>.
- [28] S Dimmeler, I Fleming, B Fisslthaler, C Hermann, R Busse, and a M Zeiher. Activation of nitric oxide synthase in endothelial cells by Akt-dependent phosphorylation. *Nature*, 399(June):601–605, 1999. ISSN 0028-0836. doi: 10.1038/21224.
- [29] K. Dormanns and Sanne Van Der Lelij. Documentation for Code Version 1 . 1. 2014.
- [30] K. Dormanns, E M J van Disseldorp, R G Brown, and T David. Neurorovascular coupling and the influence of luminal agonists via the endothelium. *Journal of theoretical biology*, 364:49–70, aug 2015. ISSN 1095-8541. doi: 10.1016/j.jtbi.2014.08.029. URL <http://www.ncbi.nlm.nih.gov/pubmed/25167790>.
- [31] K. Dormanns, R.G. Brown, and T. David. The role of nitric oxide in neurorovascular coupling. *Journal of Theoretical Biology*, 394:1–17, 2016. ISSN 00225193. doi: 10.1016/j.jtbi.2016.01.009. URL <http://linkinghub.elsevier.com/retrieve/pii/S0022519316000308>.
- [32] J P Dreier, K Körner, N Ebert, a Görner, I Rubin, T Back, U Lindauer, T Wolf, a Villringer, K M Einhäupl, M Lauritzen, and U Dirnagl. Nitric oxide scavenging by hemoglobin or nitric oxide synthase inhibition by N-nitro-L-arginine induces cortical spreading ischemia when K⁺ is increased in the subarachnoid space. *Journal of cerebral blood flow and metabolism : official journal of the International Society of Cerebral Blood Flow and Metabolism*, 18(9):978–90, sep 1998. ISSN 0271-678X. doi: 10.1097/00004647-199809000-00007. URL <http://www.ncbi.nlm.nih.gov/pubmed/9740101>.
- [33] Jens P Dreier. The role of spreading depression, spreading depolarization and spreading ischemia in neurological disease. *Nature medicine*, 17(4):

- 439–47, apr 2011. ISSN 1546-170X. doi: 10.1038/nm.2333. URL <http://www.ncbi.nlm.nih.gov/pubmed/21475241>.
- [34] Kathryn M Dunn, David C Hill-Eubanks, Wolfgang B Liedtke, and Mark T Nelson. TRPV4 channels stimulate Ca²⁺-induced Ca²⁺ release in astrocytic endfeet and amplify neurovascular coupling responses. *Proceedings of the National Academy of Sciences*, 110(15):6157–6162, 2013.
 - [35] F R Edwards, G D Hirst, and G D Silverberg. Inward rectification in rat cerebral arterioles; involvement of potassium ions in autoregulation. *The Journal of Physiology*, 404(1):455–466, 1988.
 - [36] Michelle a Erickson and William a Banks. Blood-brain barrier dysfunction as a cause and consequence of Alzheimer’s disease. *Journal of cerebral blood flow and metabolism : official journal of the International Society of Cerebral Blood Flow and Metabolism*, 33(10):1500–13, oct 2013. ISSN 1559-7016. doi: 10.1038/jcbfm.2013.135. URL <http://www.ncbi.nlm.nih.gov/articlerender.fcgi?artid=3790938&tool=pmcentrez&rendertype=abstract>.
 - [37] a a Fadel, K a Barbee, and D Jaron. A computational model of nitric oxide production and transport in a parallel plate flow chamber. *Annals of biomedical engineering*, 37(5):943–54, may 2009. ISSN 1573-9686. doi: 10.1007/s10439-009-9658-5. URL <http://www.ncbi.nlm.nih.gov/pubmed/19242805>.
 - [38] Hannah Farr and Tim David. Models of neurovascular coupling via potassium and EET signalling. *Journal of theoretical biology*, 286(1):13–23, oct 2011. ISSN 1095-8541. doi: 10.1016/j.jtbi.2011.07.006. URL <http://www.ncbi.nlm.nih.gov/pubmed/21781976>.
 - [39] Francisco Fernández-klett, Nikolas Offenhauser, Ulrich Dirnagl, Josef Priller, and Ute Lindauer. Pericytes in capillaries are contractile in vivo, but arterioles mediate functional hyperemia in the mouse brain. 2010. doi: 10.1073/pnas.1011321108.
 - [40] J A Filosa and V M Blanco. Neurovascular coupling in the mammalian brain. *Exp Physiol*, 92(4):641–646, 2007.
 - [41] J A Filosa, Adrian D Bonev, and Mark T Nelson. Calcium Dynamics in Cortical Astrocytes and Arterioles during Neurovascular Coupling. *Circulation research*, 95(10):e73—e81, 2004.
 - [42] J A Filosa, Adrian D Bonev, Stephen V Straub, Andrea L Meredith, M Keith Wilkerson, Richard W Aldrich, and Mark T Nelson. Local potassium signaling couples neuronal activity to vasodilation in the brain. *Nature neuroscience*, 9(11):1397–1403, nov 2006. ISSN 1097-6256. doi: 10.1038/nn1779. URL <http://www.ncbi.nlm.nih.gov/pubmed/17013381>.

- [43] B Fisslthaler, S Dimmeler, C Hermann, R Busse, and I Fleming. Phosphorylation and activation of the endothelial nitric oxide synthase by fluid shear stress. *Acta physiologica Scandinavica*, 168(1):81–8, 2000. ISSN 0001-6772. doi: 10.1046/j.1365-201x.2000.00627.x. URL <http://www.ncbi.nlm.nih.gov/pubmed/10691783>.
- [44] Ingrid Fleming and Rudi Busse. Endothelial Dysfunction: a Novel Therapeutic Target - NO: the Primary EDRF. *Journal of Molecular and Cellular Cardiology*, 14(31):5–14, 1999.
- [45] Paul Forsythe, Mark Gilchrist, Marianne Kulka, and A. Dean Befus. Mast cells and nitric oxide: Control of production, mechanisms of response. *International Immunopharmacology*, 1(8):1525–1541, 2001. ISSN 15675769. doi: 10.1016/S1567-5769(01)00096-0.
- [46] Helene Girouard and Costantino Iadecola. Neurovascular coupling in the normal brain and in hypertension, stroke, and Alzheimer disease. *Journal of applied physiology (Bethesda, Md. : 1985)*, 100(1):328–335, jan 2006. ISSN 8750-7587. doi: 10.1152/japplphysiol.00966.2005. URL <http://www.ncbi.nlm.nih.gov/pubmed/16357086>.
- [47] Helene Girouard, Adrian D Bonev, Rachael M Hannah, Andrea Meredith, Richard W Aldrich, and Mark T Nelson. Astrocytic endfoot Ca^{2+} and BK channels determine both arteriolar dilation and constriction. *Proceedings of the National Academy of Sciences of the United States of America*, 107(8):3811–6, feb 2010. ISSN 1091-6490. doi: 10.1073/pnas.0914722107. URL <http://www.pubmedcentral.nih.gov/articlerender.fcgi?artid=2840528&tool=pmcentrez&rendertype=abstract>.
- [48] Albert Goldbeter, Geneviève Dupont, and Michael J Berridge. Minimal model for signal-induced Ca^{2+} oscillations and for their frequency encoding through protein phosphorylation. *Proceedings of the National Academy of Sciences*, 87(4):1461–1465, 1990.
- [49] B Gonzalez-Fernandez J.M. Ermentrout, J M Gonzalez-Fernandez, and B Ermentrout. On the Origin and Dynamics of the Vasomotion of Small Arteries. *Mathematical Biosciences*, 167(2):127–167, feb 1994. ISSN 0025-5564. URL <http://www.ncbi.nlm.nih.gov/pubmed/8142694>.
- [50] James Hadfield, Michael J Plank, and Tim David. Modeling Secondary Messenger Pathways in Neurovascular Coupling. *Bulletin of mathematical biology*, pages 1–16, 2013.
- [51] C M Hai and R A Murphy. Cross-bridge phosphorylation and regulation of latch state in smooth muscle. *American Journal of Physiology - Cell Physiology*, 254:C99–C106, 1988.
- [52] C-M Hai and R A Murphy. Ca^{2+} , crossbridge phosphorylation, and contraction. *Annual Review of Physiology*, 51(1):285–298, 1989. ISSN 00664278. doi: 10.1146/annurev.physiol.51.1.285.

- [53] Catherine N Hall, Clare Reynell, Bodil Gesslein, Nicola B Hamilton, Anusha Mishra, Brad A Sutherland, Fergus M O’Farrell, Alastair M Buchan, Martin Lauritzen, and David Attwell. Capillary pericytes regulate cerebral blood flow in health and disease. *Nature*, 508(7494):55–60, 2014. ISSN 1476-4687. doi: 10.1038/nature13165. URL <http://www.ncbi.nlm.nih.gov/article/fcgi?artid=3976267&tool=pmcentrez&rendertype=abstract>.
- [54] Edith Hamel. Perivascular nerves and the regulation of cerebrovascular tone. *Journal of applied physiology (Bethesda, Md. : 1985)*, 100(3):1059–1064, 2006. ISSN 8750-7587. doi: 10.1152/japplphysiol.00954.2005.
- [55] D R Harder, R J Roman, and D Gebremedhin. Molecular mechanisms controlling nutritive blood flow: role of cytochrome P450 enzymes. *Acta physiologica scandinavica*, 168(4):543–549, 2000.
- [56] David R Harder, Chenyang Zhang, and Debebe Gebremedhin. Astrocytes function in matching blood flow to metabolic activity. *News in physiological sciences : an international journal of physiology produced jointly by the International Union of Physiological Sciences and the American Physiological Society*, 17(February):27–31, 2002. ISSN 0886-1714.
- [57] Yuji Hayashi, Masahiro Nishio, Yasuhito Naito, Hisayuki Yokokura, Yuji Nimura, Hiroyoshi Hidaka, and Yasuo Watanabe. Regulation of neuronal nitric-oxide synthase by calmodulin kinases. *Journal of Biological Chemistry*, 274(29):20597–20602, 1999. ISSN 00219258. doi: 10.1074/jbc.274.29.20597.
- [58] R A Hill, Lei Tong, Peng Yuan, Sasidhar Murikinati, Shobhana Gupta, and Jaime Grutzendler. Regional Blood Flow in the Normal and Ischemic Brain Is Controlled by Arteriolar Smooth Muscle Cell Contractility and Not by Capillary Pericytes. *Neuron*, 87(1):95–110, 2015.
- [59] Niklas Hübel and Markus a Dahlem. Dynamics from seconds to hours in hodgkin-huxley model with time-dependent ion concentrations and buffer reservoirs. *PLoS computational biology*, 10(12):e1003941, 2014. ISSN 1553-7358. doi: 10.1371/journal.pcbi.1003941. URL <http://www.ncbi.nlm.nih.gov/article/fcgi?artid=4256015&tool=pmcentrez&rendertype=abstract>.
- [60] Costantino Iadecola. Atherosclerosis and Neurodegeneration. *Atherosclerosis Thrombosis and Vascular Biology*, 23:1951–1952, 2003. doi: 10.1161/01.ATV.00000102660.99744.85.
- [61] Costantino Iadecola and Maiken Nedergaard. Glial regulation of the cerebral microvasculature. *Nature neuroscience*, 10(11):1369–1376, 2007.
- [62] C E Jahr and C F Stevens. Calcium permeability of the N-methyl-D-aspartate receptor channel in hippocampal neurons in culture. *Proceedings*

of the National Academy of Sciences of the United States of America, 90 (December):11573–11577, 1993. ISSN 0027-8424.

- [63] H. Kager, W J Wadman, and G G Somjen. Simulated seizures and spreading depression in a neuron model incorporating interstitial space and ion concentrations. *Journal of neurophysiology*, 84(1):495–512, 2000. ISSN 0022-3077.
- [64] A. J. Kanai, H. C. Strauss, G. A. Truskey, A. L. Crews, S. Grunfeld, and T. Malinski. Shear Stress Induces ATP-Independent Transient Nitric Oxide Release From Vascular Endothelial Cells, Measured Directly With a Porphyrinic Microsensor. *Circulation Research*, 77 (2):284–293, 1995. ISSN 0009-7330. doi: 10.1161/01.RES.77.2.284. URL [http://www.scopus.com/inward/record.url?eid=2-s2.0-0029087961&partnerID=tZ0tx3y1\\$& delimiter=026E30F\\$nhttp://circres.ahajournals.org/cgi/doi/10.1161/01.RES.77.2.284](http://www.scopus.com/inward/record.url?eid=2-s2.0-0029087961&partnerID=tZ0tx3y1$& delimiter=026E30F$nhttp://circres.ahajournals.org/cgi/doi/10.1161/01.RES.77.2.284).
- [65] Mahendra Kavdia and Aleksander S. Popel. Wall shear stress differentially affects NO level in arterioles for volume expanders and Hb-based O₂ carriers. *Microvascular Research*, 66(1):49–58, 2003. ISSN 00262862. doi: 10.1016/S0026-2862(03)00008-6.
- [66] Mahendra Kavdia, Nikolaos M Tsoukias, and Aleksander S Popel. Model of nitric oxide diffusion in an arteriole: impact of hemoglobin-based blood substitutes. *American Journal of Physiology. Heart and Circulatory Physiology*, 282(6):2245–2253, 2002. ISSN 0363-6135. doi: 10.1152/ajpheart.00972.2001. URL <http://www.ncbi.nlm.nih.gov/pubmed/12003834>.
- [67] Masahito Kawamura and Masahiro Kawamura. Long-term facilitation of spontaneous calcium oscillations in astrocytes with endogenous adenosine in hippocampal slice cultures. *Cell Calcium*, 49(4):249–258, 2011. ISSN 01434160. doi: 10.1016/j.ceca.2011.02.009. URL <http://dx.doi.org/10.1016/j.ceca.2011.02.009>.
- [68] Michèle Koenigsberger, Roger Sauser, Jean-Louis Bény, and Jean-Jacques Meister. Effects of arterial wall stress on vasomotion. *Biophysical journal*, 91(5):1663–1674, sep 2006. ISSN 0006-3495. doi: 10.1529/biophysj.106.083311. URL <http://www.ncbi.nlm.nih.gov/article/fcgi?artid=1544282&tool=pmcentrez&rendertype=abstract>.
- [69] Masayo Koide, Adrian D Bonev, Mark T Nelson, and George C Wellman. Inversion of neurovascular coupling by subarachnoid blood depends on large-conductance Ca²⁺-activated K⁺ (BK) channels. *Proceedings of the National Academy of Sciences of the United States of America*, 109(21):E1387–95, may 2012. ISSN 1091-6490. doi: 10.1073/pnas.1121359109. URL <http://www.ncbi.nlm.nih.gov/article/fcgi?artid=3361424&tool=pmcentrez&rendertype=abstract>.

- [70] Masayo Koide, Inna Sukhotinsky, Cenk Ayata, and George C Wellman. Subarachnoid hemorrhage, spreading depolarizations and impaired neurovascular coupling. *Stroke research and treatment*, 2013:819340, jan 2013. ISSN 2090-8105. doi: 10.1155/2013/819340. URL <http://www.ncbi.nlm.nih.gov/pmc/articles/PMC3610342/>{tool=pmcentrez}{rendertype=abstract}.
- [71] James Kozloski and John Wagner. An Ultrascalable Solution to Large-scale Neural Tissue Simulation. *Frontiers in neuroinformatics*, 5 (September):15, jan 2011. ISSN 1662-5196. doi: 10.3389/fninf.2011.00015. URL <http://www.ncbi.nlm.nih.gov/pmc/articles/PMC3175572/>{tool=pmcentrez}{rendertype=abstract}.
- [72] James Kozloski, Maria Eleftheriou, Blake Fitch, and Charles Peck. IBM Research Report. 24811, 2009.
- [73] Frank M LaFerla. Calcium dyshomeostasis and intracellular signalling in Alzheimer's disease. *Nature reviews. Neuroscience*, 3(11):862–72, nov 2002. ISSN 1471-003X. doi: 10.1038/nrn960. URL <http://www.ncbi.nlm.nih.gov/pubmed/12415294>.
- [74] J R Lancaster. Simulation of the diffusion and reaction of endogenously produced nitric oxide. *Proceedings of the National Academy of Sciences*, 91(17):8137–8141, 1994. ISSN 0027-8424. doi: 10.1073/pnas.91.17.8137. URL http://www.pnas.org/content/91/17/8137.abstract?ijkey=f4532078682d7875eb4acb22ba4820a64405f937&keytype2=tf_ipsecsha.
- [75] J R Lancaster. A tutorial on the diffusibility and reactivity of free nitric oxide. *Nitric oxide : biology and chemistry / official journal of the Nitric Oxide Society*, 1(1):18–30, 1997. ISSN 1089-8603. doi: 10.1006/niox.1996.0112. URL <http://www.ncbi.nlm.nih.gov/pubmed/9701041>.
- [76] C. LeCrux and E. Hamel. The neurovascular unit in brain function and disease. *Acta Physiologica*, 203(1):47–59, 2011. ISSN 17481708. doi: 10.1111/j.1748-1716.2011.02256.x.
- [77] Clotilde LeCrux, Xavier Toussay, Ara Kocharyan, Priscilla Fernandes, Sujay Neupane, Maxime Lévesque, Fabrice Plaisier, Amir Shmuel, Bruno Cauli, and Edith Hamel. Pyramidal neurons are "neurogenic hubs" in the neurovascular coupling response to whisker stimulation. *The Journal of neuroscience : the official journal of the Society for Neuroscience*, 31(27):9836–9847, 2011. ISSN 0270-6474. doi: 10.1523/JNEUROSCI.4943-10.2011.
- [78] Clotilde LeCrux, Ara Kocharyan, Claire H Sandoe, Xin-Kang Tong, and Edith Hamel. Pyramidal cells and cytochrome P450 epoxigenase products in the neurovascular coupling response to basal forebrain cholinergic input. *Journal of Cerebral Blood Flow & Metabolism*, 32(5):896–906, 2012. ISSN

- 0271-678X. doi: 10.1038/jcbfm.2012.4. URL <http://dx.doi.org/10.1038/jcbfm.2012.4>.
- [79] Bing Li, Shangbin Chen, Shaoqun Zeng, Qingming Luo, and Pengcheng Li. Modeling the contributions of Ca²⁺ flows to spontaneous Ca²⁺ oscillations and cortical spreading depression-triggered Ca²⁺ waves in astrocyte networks. *PLoS one*, 7(10):e48534, jan 2012. ISSN 1932-6203. doi: 10.1371/journal.pone.0048534. URL <http://www.ncbi.nlm.nih.gov/article/fcgi?artid=3485305&tool=pmcentrez&rendertype=abstract>.
- [80] Bo Liao, Yun-Min Zheng, Vishal R Yadav, Amit S Konde, and Yong-Xiao Wang. Hypoxia induces intracellular Ca²⁺ release by causing reactive oxygen species-mediated dissociation of FK506-binding protein 12.6 from ryanodine receptor 2 in pulmonary artery myocytes. *Antioxidants & redox signaling*, 14(1):37–47, 2011. ISSN 1523-0864. doi: 10.1089/ars.2009.3047.
- [81] Eng H Lo. A new penumbra: transitioning from injury into repair after stroke. *Nature medicine*, 14(5):497–500, may 2008. ISSN 1546-170X. doi: 10.1038/nm1735. URL <http://www.ncbi.nlm.nih.gov/pubmed/18463660>.
- [82] T Lu, T Hoshi, N L Weintraub, a a Spector, and H C Lee. Activation of ATP-sensitive K(+) channels by epoxyeicosatrienoic acids in rat cardiac ventricular myocytes. *The Journal of physiology*, 537 (Pt 3):811–27, 2001. ISSN 0022-3751. doi: 10.1113/jphysiol.2001.012896. URL <http://www.ncbi.nlm.nih.gov/article/fcgi?artid=2278996&tool=pmcentrez&rendertype=abstract>.
- [83] George A Mashour and Robert J Boock. Effects of shear stress on nitric oxide levels of human cerebral endothelial cells cultured in an artificial capillary system. *Brain research*, 842(1):233–8, 1999. ISSN 0006-8993. URL <http://www.ncbi.nlm.nih.gov/pubmed/10526117>.
- [84] Joseph R H Mauban, Seth T Fairfax, Mark a Rizzo, Jin Zhang, and Withrow Gil Wier. A method for noninvasive longitudinal measurements of [Ca²⁺] in arterioles of hypertensive optical biosensor mice. *American journal of physiology. Heart and circulatory physiology*, 307(2):H173–81, jul 2014. ISSN 1522-1539. doi: 10.1152/ajpheart.00182.2014. URL <http://www.ncbi.nlm.nih.gov/pubmed/24858846>.
- [85] Bernd Mayer and Benjamin Hemmens. Biosynthesis and action of nitric oxide in mammalian cells. *Trends in Biochemical Sciences*, 22(12):477–481, 1997. ISSN 09680004. doi: 10.1016/S0968-0004(97)01147-X.
- [86] Heraldo Memelli, Benjamin Torben-Nielsen, and James Kozloski. Self-referential forces are sufficient to explain different dendritic morphologies. *Frontiers in neuroinformatics*, 7(January):1, jan 2013. ISSN 1662-5196. doi: 10.3389/fninf.2013.00001. URL

<http://www.ncbi.nlm.nih.gov/pmc/articles/PMC3558683/>&tool=pmcentrez&rendertype=abstract.

- [87] Sean J Mulligan and Brian a MacVicar. Calcium transients in astrocyte endfeet cause cerebrovascular constrictions. *Nature*, 431(7005):195–199, 2004. ISSN 0028-0836. doi: 10.1038/nature02827.
- [88] S. Murphy, G. Rich, K. I. Orgren, S. a. Moore, and F. M. Faraci. Astrocyte-derived lipoxygenase product evokes endothelium-dependent relaxation of the basilar artery. *Journal of Neuroscience Research*, 38 (3):314–318, 1994. ISSN 03604012. doi: 10.1002/jnr.490380309.
- [89] W Mutch and J Hansen. Extracellular pH changes during spreading depression and cerebral ischemia: mechanisms of brain pH regulation. *Journal of cerebral blood flow and metabolism : official journal of the International Society of Cerebral Blood Flow and Metabolism*, 4(1):17–27, mar 1984. ISSN 0271-678X. doi: 10.1038/jcbfm.1984.3. URL <http://www.ncbi.nlm.nih.gov/pubmed/6693512>.
- [90] C Y Ngai and X Yao. Vascular Responses to Shear Stress : The Involvement of Mechanosensors in Endothelial Cells. pages 85–94, 2010.
- [91] K Niwa, C Haensel, M E Ross, and C Iadecola. Cyclooxygenase-1 participates in selected vasodilator responses of the cerebral circulation. *Circ Res*, 88(6):600–608, 2001. ISSN 1524-4571. doi: 10.1161/01.RES.88.6.600. URL [http://circres.ahajournals.org/cgi/content/full/88/6/600\\$& delimiter" 026E30F\\$npapers2://publication/uuid/BF76CC7E-E9DA-4583-97A7-090315DDF881](http://circres.ahajournals.org/cgi/content/full/88/6/600$& delimiter).
- [92] Krystal Nizar, Hana Uhlirova, Peifang Tian, Payam A Saisan, Qun Cheng, Lidia Reznichenko, Kimberly L Weldy, Tyler C Steed, Vishnu B Sridhar, Christopher L MacDonald, Others, Jianxia Cui, Sergey L Gratiy, Sava Sakadzic, David A Boas, Thomas I Beka, Gaute T Einevoll, Ju Chen, Eliezer Masliah, Anders M Dale, Gabriel A Silvia, and Anna Devor. In vivo Stimulus-Induced Vasodilation Occurs without IP₃ Receptor Activation and May Precede Astrocytic Calcium Increase. *The Journal of Neuroscience*, 33(19):8411–8422, 2013.
- [93] Ivar Østby, Leiv Øyehaug, Gaute T Einevoll, Erlend A Nagelhus, Erik Plahte, Thomas Zeuthen, Catherine M Lloyd, Ole P Ottersen, and Stig W Omholt. Astrocytic Mechanisms Explaining Neural-Activity-Induced Shrinkage of Extraneuronal Space. *PLoS Computational Biology*, 5(1):1–12, 2009.
- [94] L. Ostergaard, J. P. Dreier, N. Hadjikhani, S. N. Jespersen, U. Dirnagl, and T. Dalkara. Neurovascular Coupling During Cortical Spreading Depolarization and -Depression. *Stroke*, pages 1–10, 2015. ISSN 0039-2499. doi: 10.1161/STROKEAHA.114.008077. URL <http://stroke.ahajournals.org/cgi/doi/10.1161/STROKEAHA.114.008077>.

- [95] Henning Piilgaard and Martin Lauritzen. Piilgard and Lauritzen JCBFM 2009.pdf. *Journal of Cerebral Blood Flow and Metabolism*, 29:1517–1527, 2009.
- [96] M J Plank, D J N Wall, and T David. Atherosclerosis and calcium signalling in endothelial cells. *Progress in biophysics and molecular biology*, 91(3):287–313, 2006. ISSN 0079-6107. doi: 10.1016/j.pbiomolbio.2005.07.005. URL <http://www.ncbi.nlm.nih.gov/pubmed/16171849>.
- [97] J. M. Quayle, M. T. Nelson, and N. B. Standen. ATP-sensitive and inwardly rectifying potassium channels in smooth muscle. *Physiological Reviews*, 77(4):1165–1232, 1997. ISSN 0031-9333. URL [http://physrev.physiology.org.myaccess.library.utoronto.ca/content/77/4/1165\\$delimiter"026E30F\\$nhttp://physrev.physiology.org.myaccess.library.utoronto.ca/content/physrev/77/4/1165.full.pdf\\$delimiter"026E30F\\$nhttp://www.ncbi.nlm.nih.gov/pubmed/9354814](http://physrev.physiology.org.myaccess.library.utoronto.ca/content/77/4/1165$delimiter).
- [98] D. G. Rosenegger, C. H. T. Tran, J. I. Wamsteeker Cusulin, and G. R. Gordon. Tonic Local Brain Blood Flow Control by Astrocytes Independent of Phasic Neurovascular Coupling. *Journal of Neuroscience*, 35(39): 13463–13474, 2015. ISSN 0270-6474. doi: 10.1523/JNEUROSCI.1780-15.2015. URL <http://www.jneurosci.org/cgi/doi/10.1523/JNEUROSCI.1780-15.2015>.
- [99] Beverly A Rzigalinski, Peter F Blackmore, and Miriam D Rosenthal. Arachidonate mobilization is coupled to depletion of intracellular calcium stores and influx of extracellular calcium in differentiated U937 cells. *Biochimica et Biophysica Acta (BBA)-Lipids and Lipid Metabolism*, 1299(3):342–352, 1996.
- [100] Navid Safaeian and Tim David. A computational model of oxygen transport in the cerebrocapillary levels for normal and pathologic brain function. *Journal of cerebral blood flow and metabolism : official journal of the International Society of Cerebral Blood Flow and Metabolism*, 33(10):1633–41, oct 2013. ISSN 1559-7016. doi: 10.1038/jcbfm.2013.119. URL <http://www.ncbi.nlm.nih.gov/pmc/articles/PMC3790934/>{&}tool=pmcentrez{&}rendertype=abstract.
- [101] Thomas H Sanderson, Christian a Reynolds, Rita Kumar, Karin Przyklenk, and Maik Hüttemann. Molecular mechanisms of ischemia-reperfusion injury in brain: pivotal role of the mitochondrial membrane potential in reactive oxygen species generation. *Molecular neurobiology*, 47(1):9–23, feb 2013. ISSN 1559-1182. doi: 10.1007/s12035-012-8344-z. URL <http://www.ncbi.nlm.nih.gov/pmc/articles/PMC3725766/>{&}tool=pmcentrez{&}rendertype=abstract.
- [102] David M. Santucci and Sridhar Raghavachari. The effects of NR2 subunit-dependent NMDA receptor kinetics on synaptic transmission and CaMKII

- activation. *PLoS Computational Biology*, 4(10), 2008. ISSN 1553734X. doi: 10.1371/journal.pcbi.1000208.
- [103] Hwa Kyoung Shin, Andrew K Dunn, Phillip B Jones, David a Boas, Michael a Moskowitz, and Cenk Ayata. Vasoconstrictive neurovascular coupling during focal ischemic depolarizations. *Journal of cerebral blood flow and metabolism : official journal of the International Society of Cerebral Blood Flow and Metabolism*, 26(8):1018–30, aug 2006. ISSN 0271-678X. doi: 10.1038/sj.jcbfm.9600252. URL <http://www.ncbi.nlm.nih.gov/pubmed/16340958>.
- [104] Marie Simard, Gregory Arcuino, Takahiro Takano, Qing Song Liu, and Maiken Nedergaard. Signaling at the gliovascular interface. *The Journal of neuroscience : the official journal of the Society for Neuroscience*, 23(27):9254–62, oct 2003. ISSN 1529-2401. URL <http://www.ncbi.nlm.nih.gov/pubmed/14534260>.
- [105] Xiulan Sun, Guiqiong He, Hong Qing, Weihui Zhou, Frederick Dobie, Fang Cai, Matthias Staufenbiel, L Eric Huang, and Weihong Song. Hypoxia facilitates Alzheimer’s disease pathogenesis by up-regulating BACE1 gene expression. *Proceedings of the National Academy of Sciences of the United States of America*, 103(49):18727–18732, 2006. ISSN 0027-8424. doi: 10.1073/pnas.0606298103.
- [106] Xiaoqiang Tang, Yu-Xuan Luo, Hou-Zao Chen, and De-Pei Liu. Mitochondria, endothelial cell function, and vascular diseases. *Frontiers in physiology*, 5:175, jan 2014. ISSN 1664-042X. doi: 10.3389/fphys.2014.00175. URL <http://www.ncbi.nlm.nih.gov/pmc/articles/PMC3930703/>; <http://www.ncbi.nlm.nih.gov/pmc/articles/PMC3930703/tool=pmcentrez&rendertype=abstract>.
- [107] Roger J Thompson, Ning Zhou, and Brian a MacVicar. Ischemia opens neuronal gap junction hemichannels. *Science (New York, N.Y.)*, 312(5775):924–7, may 2006. ISSN 1095-9203. doi: 10.1126/science.1126241. URL <http://www.ncbi.nlm.nih.gov/pubmed/16690868>.
- [108] Cam Ha T Tran, Mark S Taylor, Frances Plane, Sridevi Nagaraja, Niko-laos M Tsoukias, Viktoryiya Solodushko, Edward J Vigmond, Tobias Furstenhaupt, Mathew Brigdan, and Donald G Welsh. Endothelial Ca²⁺ wavelets and the induction of myoendothelial feedback. *American Journal of Physiology-Cell Physiology*, 302(8):C1226—C1242, 2012.
- [109] R D Traub, J G Jefferys, R Miles, M a Whittington, and K Tóth. A branching dendritic model of a rodent CA3 pyramidal neurone. *The Journal of physiology*, 481 (Pt 1:79–95, nov 1994. ISSN 0022-3751. URL <http://www.ncbi.nlm.nih.gov/pmc/articles/PMC16790868/>; <http://www.ncbi.nlm.nih.gov/pmc/articles/PMC16790868/tool=pmcentrez&rendertype=abstract>.
- [110] T F Wiesner, B C Berk, and R M Nerem. A mathematical model of the cytosolic-free calcium response in endothelial cells to fluid shear stress.

Proceedings of the National Academy of Sciences of the United States of America, 94(8):3726–3731, 1997. ISSN 0027-8424. doi: 10.1073/pnas.94.8.3726.

- [111] Wikipedia. No Title. URL http://en.wikipedia.org/wiki/Mechanism_of_anoxic_depolarization_in_the_brain.
- [112] J Wood and J Garthwaite. Models of the diffusional spread of nitric oxide: Implications for neural nitric oxide signalling and its pharmacological properties. *Neuropharmacology*, 33(11):1235–1244, 1994. ISSN 00283908. doi: 10.1016/0028-3908(94)90022-1.
- [113] Jin Yang, John W Clark, Robert M Bryan, and Claudia S Robertson. Mathematical modeling of the nitric oxide/cGMP pathway in the vascular smooth muscle cell. *American Journal of Physiology-Heart and Circulatory Physiology*, 289(2):H886—H897, 2005.
- [114] Luqing Zhang, Panayiota Papadopoulos, and Edith Hamel. Endothelial TRPV4 channels mediate dilation of cerebral arteries: Impairment and recovery in cerebrovascular pathologies related to Alzheimer’s disease. *British Journal of Pharmacology*, 170(3):661–670, 2013. ISSN 00071188. doi: 10.1111/bph.12315.
- [115] Berislav V. Zlokovic. Neurovascular mechanisms of Alzheimer’s neurodegeneration. *Trends in Neurosciences*, 28(4):202–208, 2005. ISSN 01662236. doi: 10.1016/j.tins.2005.02.001.
- [116] M Zonta, M C Angulo, S Gobbo, B Rosengarten, K-A. Hossman, T Pozzan, and G Carmignoto. Neuron-to-Astrocyte signaling is central to the dynamic control of brain microcirculation. *Nature Neuroscience*, 6(1), 2003.
- [117] Robin Zur Nieden and Joachim W. Deitmer. The role of metabotropic glutamate receptors for the generation of calcium oscillations in rat hippocampal astrocytes in situ. *Cerebral Cortex*, 16(5):676–687, 2006. ISSN 10473211. doi: 10.1093/cercor/bhj013.